UNIVERSITA' DEL PIEMONTE ORIENTALE
Dipartimento di Scienze e Innovazione Tecnologica

PhD Thesis in "Chemistry & Biology" – XXXVth Cycle

Iron(III)-Complexes as MRI Contrast Agents

Alessandro Nucera

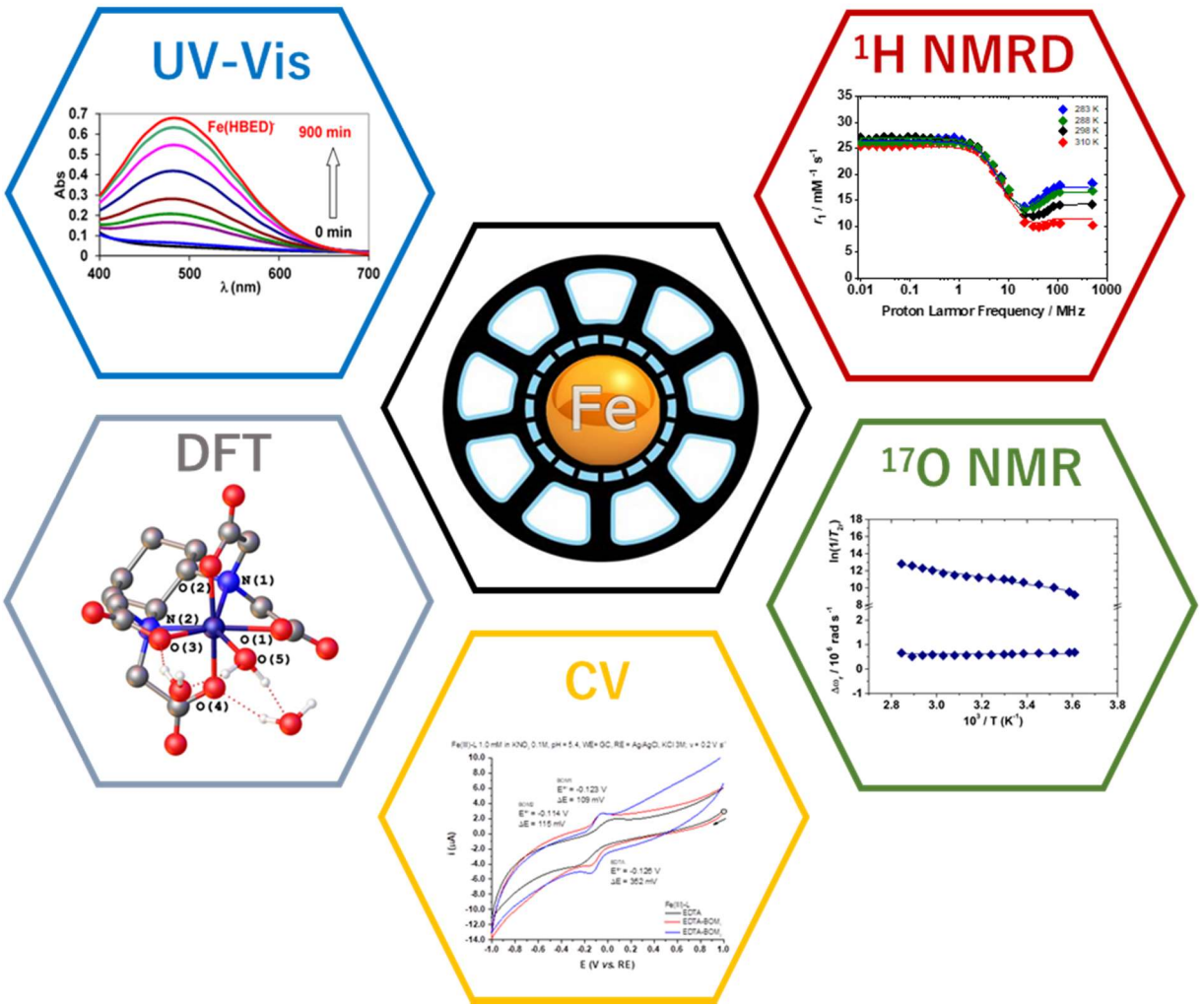

UNIVERSITÀ DEL PIEMONTE ORIENTALE

"Amedeo Avogadro"

Dipartimento di Scienze e Innovazione Tecnologica

PhD Thesis in "Chemistry & Biology" – XXXVth Cycle

Iron(III)-Complexes as MRI Contrast Agents

PhD Candidate: Alessandro Nucera

Supervisor: Prof. Mauro Botta

Ph.D. Program Co-ordinator: Prof. Gian Cesare Tron

Disciplinary scientific area: CHIM/03

A mamma e papà,

al piccolo Francesco

E a tutta la mia famiglia.

Grazie.

UNIVERSITÀ DEL PIEMONTE ORIENTALE
DOTTORATO DI RICERCA
IN CHEMISTRY & BIOLOGY

Via Duomo, 6
13100 – Vercelli (ITALY)

DECLARATION AND AUTHORISATION TO ANTIPLAGIARISM DETECTION

The undersigned ……Nucera Alessandro……student of the Chemistry & Biology Ph.D course (XXXV Cycle)

declares:

- to be aware that the University has adopted a web-based service to detect plagiarism through a software system called "Turnit.in",
- his/her Ph.D. thesis was submitted to Turnit.in scan and reasonably it resulted an original document, which correctly cites the literature;

acknowledges:

- his/her Ph.D. thesis can be verified by his/her Ph.D. tutor and/or Ph.D Coordinator in order to confirm its originality.

Date: 12/11/2022…….. Signature: … 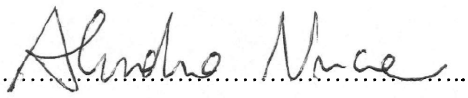 …..

XY/tcs
Percorso del file

Outline

In Magnetic Resonance Imaging (MRI), Gd(III)-based contrast agents have proven to be of great help for the diagnosis of various pathologies and for improving image quality. Although such compounds are generally considered safe, in response to concerns about patients who cannot tolerate some Gd(III) contrast agents as well as more recent reports of Gd(III) retention in the body, there has been a renewed interest in finding alternatives to using Gd(III) for MR contrast. In this regard, complexes based on endogenous ions such as Fe(III) and Mn(II) may be a viable option. While over the last 20 years, many investigations have been performed on Mn(II) complexes, there is not such a large number of publication on Fe(III) complexes. Indeed, even though it was stated by Koenig *et. al* more than 35 years ago that Fe(III) has the potential to be suitable as an MRI probe, the mechanism responsible for water proton relaxation enhancement induced by Fe(III) complexes has not been deciphered yet. This could be pursued by understanding the relationship between their chemical structure and the molecular parameters that govern relaxivity. Hence, in the context of a long-term project directed toward the development of new iron-based chelates as MRI probes, a systematic study of specific model systems is preliminary and essential for the design of new compounds for future applications. In this PhD thesis,

a detailed examination was carried out on the relaxometric properties of Fe(III)-based chelates by measuring ^{1}H longitudinal relaxation data from 0.01 up to 500 MHz and ^{17}O transverse relaxation rates (R_2) and shift ($\Delta\omega$) at 11.7 T, as a function of temperature. This multinuclear and multifrequencies time domain NMR study at low and high resolution at different temperatures allowed us to adequately describe the behavior of these paramagnetic complexes in aqueous solution, starting from model system as $[Fe(H_2O)_6]^{3+}$, $[Fe(EDTA)]^{-}$ and $[Fe(CDTA)]^{-}$. This study is also extended to specific cases that will be proposed to better understand how water proton relaxation enhancement is influenced by:

1. the interaction with macromolecules (e.g., albumin, cyclodextrin…) by using lipophilic ligands as in the case of the $[Fe(EDTA\text{-}BOM_x)]^{-}$ series;
2. the effect of the electronic parameters by investigating specific complexes;
3. the choice of the ligand structure.

These are key aspects to fill the gap on the knowledge on Fe(III)-based complexes for MRI applications. Additionally, through UV-Vis spectrophotometry, potentiometry and cyclic voltammetry, crucial properties such as thermodynamic stability, kinetic inertness and the redox behavior of such complexes will be investigated in depth. Our experimental data will also by supported by DFT calculations. Finally,

the combination of these techniques will be used for the characterization of a well-defined iron(III)-catecholate system, the Fe(III)-Tiron. Its remarkable properties led us to define this system as a possible blueprint for the rational design of novel and more biocompatible catechol-based ligands for Fe(III) complexation. The first attempts of the synthesis and the characterization of these newly designed ligands and their corresponding Fe(III) complexes will also be presented.

List of abbreviations

BCAT	3,3'-((butane-1,4-diylbis(azanediyl))bis(methylene))bis(benzene-1,2-diol)
β-CD	β-cyclodextrin
BOM	Benzyloxymehtyl
CA	Contrast agent
CDTA	2,2',2'',2'''-(cyclohexane-1,2-diylbis(azanetriyl))tetraacetic acid
DF	Desferrioxamine B
DTPA	Diethylenetriaminepentaacetic acid
ECAT	3,3'-((ethane-1,2-diylbis(azanediyl))bis(methylene))bis(benzene-1,2-diol)
EDTA	Ethylenediaminetetraacetic acid
EDTA-BOM	2,2'-((2-((2-(benzyloxy)-1-carboxyethyl)-(carboxymethyl)-amino)-ethyl)-azanediyl)diacetic acid
EDTA-BOM_2	2,2'-(4,9-dicarboxy-1,12-diphenyl-2,11-dioxa-5,8-diazadodecane-5,8-diyl)diacetic acid
EHBG/HBED	N,N'-bis(2-hydroxybenzyl)ethylenediamine-N,N'-diacetate
EHPG	N,N'-ethylenebis-(2-hydroxyphenylglicinate)
FAC	Ferric ammonium citrate
GBCA(s)	Gadolinium-based contrast agent(s)
HA^-/A	Ascorbate anion/Ascorbic acid
HCAT	3,3'-((hexane-1,6-diylbis(azanediyl))bis(methylene))bis(benzene-1,2-diol)
HOPO	Hydroxypyridinone
HSA	Human serum albumin

IS	Inner sphere
MRI	Magnetic resonance imaging
NMR	Nuclear magnetic resonance
NMRD	Nuclear Magnetic Relaxation Dispersion
NOTA	1,4,7-Triazacyclononane-1,4,7-triacetic acid
OS	Outer sphere
PeCAT	3,3'-((pentane-1,5-diylbis(azanediyl))bis(methylene))bis(benzene-1,2-diol)
PipCAT	3,3'-(piperazine-1,4-diylbis(methylene))bis(benzene-1,2-diol)
Poly-β-CD	Poly-β-cyclodextrin
PRE	Paramagnetic relaxation enhancement
PyC3A	2,2'-((2-((carboxymethyl)(pyridin-2-ylmethyl)amino)cyclohexyl)azanediyl)diacetic acid
ROS	Reactive oxygen species
SAL	N,N,N′-Tris[(2-hydroxyphenyl)methyl]ethan-1,2-diamine
SPIO	Superparamagnetic iron oxide
SS	Second sphere
TACN	1,4,7-triazanonane
Tiron®	disodium 4,5-dihydroxy-1,3-benzendisulfonate
USPIO	Ultrasmall superparamagnetic iron oxide
W1/2	Line width at half height of NMR signals

List of symbols

$A_H/\hbar$	Hyperfine coupling constant with hydrogen or Scalar coupling constant
a_{MH}	Distance of closest approach of a water molecule to the metal center in the outer-sphere
$A_O/\hbar$	Hyperfine coupling constant with oxygen
B	Magnetic field
C_{OS}	outer-sphere contribution to the chemical shifts
Δ^2	Mean-squared energy of the zero-field splitting
ΔH_M	Water exchange enthalpy variation
D_{MH}	Translational diffusion coefficient
$\Delta\omega$	Chemical shifts difference
E^0	Reduction potential
$E_{1/2}$	Half-wave reduction potential
E_Δ	Activation energy for the modulation of the static zero-field splitting
E_D	Activation energy of the diffusion
E_R	Activation energy associated with the rotation
E_V	Activation energy of the modulation of the transient zero-field splitting
g	Electron g-factor
γ_I	Nuclear gyromagnetic ratio
γ_S	Electron gyromagnetic ratio
$J(\omega)$	Spectral density function
k_0	Rate of spontaneous dissociation
K_A	Affinity constant
K_D	Dimerization constant

k_d	Pseudo-first-order rate constant
k_{ex}	Water exchange rate
k_{HA}	Rate constant characterizing the ascorbate anion assisted reduction
K_i^H	Protonation constant of the ligand
K_{MHL}	Protonation constant of the complex
K_{ML}	Thermodynamic stability constant
M	Magnetization vector
μ_B	Bohr magneton
μ_{eff}	Magnetic moment
n	Binding sites
p_m	Molar fraction of bound water molecules
q	Number of coordinated water molecule(s)
R_1	Longitudinal relaxation rate
r_1 / r_{1p}	Relaxivity
r_1^b	Relaxivity of the bound chelate
r_1^f	Relaxivity of the free chelate
R_2	Transverse relaxation rate
r_{MH}	Distance between electron and nuclear spins (Metal to hydrogen distance)
S	Electron spin
T_1	Longitudinal relaxation time
$t_{1/2}$	Half-lifetime
T_{1e}	Longitudinal electronic relaxation time
T_{1M}^H	Proton longitudinal relaxation time of inner sphere water molecules
T_2	Transverse relaxation time
T_{2e}	Transverse electronic relaxation time

τ_C	Correlation time
τ_M	Mean residence lifetime of bound water molecule(s)
τ_R	Rotational correlation time
τ_V	Correlation time associated with the modulation of the zero-field splitting
ω_I	Nuclear Larmor frequency
ω_S	Electron Larmor frequency

Contents

1 Introduction

Over the past 40 years, magnetic resonance imaging has experienced exponential growth in the field of diagnostic techniques. This is also due to the use of contrast agents, metal-based probes which are necessary to improve the diagnostic performance of this technique. The compounds used in medicine today are all Gd(III)-based. However, in light of recent concerns about some of these compounds, research has shifted to alternatives. In this dissertation, the case of Fe(III) is discussed. To fully understand this work, this introductory section provides information on MRI, paramagnetic relaxation theory, and a general overview of MRI probes studied in the past. It also describes how this research will be organized. This is the first step in understanding the work that will be proposed in the next chapters.

1.1 Magnetic Resonance Imaging and Contrast Agents

The 1970s and especially the 1980s were the decades of the advent and amazing growth of magnetic resonance imaging (MRI), which quickly became one of the most important techniques for clinical diagnostics and biomedical research. The technique is essentially based on measuring the relaxation times of the hydrogen nuclei of the water molecules inside the organism. The intrinsic contrast, i.e., the discrimination of the different parts of the body, is determined by the difference in the relaxation times (T_1 and/or T_2) of the protons of the water molecules, which depend on the

dynamic properties of the molecule itself. The strength of MRI lies in its ability to obtain high spectral resolution images of virtually the entire human body without ionizing radiations. Furthermore, no substantial negative effects of the magnetic fields and radio waves employed on the human body have been identified. Although this technique offers numerous advantages, there is a strong limitation, namely its sensitivity. To increase the diagnostic value of NMR images, exogenous substances called contrast agents (CA) are usually used. CAs are chemical compounds administered to the patient to increase contrast in the image and to distinguish healthy tissue from diseased tissue. These probes are paramagnetic coordination complexes that can accelerate the process of nuclear relaxation by interacting with water protons, increasing the sensitivity of the technique. Paramagnetic complexes are used because the electronic magnetic moment is 680 times larger than the nuclear moment, which allows an efficient increase in the relaxation rate. Out of the approximately 95 million MRI scans per year that have been performed worldwide in recent years, about 40 percent of these have required the use of a CA. It is obvious, therefore, how important it is to know and study in detail the properties of these metal probes.

A paramagnetic ion is not necessarily able to effectively decrease the relaxation time of interacting nuclei. To achieve a significant increase in the relaxation rate, the unpaired electrons must be isotropically distributed. Therefore, the ion must have an external electronic configuration in which each electron occupies an orbital. Among the various paramagnetic ions studied throughout history, Gd(III) has been the most commonly used, since in this oxidation state it is the element of the periodic table with the highest spin multiplicity (7 unpaired electrons distributed isotropically in the 4*f* orbitals), which is accompanied by a high

magnetic moment (μ_{eff} = 7.94 B.M.) and long electronic relaxation times ($\approx 10^{-9}$ - 10^{-10} s). In addition to choosing the most suitable ion, other aspects such as solubility in water and stability over time must be considered when developing a contrast agent:

- *Effectiveness,* that is, how much a CA increases the relaxation rate of water protons;
- *Distribution in vivo,* because to have diagnostic value, a contrast agent should ideally be in a target tissue or tissue compartment relative to the other body regions;
- *Toxicity and stability*, since it is necessary to prevent the complex from dissolving by releasing the free ion and the ligand;
- *The retention time in the body and metabolism,* because it is necessary to minimize exposure to CA, so as to reduce the possibility of internalization in the cells and ensure efficient excretion.

In the past, more than 800 different Gd(III) complexes have been intensively studied, and some of them are now used in clinical practice. Despite their remarkable properties, there are concerns about the long-term toxicity of some Gd(III) chelates, which has necessitated the search for alternatives based on potentially less toxic paramagnetic metals. In this regard, Fe(III) chelates could be a possible solution. However, the available literature on the use of these probes as T_1-shortening contrast agents is very sparse. In the following sections, we will not only discuss the theory of paramagnetic

relaxation, but also how we intend to lay a solid foundation for the future development of Fe(III)-based MRI probes.

1.2 Paramagnetic relaxation enhancement

In NMR experiments, a nucleus can be investigated only if it has its magnetic moment, which is granted in any system with a total nuclear spin moment $S \neq 0$. When an external magnetic field is applied, these nuclei can align themselves according to the magnetic field or against it, producing two different energetic states. This phenomenon produces a macroscopic magnetization that is assumed to be parallel to the magnetic field across the z-axis. When one or more radio frequency pulses are applied, they can create a controlled disturbance. The natural tendency of the system is to return to the equilibrium state, and this is possible thanks to relaxation. The time function representing the relaxation of the z-component of the magnetization to its equilibrium value depends exponentially on a time constant called T_1, the longitudinal (or spin-lattice) relaxation time, while the time dependence of the perpendicular components is defined by T_2, the transverse (or spin-spin) relaxation time, and is associated with the decay of its value to zero. The relaxation is possible thanks to the interactions of the resonant nucleus with local magnetic fields generated by Brownian motions. In paramagnetic molecules, such as CAs used in MRI, there are also unpaired electrons that affect relaxation. Electron relaxation provides fluctuating magnetic fields that can significantly increase the relaxation rate of water proton nuclei.[1] Nuclear relaxation can arise by contact, if the spin density in the resonant nucleus is referred to, or dipolar, if

electron relaxation is sensed by the resonant nucleus through dipolar coupling. These are also referred to as metal-centered and ligand-centered relaxation. In addition to electron relaxation, other mechanisms can cause relaxation. These mechanisms are sudden and short motions that provide a range of frequencies that can be used by the interacting nuclei to relax, and they are *rotation* and *chemical exchange*. There is also an additional effect, called *Curie spin relaxation*, where the resonating nucleus senses the local magnetic field induced by the electronic magnetic moment. The synergy of these effects enables what is known as *paramagnetic relaxation enhancement* (PRE). As we have already discussed, MRI is based on the different relaxation rates of water proton nuclei in the organism, which naturally behave differently depending on where they are found (e.g. bound to proteins, free...). To improve the sensitivity of MRI scans, the contrast of damaged/diseased tissue can be increased by accelerating the longitudinal and/or transverse relaxation rate of the hydrogen atoms of the water molecules in that tissue. Thanks to the PRE effect, paramagnetic agents can fulfill this requirement. Nevertheless, not all paramagnetic compounds can lead to an effective increase and each complex acts in a different way. It is important to know the relationship between the chemical structure of the probe and the molecular and dynamic parameters that affect relaxation. Only then can their synthesis and design be optimized. The dynamics of these systems can be studied by introducing the correlation function. This is a time function that, in the absence of constraints, can be expressed as: [2]

$$C(t) = \left(\sum_i \frac{1}{4}\right) e^{(-t/\tau_C)} \qquad \text{(Eq.1)}$$

τ_C is known as correlation time and $C(t)$ it is the time constant that decays to zero. By applying the Fourier transform to this function, it becomes a Lorentzian defined in the frequencies domain, also known as *spectral density function*.

$$J(\omega) = \frac{\tau_C}{1 + \omega^2 \tau_C^2} \qquad \text{(Eq.2)}$$

$J(\omega)$ describes the distribution of frequencies useful for inducing relaxation while τ_C is related to the time values associated with the different physical phenomena that can cause relaxation. These are the electronic relaxation correlation times T_{ie}, where i can be 1 or 2, the rotational correlation time τ_R, associated with the rotation of the complex, and the exchange correlation time τ_M, which is the mean residence lifetime of a water molecule bound to the metal center. Each of them can contribute to relaxation, however usually one of them prevails over the other. An additional distinction must also be shown. In dipolar coupling, the correlation time can be expressed as:

$$\left(\frac{1}{\tau_{ci}}\right)^{dip} = \frac{1}{\tau_R} + \frac{1}{\tau_M} + \frac{1}{T_{ie}} \qquad (i = 1,2) \qquad \text{(Eq.3)}$$

In the contact coupling regime, the modulation is only due to chemical exchange and electron relaxation:

$$\left(\frac{1}{\tau_{ci}}\right)^{con} = \frac{1}{\tau_M} + \frac{1}{T_{ie}} \qquad (i = 1,2) \qquad \text{(Eq.4)}$$

These parameters are obtained by studying the dependence of relaxation times on the magnetic field (or Larmor proton frequency) by obtaining dispersion curves. These are called Nuclear Magnetic Relaxation Dispersion (NMRD) profiles. Using a set of suitable equations, these curves can be fitted to obtain such parameters. In the following section, we will explain these equations in more detail along with the concept of relaxivity.

1.3 Relaxivity: background and theory

Although long electron relaxation times and high magnetic moment values are important criteria in choosing the right paramagnetic probe, many other parameters affect PRE. The effectiveness of a CA is indicated by the "relaxivity" (r_1 or $r_{1\rho}$), which is the increase in the longitudinal relaxation rate (R_1) of water proton nuclei normalized to a 1 mM concentration of the paramagnetic ion. In the presence of a paramagnetic species, the observed longitudinal proton relaxation rate (R_1^{obs}) is due to two separate contributions, the diamagnetic term (R_1^d) and the paramagnetic term (R_1^p), the latter being proportional to the concentration of the paramagnetic agent [3]:

$$R_1^{obs} = R_1^d + R_1^p = R_1^d + r_1[CA] \qquad \text{(Eq.5)}$$

Longitudinal relaxivity, r_1, is generally assumed to be the result of the contributions of the inner sphere (r_1^{IS}), the second sphere (r_1^{SS}) and the outer sphere (r_1^{OS}) [4]:

$$r_1 = r_1^{IS} + r_1^{SS} + r_1^{OS} \qquad \text{(Eq.6)}$$

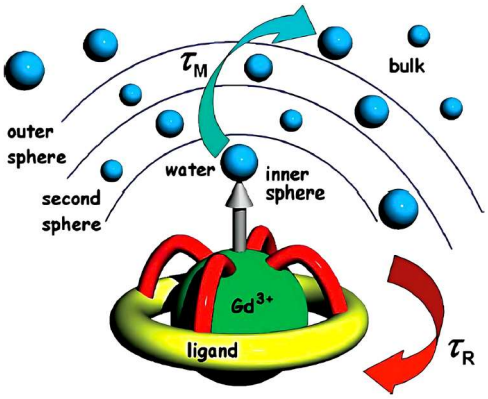

Figure 1. Different contribution to relaxivity in paramagnetic probes.[5]

The outer sphere contribution r_1^{OS} is due to water molecules that diffuse near the paramagnetic complex and arises from the interaction between the nuclear spin of water protons and the electron spin of the paramagnetic ion. This interaction is a long-range coupling that can be described by Freed's model [6]:

$$r_1^{OS} = \frac{32N_A\pi}{405}\left(\frac{\mu_0}{4\pi}\right)^2 \frac{\gamma_S^2\gamma_I^2}{a_{MH}D_{MH}} S(S+1)[3J_{OS}(\omega_I;T_{1e}) + 7J_{OS}(\omega_I;T_{2e})] \quad \text{(Eq.7)}$$

$$J_{OS}(\omega_I;T_{ie}) = Re\left[\frac{1+\frac{1}{4}\left(i\omega\tau_{MH}+\frac{\tau_{MH}}{\tau_{ie}}\right)^{\frac{1}{2}}}{1+\left(i\omega\tau_{MH}+\frac{\tau_{MH}}{\tau_{ie}}\right)^{\frac{1}{2}}+\frac{4}{9}\left(i\omega\tau_{MH}+\frac{\tau_{MH}}{\tau_{ie}}\right)+\frac{1}{9}\left(i\omega\tau_{MH}+\frac{\tau_{MH}}{\tau_{ie}}\right)^{\frac{3}{2}}}\right] \quad \text{(Eq.8)}$$

$$\tau_{MH} = \frac{a_{MH}^2}{D_{MH}} \quad \text{(Eq.9)}$$

Where a_{MH} is the distance of closest approach of a water molecule to the metal center in the outer-sphere, D_{MH} is the relative translational diffusion coefficient (calculated as sum of the self-diffusion coefficients of water molecules and the metal complex), S is the electron spin, γ_S and γ_I are respectively the electron and nuclear gyromagnetic ratios and T_{1e} and T_{2e} are the longitudinal and

transverse electron relaxation times. These are usually approximated as:

$$\frac{1}{T_{1e}} = \frac{1}{25}\Delta^2\tau_V\{4S(S+1)-3\}\left(\frac{1}{1+\omega_S^2\tau_V^2}+\frac{4}{1+4\omega_S^2\tau_V^2}\right) \quad \text{(Eq.10)}$$

$$\frac{1}{T_{2e}} = \frac{1}{50}\Delta^2\tau_V\{4S(S+1)-3\}\left(\frac{5}{1+\omega_S^2\tau_V^2}+\frac{2}{1+4\omega_S^2\tau_V^2}+3\right) \quad \text{(Eq.11)}$$

In Eq.10 and 11, τ_V is the correlation time associated with the modulation of the zero-field-splitting (ZFS) interaction, Δ^2 is the mean-square energy of the ZFS and ω_S is the electron Larmor frequency.[7]

The second sphere contribution r_1^{SS} arises from water molecules hydrogen-bonded to polar groups on the ligand molecules.[8] This contribution is detectable only if the mean residence time of a water molecule in the second shell is long enough to allow relaxation, and this could be the case if it is longer than the value of self-diffusion of the solvent molecules. There are cases where this influence is significant, as in the case of Gd(III)-DO3A-NP2.[8]

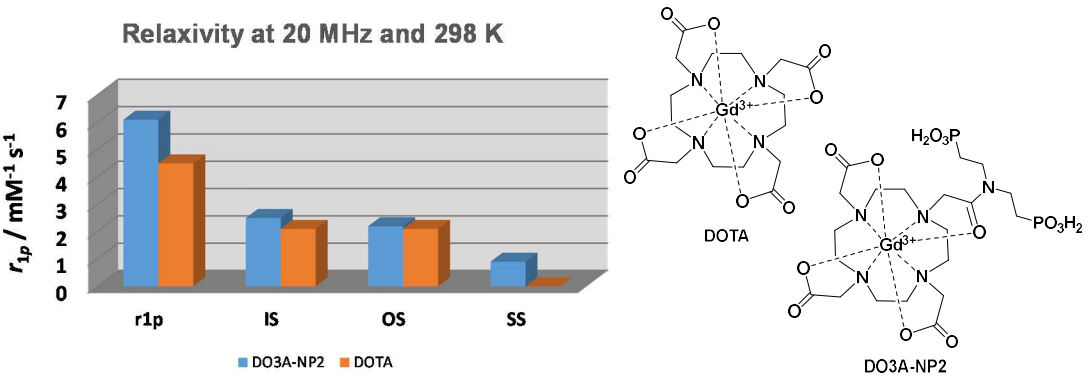

Figure 2. Relaxivity contributions for Gd(III)-DOTA and Gd(III)-DO3A-NP2.[8]

In Fig. 2 the two complexes show comparable values for r_1^{IS} and r_1^{OS}, however the total relaxivity for Gd(III)-DO3A-NP2 is much higher. The presence of a second shell of water molecules, which arise from the interaction with the $-PO_3H_2$ groups, determines a higher relaxivity value.

Finally, the inner sphere contribution r_1^{IS} to the total relaxivity is given by the following equation:

$$r_1^{IS} = \frac{1}{1000} \times \frac{q}{55.55} \times \frac{1}{T_{1m}^H + \tau_M} \qquad \text{(Eq.12)}$$

Here q stands for the number of coordinated water molecules, τ_M is the mean residence lifetime of a water molecule in the inner coordination sphere, and T_{1m}^H is the proton longitudinal relaxation time of inner sphere water molecules. The proton relaxation mechanism is determined by a dipole-dipole interaction (DD), which depends on the magnetic field, and by a scalar or contact contribution (SC). The latter contribution is, with some exceptions, generally negligible in the study of longitudinal relaxation. T_{1m}^H is defined by the Solomon-Bloembergen-Morgan equations [9-12]:

$$\left(\frac{1}{T_{1m}^H}\right)^{DD} = \frac{2}{15}\left(\frac{\mu_0}{4\pi}\right)^2 \frac{\gamma_I^2 g^2 \mu_B^2}{r_{M-H}^6} S(S+1) \times \left[\frac{3\tau_{d1}}{1+\omega_I^2\tau_{d1}^2} + \frac{7\tau_{d2}}{1+\omega_S^2\tau_{d2}^2}\right] \qquad \text{(Eq.13)}$$

$$\left(\frac{1}{T_{1m}^H}\right)^{SC} = \frac{2}{3} S(S+1) \left(\frac{A_H}{\hbar}\right)^2 \frac{\tau_{e2}}{1+\omega^2\tau_{e2}^2} \qquad \text{(Eq.14)}$$

$$\frac{1}{\tau_{di}} = \frac{1}{\tau_M} + \frac{1}{\tau_R} + \frac{1}{T_{ie}} \qquad i = 1,2 \qquad \text{(Eq.15)}$$

$$\frac{1}{\tau_{e2}} = \frac{1}{\tau_M} + \frac{1}{T_{2e}} \qquad \text{(Eq.16)}$$

In these equations, μ_B is the Bohr magneton, g is the electron g factor, r_{M-H} is the metal to hydrogen distance and $A_H/\hbar$ is the scalar coupling constant.

The following section will address how inner sphere relaxivity is influenced by the different mentioned parameters.

i) Hydration number (q)

As can be seen in Eq. 12, r_1^{IS} is directly proportional to the number of coordinated water molecules (q). However, if an attempt is made to increase the number of bound water molecules by decreasing the denticity of the ligand, the thermodynamic stability of the complex is lowered. It is also important to note that because of the many different parameters that can affect relaxivity, the NMRD profiles of systems with different q values are not correlated by a simple scalar factor.

ii) Electronic relaxation

Empirically, this parameter is related to the symmetry and stereochemical rigidity of the coordination cage,[13] for which labile and/or low-symmetry complexes are characterized by higher Δ^2 values and therefore by lower relaxivity values at low magnetic fields.

iii) Rotational correlation time (τ_R)

The contribution of the rotational correlation time is generally only appreciable at high magnetic field values (≥ 20 MHz). An increase in τ_R is generally associated with an increase in relaxivity. τ_R is inversely proportional to temperature and directly proportional to the molecular weight of the complex. This means that it is possible to design complexes with a higher molecular weight to achieve an increase in the relaxation rates of the water proton nuclei.

iv) Water exchange rate (k_{ex})

The water exchange rate $k_{ex}\,(=1/\tau_M)$, as well as the rotational correlation time, mainly affect the high-field region of the NMRD profiles. Normally, systems characterized by fast rotation and low molecular weight are not particularly affected by the water exchange rate. This is related to the relative weights of the terms in Eq. 12. However, the value of the mean residence time must be treated carefully. An excessively slow exchange brings the term $\frac{1}{T_{1m}^{H}+\tau_M}$ in Eq. 12 close to zero, which translates into a decrease in relaxivity. Moreover, too fast an exchange would prevail over the terms included in the correlation time, which would have the same effect. In general, the optimal values of τ_M are between 10^{-7}-10^{-8} s.

In the case of Gd(III) and Mn(II) complexes, the effect that each of these parameters has on water proton relaxation is well known. This is not true for Fe(III) complexes. In fact, the available literature is very sparse and fragmentary. One of the objectives of this thesis is to investigate these aspects in detail in order to address the optimal way to develop new Fe(III)-based MRI probes.

1.4 Paramagnetic probes in MRI

Like platinum in cancer therapy and technetium in nuclear medicine studies, the unique magnetic properties of the Gd(III) ion have placed it at the center of medicine's revolutionary growth in the field of MRI. Being a paramagnetic ion, in solution it causes a considerable increase in the relaxation rate of the protons of the water molecules with which the paramagnetic species interacts, thanks to the fluctuation time of the dipolar coupling between the electronic magnetic moment of the metal ion and the nuclear magnetic moment of solvent nuclei. In the +3 oxidation state, its external electronic configuration is $4f^7$, and the seven unpaired electrons (S = 7/2) guarantee a high effective magnetic moment (μ_{eff}=7.94 B.M.). Despite its remarkable properties, the ion has a high toxicity (LD_{50} $GdCl_3 \cdot 6H_2O$ = 0.3-0.5 mmol/kg in rats), since it does not perform physiological functions in mammals and, even at very low doses (10-20 μmol/kg), it can cause the precipitation of nucleic acids in vitro or antagonize Ca^{2+} ions. The main strategy to exploit Gd(III) in diagnostics is to form stable complexes with suitable ligands. The use of a chelator allows to lower the toxicity of the metal ion, making its pharmaceutical use possible (for example, Gd(III)-DTPA has an LD_{50} of 10 mmol/kg). A great advantage of this element is the high coordination number (C.N. = 8 – 9), which provides complexes with high thermodynamic stability.[14] All the FDA-approved Gadolinium-based contrast agents (GBCAs, Figure 3) are nona-coordinated complexes, where eight positions are occupied by the ligand and a molecule of water binds in the ninth site. GBCAs are generally polyaminocarboxylates complexes with extremely high thermodynamic stability ($\log K_{GdL} \approx 22$ - 26) and kinetic inertia, which

guarantees their safety at the recommended dosage, with an excellent effect in accelerating the relaxation times of water protons.

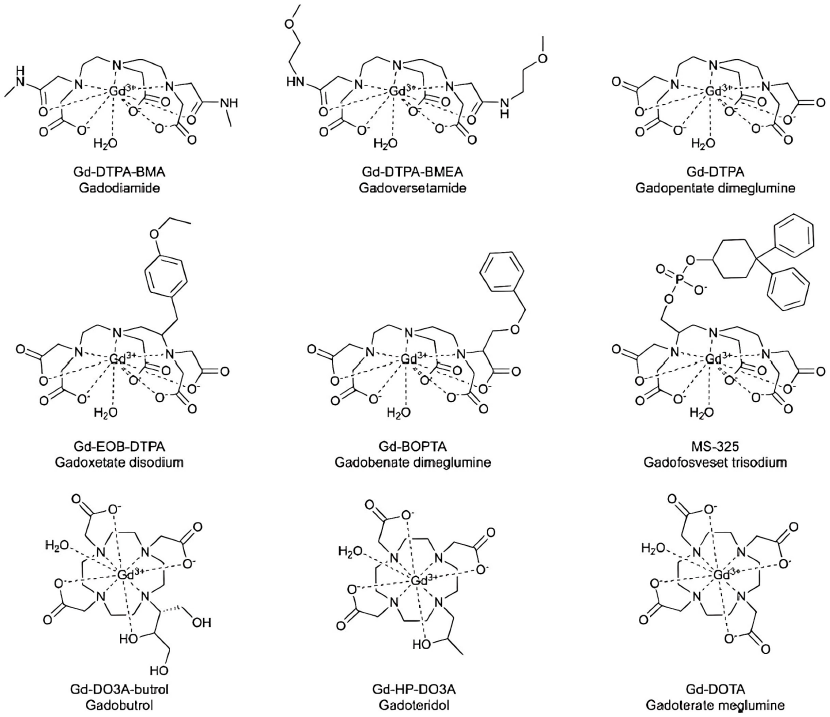

Figure 3. Structures and commercial names of Gadolinium-based contrast agents.[15]

The first approved contrast agent for clinical practice was Gd(III)-DTPA (Magnevist®, Schering), used for more than twenty million patients over ten years. With the aim of improving the properties of a contrast agent, a wide range of gadolinium-based agents have been developed, and some of them have found use in clinical analysis: Gd(III)-DOTA (Dotarem®, Guerbet), Gd(III)-DTPA-BMA (Omniscan®, Nycomed), Gd(III)-HPDO3A (Prohance®, Bracco) used for example to identify lesions of the blood-brain barrier, Gd(III)-EOB-DTPA (Eovist®, Schering) and Gd(III)-BOPTA (Multihance®, Bracco) particularly

suitable for imaging the liver. In addition to these systems, there are also studies on higher molecular weight complexes like covalent adducts between Gd(III)-DTPA and some macromolecular systems such as albumin, dextran, liposomes, dendrimer systems or oligopeptides (to obtain agents with improved efficacy and modified distribution). GBCAs have been shown to be essential for magnetic resonance imaging and they are considered safe and effective. They have an excellent toxicity profile and are considered to be among the safest pharmaceuticals. In facts, the rate of immediate adverse events is very low (<1 per thousand injections) and usually mild and severe adverse events occur at about once per 40000 injections.[16] However, despite all advances accomplished with GBCA-enhanced MRI, there is concern about the long-term safety of some of these agents. Over the last decade these concerns have increased, starting from 2006, when the use of GBCAs was connected to the development of the nephrogenic systemic fibrosis (NSF), although initially it was detectable only in patients with impaired renal function.[17,18] Unfortunately, these concerns grew firstly in 2016, when NSF was detected in four patients with normal renal function and moreover, reports have also shown (in patients that underwent multiple MRI scans with contrast) the presence of intact gadolinium complexes accumulations in the central nervous system as well as in skin and bones. [19-22] The long-term effect of these deposits is still unknown, therefore it is not clear if the complex remains intact, if it binds to macromolecular systems such as proteins or if it can release Gd(III) and the free ligand (Fig.4).

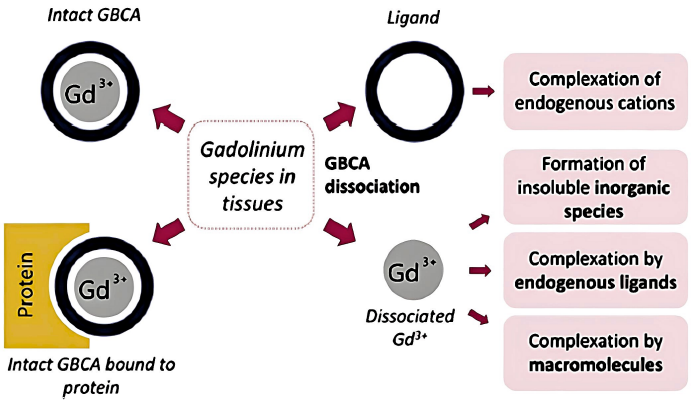

Figure 4. The possible pathways that tissue accumulations of gadolinium complexes can follow.[15]

Accordingly, there is a potential clinical need for alternative that can replace gadolinium-based chelates as T_1-shortening contrast agents. Finding new candidates could be challenging, since there are not many elements that have both efficient magnetic properties and high biocompatibility. The research therefore turned in parallel towards the study of the *d*-block elements. In particular, it was focused on endogenous elements that could meet the requirements to become MRI probes. Fe(III)- and Mn(II)-based contrast agents may represent viable alternatives for contrast enhancement at T_1-weighted MRI. Manganese is an endogenous ion and living organisms are able to tolerate small excesses in organs and tissues. Biologically, it is an essential element. In serum it must have a concentration between 0.5 - 1.2 μg/L. It also plays a role in a number of enzymatic processes acting as a cofactor, as in manganese superoxide dismutase. Despite being more tolerable than Gd(III) (LD_{50} $MnCl_2$ = 2 mmol/kg in rats), in high quantities it has a neurotoxic effect, also associated with "manganism", a pathology with characteristics and symptoms similar to Parkinson's disease.

High-spin Mn(II) (S = 5/2) has a good magnetic moment (μ_{eff} = 5.94 B.M.) and long electronic relaxation times ($\approx 10^{-8}$-10^{-10} s, compared to 10^{-9}-10^{-10} s for Gd(III)). The quantification of the increase in the relaxation rate of the water proton nuclei can be easily performed by studying the NMRD profile of the aquaions. The NMRD profiles comparison between the $[Mn(H_2O)_6]^{2+}$ and $[Gd(H_2O)_8]^{3+}$ immediately displays the effective potential of manganese.

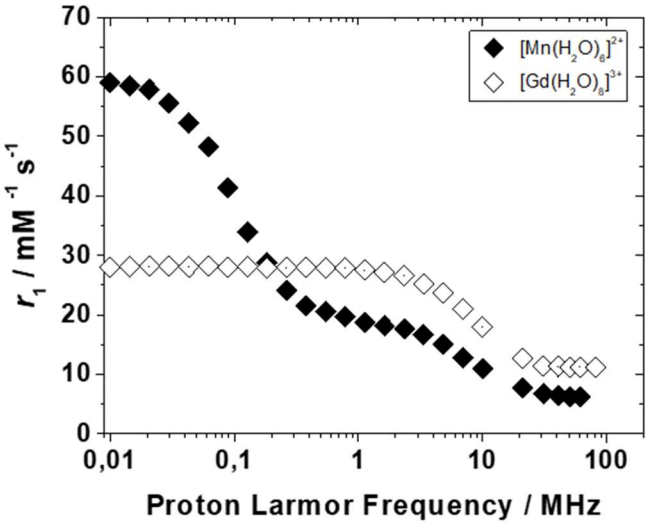

Figure 5. ^{1}H NMRD profiles of $[Mn(H_2O)_6]^{2+}$ ($[Mn^{2+}]$=3.85 mM, pH=3.94) and $[Gd(H_2O)_8]^{3+}$ ($[Gd^{3+}]$=3.28 mM, pH=4.05) measured at 25 °C.

As one would expect, at proton Larmor frequencies higher than 1 MHz, the r_1 of the hydrated Mn(II) is lower than that of the $[Gd(H_2O)_8]^{3+}$. Different aspects would play against Mn(II) and these can be derived from the equations reported above: the lower spin of manganese, since any contribution that depends on the term S(S+1) should be 1.8 times less than Gd(III), the magnetic moment (5.94 B.M. vs. 7.94 B.M. for Gd(III)), the lower hydration number, since inner

sphere relaxivity is directly proportional to the number of bound water molecules, and the lower molecular weight, which translates in a lower rotational correlation time. Nevertheless, the relaxivity values for Mn(II) are very interesting (r_1 at 20 MHz and 298 K for $[Mn(H_2O)_6]^{2+}$ is 7.7 mM^{-1} s^{-1}, for $[Gd(H_2O)_8]^{3+}$ is 12.7 mM^{-1} s^{-1}) thanks to a lower metal-hydrogen distance (r_{MnH} = 2.83 Å vs. r_{GdH} = 3.1 Å), from which the inner sphere relaxivity depends on the sixth power, but that still does not allow to totally compensate the other effects. At low magnetic fields the relaxivity for Mn(II) is much higher thanks to the presence of a scalar contribution. This term is usually negligible for Mn(II) complexes other than the aquaion, but its importance is minor since the range of proton Larmor frequencies at which it generally occurs is far from the magnetic fields used in the clinical setting. Low molecular weight Mn(II) complexes, which have been largely studied over the last two decades,[23] have generally lower values of relaxivity than the gadolinium counterparts and this is due to the lower number of unpaired electrons. Most of Mn(II) complexes have rather fast water exchange rates, so it is usually not a limiting factor for relaxivity, and the possible approach to improve the performance of such compounds is to increase the rotational correlation time. *In vivo* applications require a detailed study of the system's kinetics and thermodynamic stability. Compared to gadolinium complexes, the thermodynamic stability of manganese compounds is lower, due to the lower charge and the absence of the stabilizing energy of the ligand field associated with the high spin d^5 electronic configuration. As regards the kinetic inertia, the rates of the transmetallation reactions with endogenous ions such as Ca(II), Zn(II) and Cu(II) and proton-assisted dissociations are crucial because these lead to the

dissociation of the complex, thus releasing Mn(II). In the pharmaceutical field, only two Mn(II)-based contrast agents have been clinically approved: liver-specific Mn-DPDP (DPDP = Dipyridoxaldiphosphate, Teslascan®), and an oral contrast agent containing manganese(II) chloride (LumenHance®), however both did not find commercial success and have been removed from the market. The directives for the production of new drugs focus on the search for new manganese-based compounds, both in the form of biocompatible complexes, and in the form of organic and inorganic nanoparticles. While for manganese(II) a large and in-depth study has been carried out over the last 20-30 years,[23] the same cannot be said for iron(III). To be precise, the main iron(III)-containing compounds used as contrast agents are called superparamagnetic contrast agents. They consist of a colloidal suspension of iron oxide nanoparticles. When used in MRI, they reduce the intensity of T_2 signals in the tissues where they accumulate (they are also called "negative" contrast agents). As we will show in Chapter 2, there is no such an extensive literature on Fe(III) chelates, especially used as positive contrast agents. A detailed study of the intrinsic properties of the ion and its complexes is crucial to fully understand the behavior of this element. Therefore, as part of a long-term project aimed to explore new iron(III) chelates as MRI probes, with this dissertation we want to provide all the information that is still missing. The cornerstone of this research will be to understand the relationship between all the parameters we have seen so far and the molecular structure of these complexes. This is the starting point that will allow us to optimize the chemical structure to obtain the desired properties. To this end, we have decided to apply a multi-technical approach.

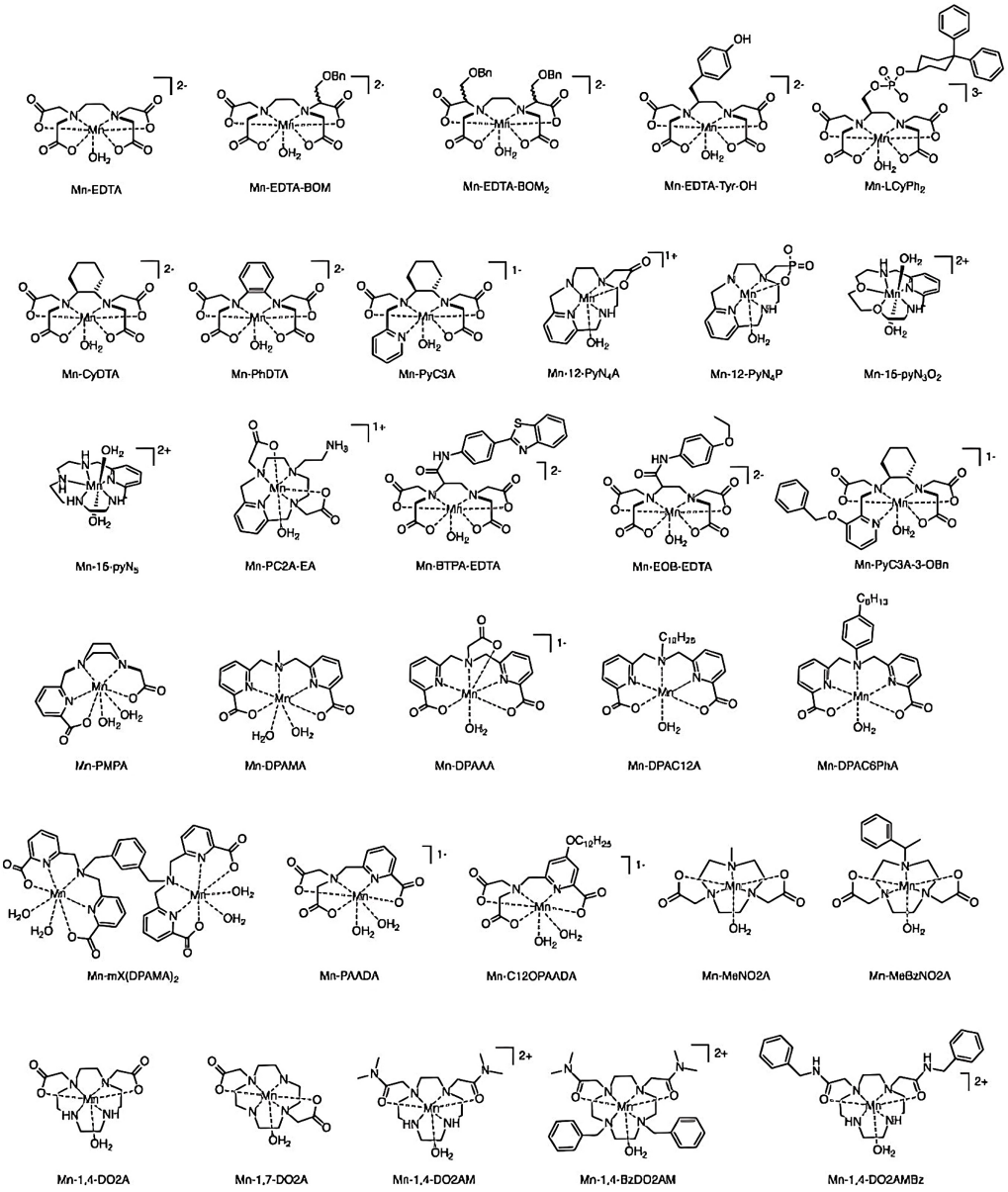

Figure 5. Representative examples of Mn^{2+} complexes considered as T_1 relaxation agents.[24]

For a meaningful design of MRI probes, it is essential to analyze the structural and dynamic aspects of these complexes and their interaction with water. Unfortunately, due to the properties of these complexes, it is not possible to fully determine these aspects using NMR analysis and/or other routine analyzes. Instead, this can be done by studying the relaxation rates as a function of the applied magnetic field: the technique that allows this type of measurement is called **relaxometry**. As described by Koenig and Brown,[25] " *"relaxometry" is a relatively new word to indicate a long-established activity: the measurement of the magnetic relaxation rates of solvent nuclei in aqueous systems to explore the nature of solutes*". Since its first applications in the 1950s, the use of this technique has led to improvements in theory and greater clarity of the relaxation mechanisms. In this work, a detailed study of the relaxometric properties of various Fe(III) complexes has been carried out, starting with the hexaaquairon(III), by measuring ^{1}H longitudinal relaxation data from 0.01 to 500 MHz and ^{17}O transverse relaxation rates (R_2) and shift ($\Delta\omega$) at 11.7 T as a function of temperature.[8] The availability of (i) a wider range of magnetic fields, (ii) relaxation data as a function of temperature, and (iii) ^{17}O displacement and relaxation data measured at high magnetic field strength allows us to obtain very accurate values of the structural and dynamic parameters that adequately describe the behavior of paramagnetic complexes in aqueous solution.[26] These measurements will be complemented by DFT calculations, cyclic voltammetry, UV-Vis spectrophotometry and potentiometry, which are essential to be able to support our data but also asses properties such as the redox behaviour, the thermodynamic stability and the kinetic inertness of such complexes.

1.5 Notes and References

(1) Bertini, I.; Luchinat, C.; Parigi, G.; Ravera, E. *Elsevier*, **2017,** 77–126.

(2) Stokes G. *Trans. Cambridge Philos. Soc*. **1956**, 9,5.

(3) Kim, W. D.; Kiefer, G. E.; Maton, F.; McMillan, K.; Muller, R. N.; Sherry, A. D. *Inorg. Chem.* **1995**, 34, 8, 2233-2243

(4) Caravan, P.; Farrar, C. T.; Frullano, L.; Uppal, R. *Contrast Media Mol. Imaging* **2009**, 4 (2), 89–100.

(5) Hermann, P.; Kotek, J.; Kubíček, V.; Lukeš, I. *Dalton Trans.* **2008**, 23, 3027–3047.

(6) Freed, J. H. *J. Chem. Phys*. **1978**, 68 (9), 4034–4037.

(7) McLachlan, A. D.; Longuet-Higgins, H. C. *Proc. R. Soc. Lond. Ser. Math. Phys. Sci.* **1964**, 280 (1381), 271–288.

(8) Aime S., Botta M., Terreno E. *Adv. Inorg. Chem*. **2005**, 57, 173–237.

(9) Solomon, I. *Phys. Rev.* **1955**, 99 (2), 559–565.

(10) Solomon, I.; Bloembergen, N. *J. Chem. Phys.* **1956**, 25 (2), 261–266.

(11) Bloembergen, N. *J. Chem. Phys.* **1957**, 27 (2), 572–573.

(12) Bloembergen, N.; Morgan, L. O. *J. Chem. Phys.* **1961**, 34 (3), 842–850.

(13) Borel, A.; Kang, H.; Gateau, C.; Mazzanti, M.; Clarkson, R. B.; Belford, R. L. *J. Phys. Chem. A* **2006**, 110 (45), 12434–12438.

(14) Powell, D.H.; Ni Dhubhghaill, O. M.; Pubanz, D.; Helm, L.; Lebedev, Y. S.; Schlaepfer, W.; Merbach, A. E. *J. Am. Chem. Soc.* **1996**, 118, 9333-9346.

(15) Le Fur, M.; Caravan, P. *Metallomics,* **2019**, 11 (2), 240–254.

(16) Prince, M. R.; Zhang, H.; Zou, Z.; Staron, R. B.; Brill, P. W. *AJR Am. J. Roentgenol.* **2011**, 196 (2), W138-143.

(17) Grobner, T. *Nephrol. Dial. Transplant.* **2006**, 21 (4), 1104–1108.

(18) Centers for Disease Control and Prevention (CDC). St. Louis, Missouri, 2002-2006. *MMWR Morb. Mortal. Wkly. Rep.* **2007**, 56 (7), 137–141.

(19) European Medicines Agency, Https://Www.Ema.Europa. Eu/Documents/Press-Release/Emas-Final-Opinion-Confirmsrestrictions-Use-Linear-Gadolinium-Agents-Body-Scans_en.Pdf, 2017, EMA/457616/2017.

(20) Kanda, T.; Ishii, K.; Kawaguchi, H.; Kitajima, K.; Takenaka, D. *Radiology*, **2013**, 270 (3), 834-841.

(21) McDonald, R. J.; McDonald, J. S.; Kallmes, D. F.; Jentoft, M. E.; Murray, D. L.; Thielen, K. R.; Williamson, E. E.; Eckel, L. J. *Radiology,* **2015**, 275 (3), 772–782.

(22) Roberts, D. R.; Lindhorst, S. M.; Welsh, C. T.; Maravilla, K. R.; Herring, M. N.; Braun, K. A.; Thiers, B. H.; Davis, W. C. *Invest. Radiol.* **2016**, 51 (5), 280–289.

(23) Botta, M.; Carniato, F.; Esteban-Gómez, D.; Platas-Iglesias, C.; Tei, L. *Future Med. Chem.* **2019**, 11 (12), 1461–1483.

(24) Gupta, A.; Caravan, P.; Price, W. S.; Platas-Iglesias, C; Gale, E. M. *Inorg. Chem.* **2020**, 59, 6648 – 6678

(25) Koenig, S. H.; Brown, R. D., *Prog. Nucl. Magn. Reson. Spectrosc.* **1990**, 22 (6), 487–567.

(26) Aime, S.; Botta, M.; Esteban-Gómez, D.; Platas-Iglesias, C. *Mol. Phys.* **2019**, 117 (7–8), 898–909.

2 Fe(III)-based probes in MRI

Gd(III), high-spin Mn(II) and high-spin Fe(III) were the main metal ions investigated for use as contrast agents for MRI. Despite the efficacy of Gd(III) complexes, current concerns about Gd(III) retention in the body have rekindled interest in Mn(II) and Fe(III) as alternatives. High-spin Fe(III) complexes were developed in the early days of MRI contrast agents, but progress has slowed in recent years. In this chapter we will review some different types of Fe(III) complexes that have been studied as potential MRI probes.

2.1 An overview on Fe(III) complexes as MRI probes

In order to understand why Fe(III) is a potential candidate for the synthesis of new MRI probes, it is necessary to analyse in detail its biochemical role along with its chemical, physical, and magnetic properties. We have already discussed in the previous chapter the characteristics that a metal ion must have to be suitable. Thus, the high-spin Fe(III) that has a d^5 external electronic configuration (S = 5/2), satisfies the requirement of having an excellent magnetic moment (5.92 B.M.). In addition, although its electronic relaxation times are shorter than Gd(III) and Mn(II) ($\approx 10^{-9}$-10^{-11} s), they still remain compatible with the technique. The main advantage of using Fe(III) is that it is an endogenous ion whose biochemistry within the body has been extensively studied. On a biological level it is, among the various

paramagnetic metals, the most tolerated by living organisms. The concentration of iron normally present in the body is about 1 mmol/kg (LD_{50} = 30 mg/kg in rats) and is mainly localized in red blood cells, muscles, endothelial reticulum and can be incorporated into various types of proteins: functional (haemoglobin, myoglobin and some enzymes), storage (ferritin and hemosiderin), and transport (transferrin). Although the short-term toxicity of iron(III) is comparable to that of gadolinium(III), the long-term toxicity should be lower, thanks to the presence of these Fe(III)-specific proteins.

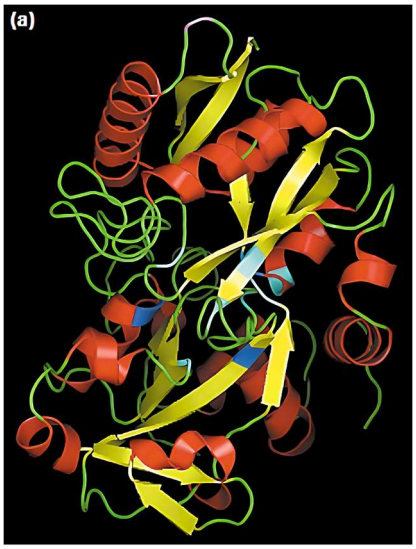

Figure 1. Structure of Transferrin.[1]

A common problem for humans is iron deficiency, which leads to anaemia. The daily intake of iron is 7 mg for men and 11 mg for women, both quantities that can be taken with a normal diet. Like any other metal ions, it can be administered only as a stable coordination complex. The iron-containing compounds that have been used as contrast agents are called superparamagnetic contrast agents. They consist of a colloidal suspension of ferric oxide nanoparticles.[2] When

used in MRI, they reduce the intensity of T_2 signals in the tissues in which they accumulate (they are also called "negative" contrast agents). There are two major categories of these compounds: superparamagnetic iron oxide (SPIO[3]) and ultrasmall superparamagnetic iron oxide (USPIO[4]). Two decades ago, SPIO was the first nanoparticle MRI contrast agent used as a liver contrast agent. SPIO and USPIO compounds such as Feridex I.V. ®, Resovist®, Sinerem® and Clariscan® have been clinically approved in the past, however they are now almost all removed from the market, with the exception of Lumirem®/GastroMARk® (oral contrast agent). The nanometric dimensions and the shape of the particles of this class of agents allow a different biodistribution and different applications. Even though iron has found some temporarily application as negative contrast agent, the use of colloidal suspensions can easily encounter difficulties in the pharmacological field. In addition, the images obtained according to negative contrast turn out to be diagnostically less effective and more difficult to interpret. The ability to seek a new viable alternative to commercially available drugs can be undertaken as the new challenge in this area. While gadolinium and manganese have been mainly used as T_1-shortening MRI probes, the literature on iron as a positive contrast agent is relatively less extensive.

One of the main problems in the research of new iron(III) based MRI probes is related to its quite complex solution chemistry. In the case of gadolinium, as previously reported, the most typical approach is to use an octa-dentate ligand capable of producing a very stable complex, leaving a free coordination site for a water molecule. This approach becomes more difficult for iron: a hexa-dentate ligand should be used so as to be able to leave the seventh position free for

a molecule of water, but the thermodynamic stability of the complex is impaired. Furthermore, the main toxicity effect that iron can manifest is connected to its redox activity and the consequent formation of reactive oxygen species (ROS) according to the following mechanism, also known as *Fenton's reaction*.

$$Fe^{3+} + O_2^{\cdot-} \longrightarrow Fe^{2+} + O_2$$

$$Fe^{2+} + H_2O_2 \longrightarrow Fe^{3+} + OH^- + OH^{\cdot}$$

Scheme 1. Fenton's reaction

Although it was demonstrated how the direct coordination of oxygen in the free site doesn't necessarily lead to the formation of ROS,[5] any model of this type needs to be accurately studied in this respect. In addition, interaction with organic substrates in the body, such as ascorbic acid (≈ 43 μM in human plasma), must also be considered, as its reducing character facilitates the Fenton reaction.[6]

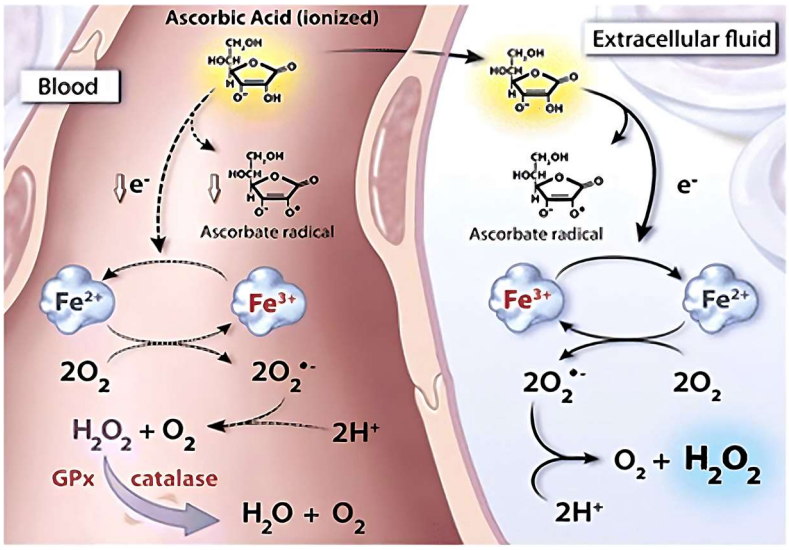

Figure 2. Interaction of ascorbic acid with Fe(III).[7]

As reported in literature,[8] the affinity of Fe(III) with amino ligands is very low. Complexes based on simple amines do not exist in aqueous solution, for example the addition of ammonia to solutions containing the ferric ion only promotes its precipitation, due to the increase in the basicity of the system. The hard nature of the ferric ion suggests a better interaction with ligands containing oxygen-based electron donor groups. One of the examples of complex that have found insights in the field of MRI probes is the ferric ammonium citrate (or FAC). This complex showed a relaxivity at 16 MHz and 37 °C of 1.60 mM^{-1} s^{-1} and it was the major component of two different drugs: Geritol®, which however didn't find success since the drug contained 12% of ethanol, and FerriSeltz®, a mixture of FAC, tartaric acid, sodium bicarbonate, aspartame and different flavours. The latter passed phase II and III trials in the U.S. and it was indicated as a valid bowel contrast agent with just minor side effect.[9-11]

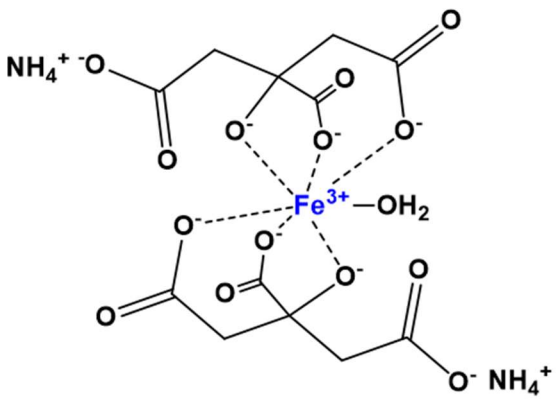

Figure 3. Structure of FAC.

Chelating ligands with both amino and oxygen groups, such as EDTA or CDTA, are able to complex the ion. Both ligands are capable of

forming heptacoordinate chelates, in which the seventh coordination site is occupied by a water molecule.

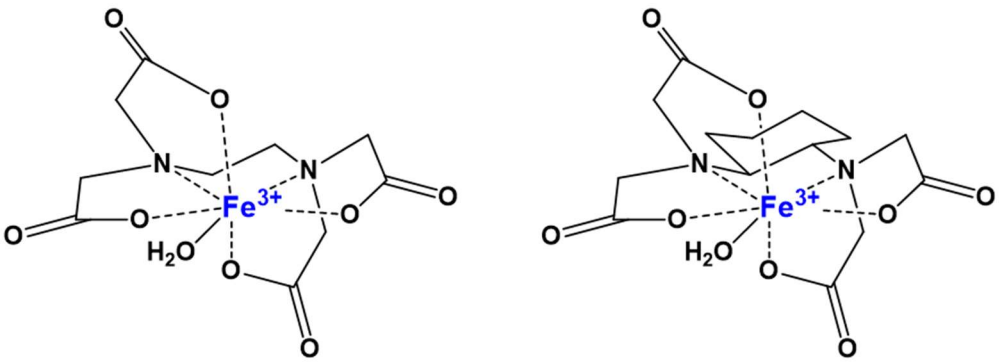

Figure 4. Structures of $[Fe(EDTA)]^-$ (left) and $[Fe(CDTA)]^-$ (right).

These complexes have been studied extensively in the past, structurally[12,13] and in terms of thermodynamic stability[14] (for $[Fe(EDTA)]^-$ $\log K$ = 25.5, for $[Fe(CDTA)]^-$ $\log K$ = 27.5). In this thesis, the relaxometric profiles of these two complexes will be later explored. The $[Fe(EDTA)]^-$ complex cannot be administered directly, as at physiological pH values the coordinated water molecule transforms into a hydroxyl group,[15] which leads to a sudden drop in relaxivity. $[Fe(CDTA)]^-$ was studied and evaluated by Boehm-Sturm *et al.*,[16] although the analysis shows that even if the complex has an interesting contrast enhancement effect (r_{1p} is 2.2 mM^{-1} s^{-1} at 40 MHz and room temperature), it is also true that the quantity required compared to the Gd(III) counterparts is greater, which is something that generally must be avoided for the patient's safety. Polyaminocarboxylates are the most studied type of ligand for paramagnetic ions in MRI, especially because they show relatively high stability constants, and with iron(III) there are reported values of $\log K$ between 25 and 40.[17] One of the first compounds in this

category that has been studied as an hepatobiliary agent was the iron(III) N,N'-ethylenebis-(2-hydroxyphenylglicinate) or $[Fe(EHPG)]^-$ (Fig. 5).[18]

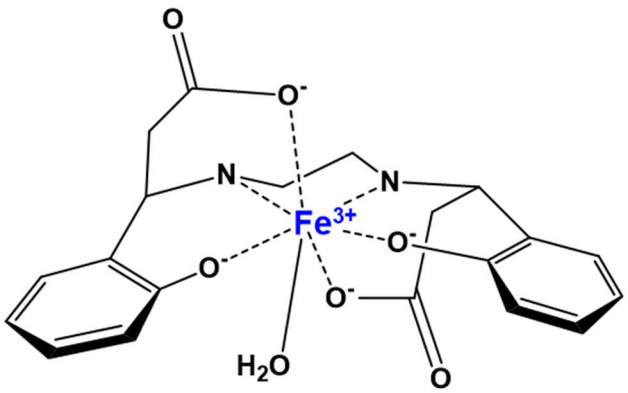

Figure 5. Structure of $[Fe(EHPG)]^-$.

The ligand EHPG can be found in plants, so it has a natural origin.[19] It exists in two different isomers (*rac*-EHPG and *meso*-EHPG), which differentiate in both stability constants (for *rac*-EHPG log*K* = 35.45, while for *meso*-EHPG log*K* = 33.28[20]) and affinities to human serum albumin.[21] It was also reported that they have different biodistribution *in vivo*.[20] Nonetheless, this compound was tested on animals and it produced a good enhancement in a T_1-weighted image.[22] The r_1 value of the mixture of the stereoisomers at 10.7 MHz is 0.9 mM^{-1} s^{-1} but, thanks to the dependence of the relaxivity on the magnetic field which, in the case of iron(III) tends to increase as the strength of the field increases, at 300 MHz and 37 °C r_1 is 1.3 mM^{-1} s^{-1}.[21] This complex has a reported LD_{50} in mice between 3.4 and 8.0 mmol kg^{-1}.[23,24]

Starting from $[Fe(EHPG)]^-$, there have been studies about several derivatives to understand how changing the nature of the ligand could affect the interaction between the metal ion and the water

molecules.[25] For instance the bromine-substituted complex, the Fe-5-Br-EHPG, which again showed different properties between the two stereoisomers *rac* and *meso* (at 20 MHz and 37 °C, 0.84 mM^{-1} s^{-1} for *rac*-Fe-5-Br-EHPG and 1.03 $mM^{-1}s^{-1}$ for *meso*-Fe-5-Br-EHPG), or the ethyl-substituted complex, which provided an r_1 value of 0.96 $mM^{-1}s^{-1}$.[26,27] Nonetheless, their Gd(III)-based counterparts still showed better enhancement. The structure of the EHPG ligand was therefore studied and modified, which led to the N,N'-bis(2-hydroxybenzyl)ethylenediamine-N,N'-diacetate, better known as HBED or EHBG (Fig. 6)

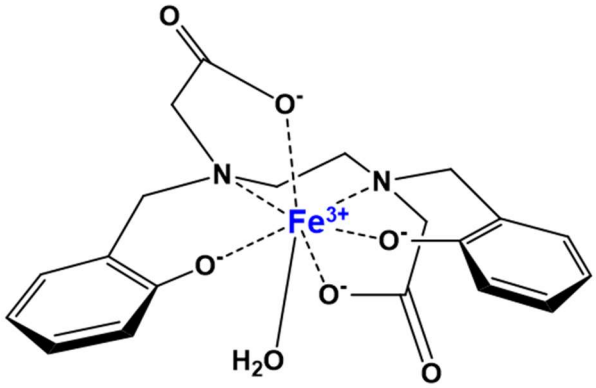

Figure 6. Structure of $[Fe(HBED)]^-$.

The main differences of the HBED ligand are the lack of stereocenters and the higher stability of the iron(III) complex, with a log*K* of 39.68 but, even though it has a slightly higher relaxivity (1.1 mM^{-1} s^{-1} at 10.7 MHz and 37 °C), it has been reported its higher toxicity, with an LD_{50} in mice of 2.0 mmol kg^{-1}.[22,28] Once again the structure has been opportunely modified, with the introduction of hydrogen-bonding groups (-OMe or -NHAc), or lipophilic groups (-Me_2 or -Ph).[29] These complexes showed good relaxivity, high stability and no redox activity. An interesting work has recently been published on the study of

analogues of FeHBED.[30] The structures shown in Fig.7 allowed to better understand the effect that structural modification can have on the properties of the complexes. Although the recorded relaxivity values are not extremely high, MR images in mice showed useful contrast of vasculature and tumoral tissue, which has brought a renewed interest of this ligand framework.

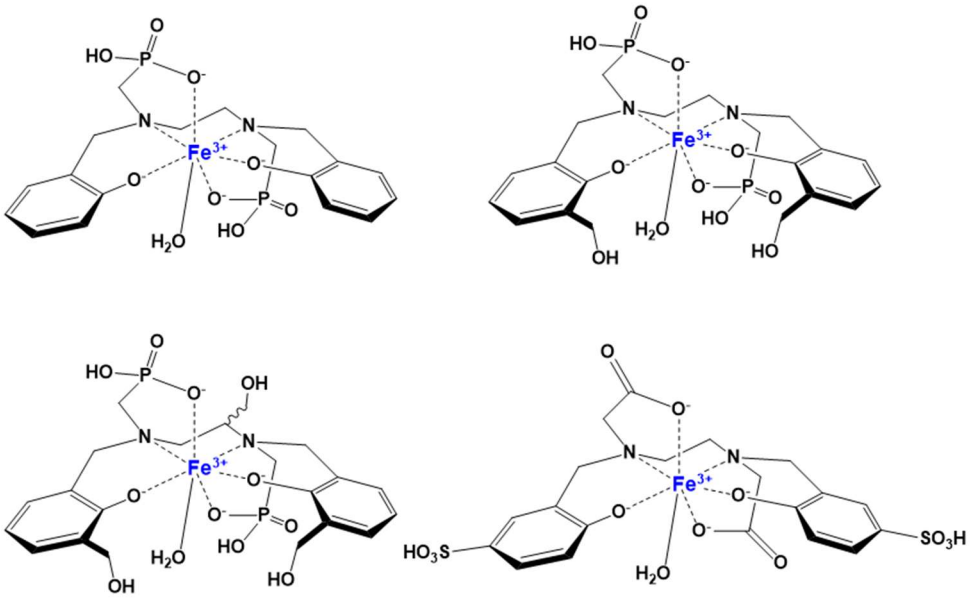

Figure 7. Structure of Fe(HBED) analogues.

The knowledge regarding how the variation of the ligand might affect the interaction between the metal ion and the water molecules is fundamental. It is exactly this kind of approach that allows the design of smart compounds, like the case of [Fe(PyC3A)].[31] This complex shares some similarities with the structures mentioned above, with a relatively higher relaxivity (at 37 °C, r_1 is 1.8 mM^{-1} s^{-1} at 60 MHz, 2.2 mM^{-1} s^{-1} at 500 MHz). The main feature of this compound is its redox-activity: the complex can be injected in the reduced form, $[Fe(PyC3A)]^-$ (which has a relaxivity ten times lower than the Fe(III) complex) and,

in the presence of oxidizing agents (e.g. ROS), the switch to the $[Fe(PyC3A)]^+$ allows a sensitive improvement in the contrast. This of course allows the complex to be site-specific, in facts it was used as a selective agent for acutely inflamed tissues. This is the first example of this kind of activity, and it opens a much wider range of possibilities.

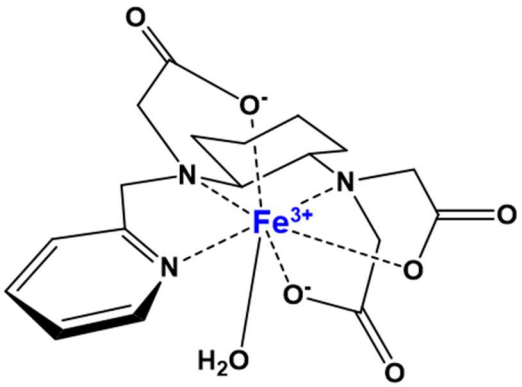

Figure 18. Structure of [Fe(PyC3A)].

All the structures shown so far are linear complexes. Another strategy for having more stable MRI probes is to use macrocyclic ligands. In fact, the FDA approved complexes for clinical use (reported in the previous chapter) are all macrocyclic compounds based on the 1,4,7,10-tetrakis(carboxymethyl)-1,4,7,10-tetraazacyclododecane (DOTA). The complex with DOTA was also investigated in the case of Fe(III), as well as that of a derivative having one less donor group, the 10-(2-hydoxypropyl)-1,4,7,10-tetraazacyclododecane-1,4,7-triacetate (DO3A). The abundance of donor groups does not allow the presence of a directly coordinated water molecule and they have obviously shown extremely low relaxivity (respectively 0.4 mM^{-1} s^{-1} and 0.5 mM^{-1} s^{-1} at 40 °C and 20 MHz).[32] Furthermore, considering the size of the ferric ion, a twelve-membered ring could be less selective for Fe(III),

thus allowing its reduction by reducing agents. Another strategy could imply the use of a lower membered ring (e.g. 1,4,7-triazonane, TACN). This approach for example was reported recently by Snyder *et al.* where Fe(III) complexes using TACN-based ligand were studied as a promising class for the development of new MRI probes.[33]

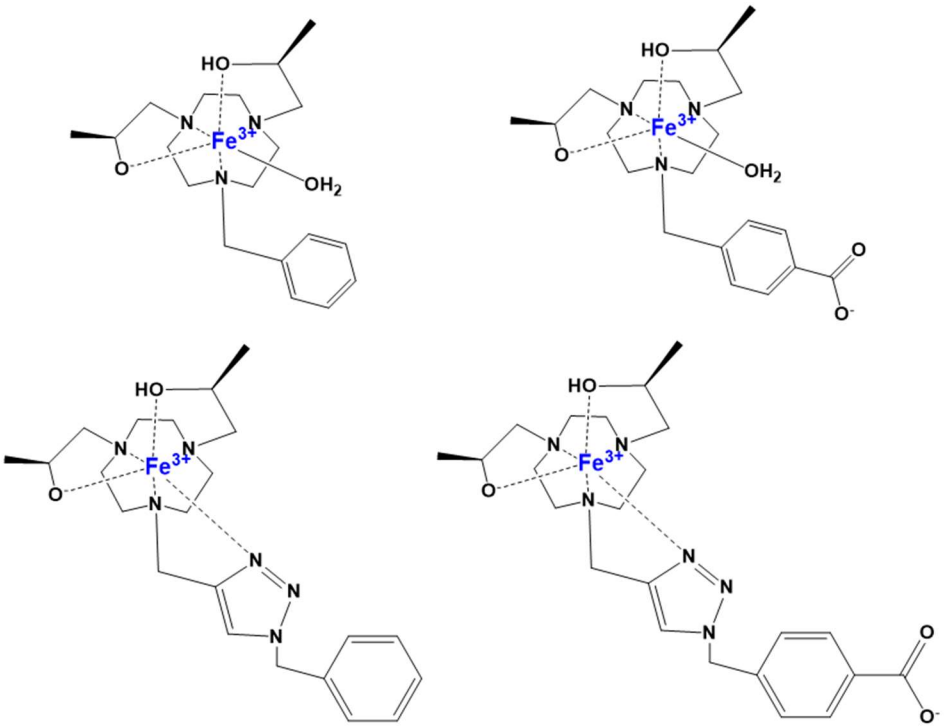

Figure 9. Fe(III) macrocyclic complexes reported in literature.[33]

Another class of iron(III) complexes that have been explored as possible positive contrast agents are the microbial desferrioxamine B (DF).[34] It has been reported a dangerous drop in blood pressure after the administration of the Fe(III) complex of DF.[35] From here, many different complexes have been synthetized and characterized (Fig. 11).[36] The general approach was to increase the lipophilicity of the complex so as to promote the liver uptake.[37]

Between these compounds, one of the most interesting and promising was the polyethylene-glycol conjugated, the Fe(III)-PEG-DF. The reported relaxivity at 20 MHz and 37 °C is 1.35 mM^{-1} s^{-1}, which is comparable to that of Fe-DF, but the blood pressure after the injection remains unchanged and the complex shows an LD_{50} in mice of 7.7 mmol kg^{-1}.[35] Interestingly, the enhancement profile of dog kidneys produced by the administration of 0.2 mmol kg^{-1} was comparable to that of Gd(III)-DTPA.[35]

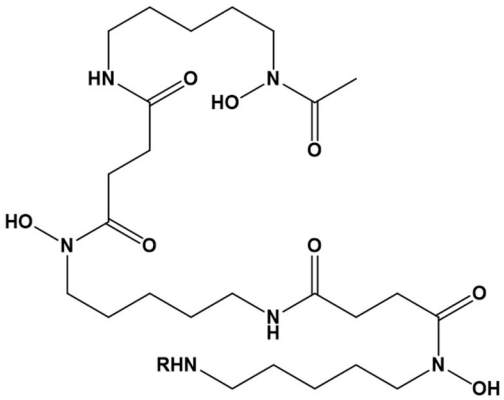

Figure 10. Structure of desferrioxamine B (R=H).

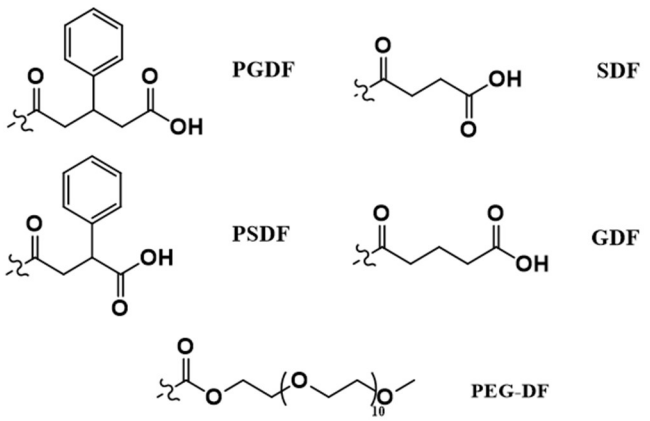

Figure 11. R groups of the derivatives of desferrioxamine B.

Finally, a relatively new and promising class of ligands for Fe(III) complexation might be represented by the amino-phenols.[38] Kuznik *et al*. proposed new structures starting from the N,N,N'-Tris[(2-hydroxyphenyl)methyl]ethan-1,2-diamine (sal) skeleton, and they showed how different variations might affect relaxivity. For the [Fe(sal)] complex, the recorded relaxivity at 16.5 MHz and 37 °C is 0.85 mM^{-1} s^{-1}. Initially, they determined that the introduction of methoxy groups in the ligand increased the relaxivity up to 1.22 mM^{-1} s^{-1}. Secondly, they tried to modulate the charge, in order to obtain positive and neutral complexes.

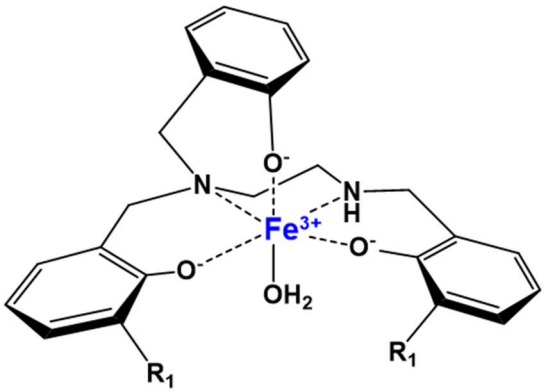

Figure 12. Structure of [Fe(sal)] (R_1=H).

For the positively charged complex, they substituted one of the aromatic arms with a pyridine, thus obtaining the $[Fe(salpy)]^+$ (Fig. 14), which has a higher relaxivity then its neutral counterpart (at 16.5 MHz and 37 °C r_{1p} is 1.09 mM^{-1} s^{-1}) and, by introducing a methoxy group on the ligand, they obtained the highest relaxivity of the study, which is equal to 1.39 mM^{-1} s^{-1} in the same conditions, and 2.39 mM^{-1} s^{-1} at 300 MHz and 22 °C, which is at the level of GBCAs. An attempt was also made to modify the other two aromatic arms by introducing two

naphthalene groups (Fig 14), as in the case of $[Fe(naphpy)]^+$, which however lowered the relaxivity to 1.03 mM^{-1} s^{-1} (300 MHz, 22 °C).

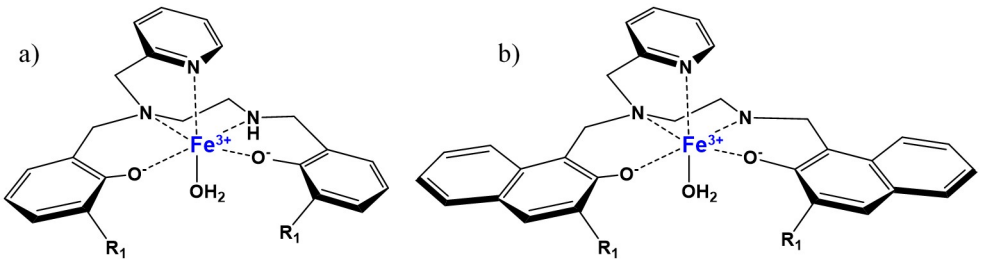

Figure 14. Structures of $[Fe(salpy)]^+$ (a) and $[Fe(naphpy)]^+$ (b) (R_1=H).

2.2 The future of Iron(III)-based contrast agents

It is clear that the ideal iron(III)-based probe would be the one having a high relaxivity and sublime thermodynamic stability and kinetic inertness. As far as the latter are concerned, we could take inspiration from nature, in particular from *siderophores*. These are compounds that exist naturally, generally produced by microorganisms, fungi and grasses, with high affinity towards Fe(III). Siderophores are among the strongest known chelating agents of Fe(III). A classic example of siderophores are catechols, whose generic structure is shown in Fig.15.

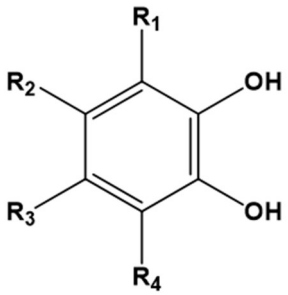

Figure 15. Generic catechol structure;

They are very weak acids and at low pH values they form transient Fe(III) complexes before decreasing to Fe(II) and *o*-quinone. At high pH, however, they can form very stable tris-catecholated complexes.[39] The progenitor of what will later be Fe(III)-siderophore complexes is enterobactin, which is an Fe(III)-sequestering agent naturally found in microorganisms (such as *Escherichia coli*). The high spin Fe(III)-enterobactin has a redox potential of -750 mV at pH=7 and is too negative to allow the reduction to Fe(II) and the value of the stability constant is one of the highest known of any other metal complex ($\log K \approx 52$).[40]

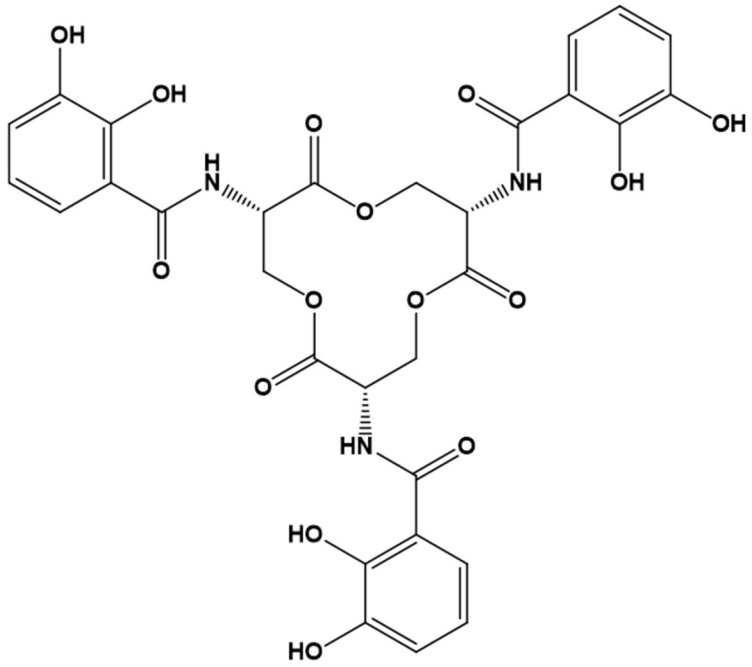

Figure 16. Structure of eneterobactin.

Precisely on the basis of this high thermodynamic stability guaranteed by the presence of catecholic groups, new ligand structures containing catecholic functionalities will be proposed in the final parts of this thesis. Their corresponding Fe(III) complexes have been

investigated and fully characterized. In the future, it will also be necessary to evaluate the use of different Fe(III)-specific functionalities, such as hydroxypyridinones (HOPOs) and hydroxamates, which have been analyzed extensively in terms of thermodynamic stability for Fe(III) complexes.[41-47] However, a detailed analysis of their relaxometric properties is lacking yet essential for understanding their diagnostic potential.

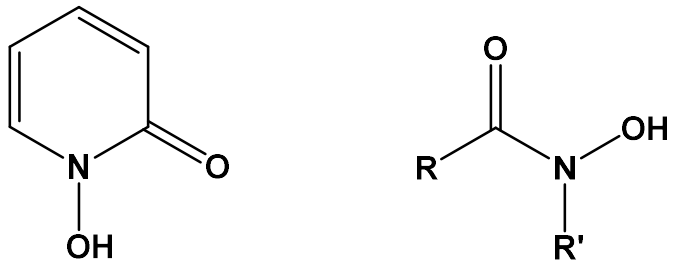

Figure 17. Generic structures of hydroxypyridinone (left) and hydroxamic acid (right).

Indeed, although the thermodynamic stability and kinetic inertia of these complexes are undeniably critical, rational design of new ligands also involves exploiting the correlations that exist between structure and efficacy. For example, in the case of Gd(III)- and Mn(II)-based complexes it is well known that the best strategies are based on increasing molecular weight (for an increase in rotational correlation time) or modulating exchange (e.g., working on charge or steric hindrance). However, this has not yet been explored in the case of Fe(III).

The same considerations that have been made previously on Mn(II) (Chapter 1) can also be applied to the case of Fe(III), since they share the same electron spin and they have similar molecular weights, but in the Fe(III) aquaion the metal-hydrogen distance is even smaller (r_{FeH}

= 2.69 Å), therefore its effect on relaxivity is even more advantageous. The case of the aquaion will be more critically discussed in the following chapter. However, we can anticipate that even though the ferric ion binds a lower number of water molecules than gadolinium (6 vs 8/9), the relaxivity values are perfectly comparable ($^{298}r_1$ at 60 MHz for $[Fe(H_2O)_6]^{3+}$ is 12.9 mM^{-1} s^{-1}, for $[Gd(H_2O)_8]^{3+}$ is 11.2 mM^{-1} s^{-1}). Unlike Gd(III), at high magnetic fields (>60 MHz) it is interesting to note that the relaxivity of Fe(III)-based complexes tends to increase ($^{298}r_1$ at 120 MHz for $[Fe(H_2O)_6]^{3+}$ is 14.2 mM^{-1} s^{-1}, for $[Gd(H_2O)_8]^{3+}$ is 11.5 mM^{-1} s^{-1}). This property can be of great help, considering how diagnostics is moving towards the use of instruments that work on even higher magnetic fields in order to improve the sensitivity of the technique. We have also performed simulations that allow us to better understand the intrinsic potential of Fe(III). Let us consider well-known Gd(III) and Mn(III)-based complexes such as $[Gd(DTPA)]^-$ and $[Mn(EDTA)]^{2-}$, both complexes having an hydration number q = 1. At the clinical magnetic field of 1.5 T, for a τ_M of 50 ns and a τ_R of 100 ps these complexes would reach a r_1 value of 3.8 mM^{-1} s^{-1} for $[Gd(DTPA)]^-$ and 3.0 mM^{-1} s^{-1} for $[Mn(EDTA)]^{2-}$. If the rotational correlation time is fixed at 1 ns, these would skyrocket to 27.8 mM^{-1} s^{-1} and 22.7 mM^{-1} s^{-1}. This τ_R value can be achieved for instance in adduct systems with macromolecules such as albumin. In order to obtain an effective comparison, we considered a generic Fe-L complex for which specific electronic parameters have been rationally hypothesized (Δ^2 = $1x10^{21}$ s^{-2}, τ_V = 5 ps). Thanks to the simulation shown below, it is clear how Fe(III) cannot guarantee competitive performance at 1.5 T.

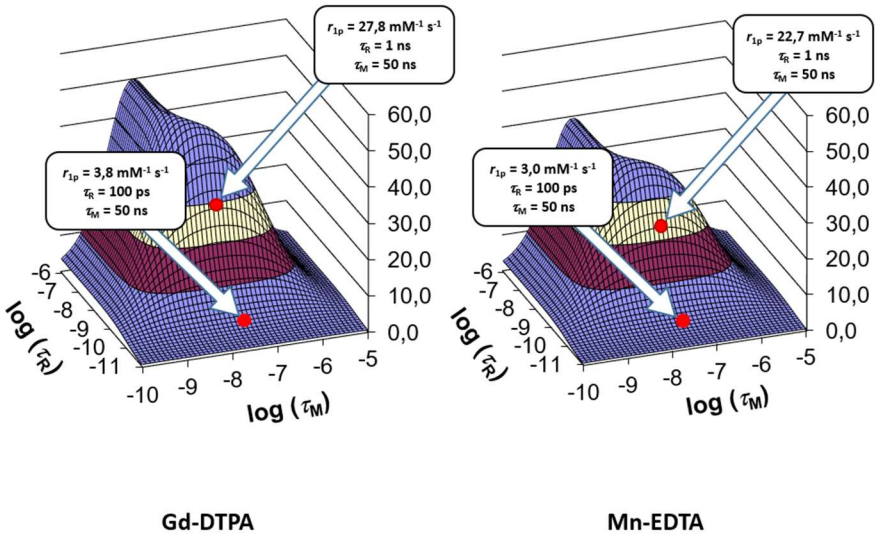

Figure 18. Simulations of the values of r_1 for $[Gd(DTPA)]^-$ and $[Mn(EDTA)]^{2-}$ at 1.5 T.

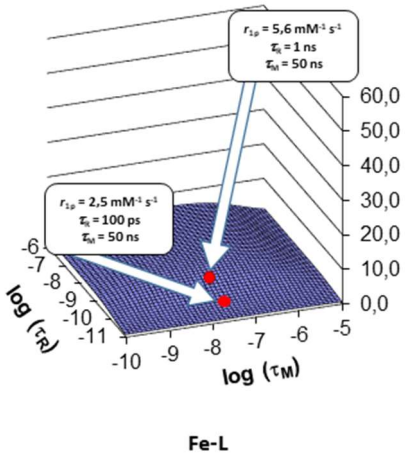

Figure 19. Simulations of the values of r_1 for Fe-L at 1.5 T.

Considering how the development of instrumentation is moving towards the use of stronger magnetic fields, we evaluated the same simulations at 3 and 7 T.

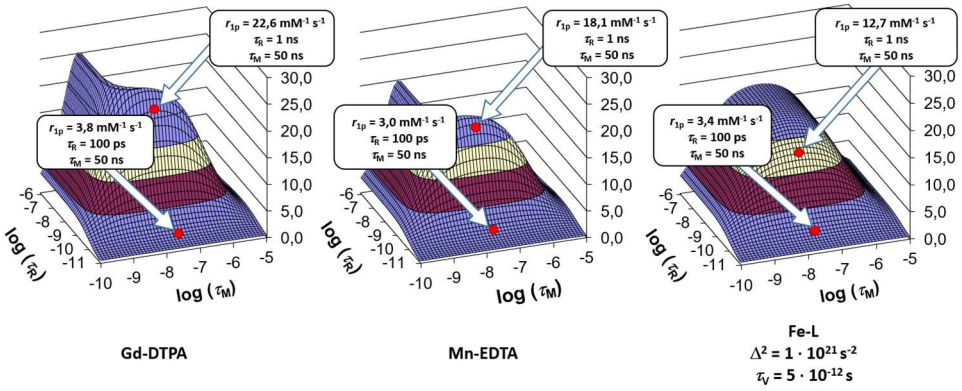

Figure 20. Simulations of the values of r_1 for $[Gd(DTPA)]^-$, $[Mn(EDTA)]^{2-}$ and Fe-L at 3 T.

Surprisingly, although in the case of $[Gd(DTPA)]^-$ and $[Mn(EDTA)]^{2-}$ the values do not change much, there is a remarkable increase for Fe-L, with values that can theoretically be 3.4 mM^{-1} s^{-1} (τ_R = 100 ps, τ_M = 50 ns) and 12.7 mM^{-1} s^{-1} (τ_R = 1 ns, τ_M = 50 ns). This is a particularly relevant property because it allows to optimize magnetic probes suitable for the magnetic field of clinical scanners that will be used in the next decade (≥ 3 T). Although it is still difficult to develop the instrumentation that can reach high fields such as 7 T, the study of the simulation allows us to highlight the importance of this peculiar behaviour that has never been studied so far. For this magnetic field value, the Fe(III)-based complex would be the only one with effectively applicable properties (Fig. 21). Furthermore, although τ_R and τ_M are still key parameters, we discovered that electronic parameters need to be treated carefully. By considering the same values of τ_R = 50 ps and τ_M = 10 ns, we determined how relaxivity can change by studying decreasing values of the mean-squared energy of the ZFS (Δ^2) (Fig. 22).

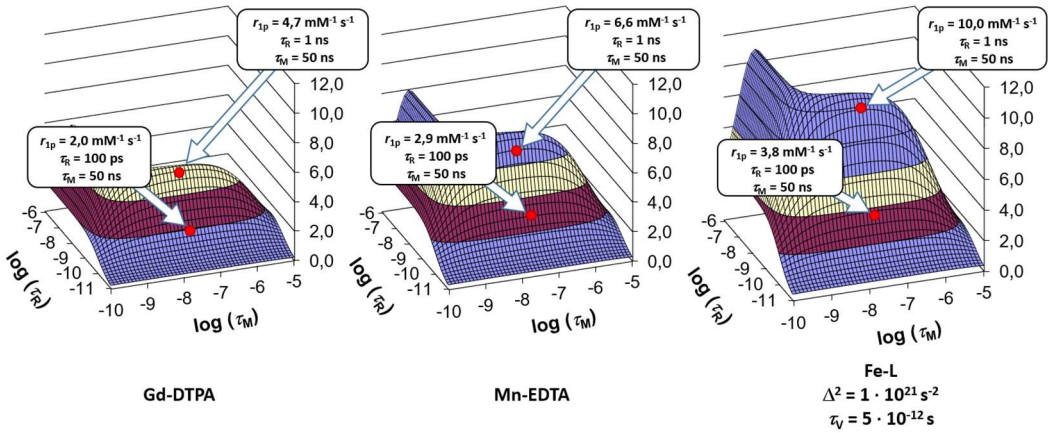

Figure 21. Simulations of the values of r_1 for $[Gd(DTPA)]^-$, $[Mn(EDTA)]^{2-}$ and Fe-L at 7 T.

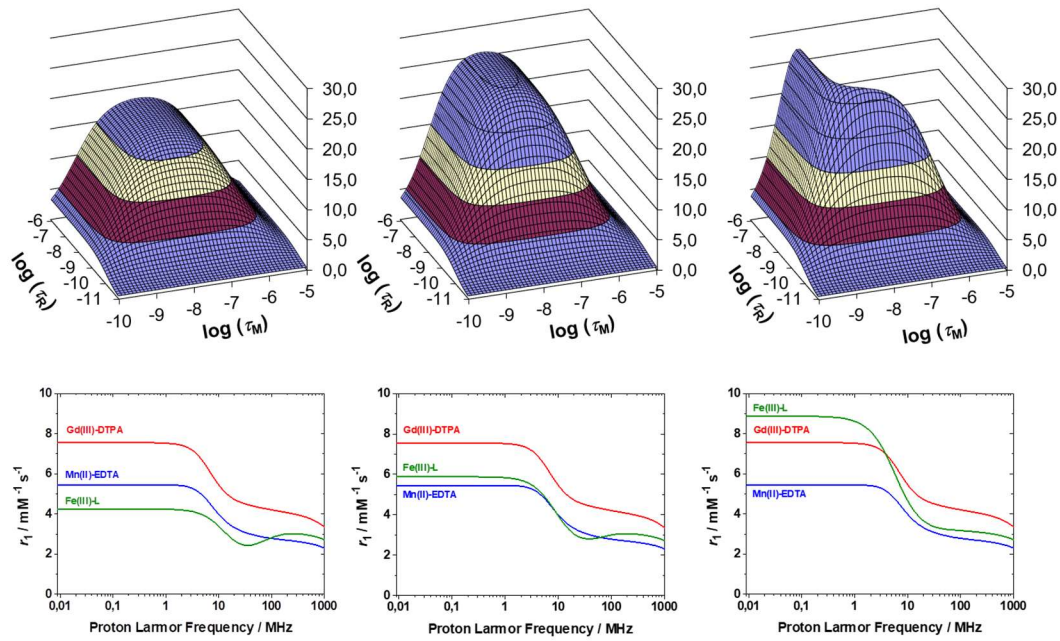

Figure 22. Simulations of the values of r_1 for Fe-L complexes with different values of Δ^2 at 3 T (from left to right, Δ^2 is 1x10^{21} s^{-2}, 5x10^{20} s^{-2} and 1x10^{20} s^{-2}).

Once we have theorized the best set of electronic parameters, we have assessed the effect of molecular thumbling. Considering τ_R values of 50, 75 and 100 ps, from the NMRD simulations we note a considerable increase in the relaxivity of the complex. All these different cases confirm the intrinsic potential of this new class of probes and how a complete and thorough study is crucial for their optimization.

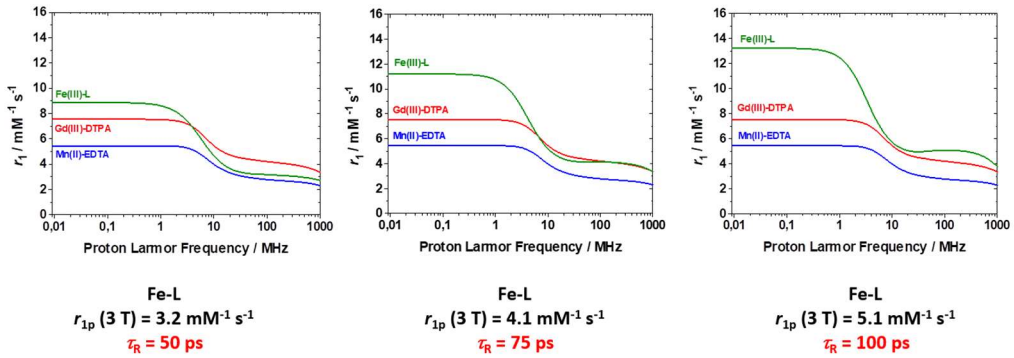

Figure 23. Simulated NMRD profiles of Fe-L (Δ^2 = 1x10^{20} s^{-2}).

The possibility of looking for alternatives, for example by changing already known structures or exploring new ligands, is certainly tempting and worth analysing in depth. Thus, the project in this dissertation will start from the characterization of already known structures as a starting point, also by taking advantage of the technological improvement of the technique and the instrumentation. This is necessary to understand how structural features affect relaxivity. Then, both derivatives of these known ligands and innovative structures that have been rationally designed will be studied. Ultimately, the focal point of this thesis is to provide the reader and future research with the basic knowledge necessary for the study, development and optimization of this class of compounds.

2.3 Notes and References

(1) Gomme, P. T.; McCann, K. B. *DDT*, **2005**, 10 (4), 267 – 273.

(2) Laurent, S.; Vander Elst, L.; Muller, R. N.; Merbach, A., Helm, L., Toth, E., *The Chemistry of Contrast Agents in Medical Magnetic Resonance Imaging*, second ed.; Eds. Wiley, **2013,** 427 – 447.

(3) Qiao, R.; Yang, C.; Gao, M. *J. Mater. Chem*. **2009**, 19 (35), 6274–6293.

(4) Zhao, X.; Zhao, H.; Chen, Z.; Lan, M. *Journal of Nanoscience and Nanotechnology*, **2014**, 14 (1), 210-220.

(5) Welch, K. D.; Davis, T. Z.; Van Eden, M. E.; Aust, S. D. *Free Radic. Biol. Med.*, **2002**, 32 (7), 577–583.

(6) W. H. Koppenol, R. H. Hider. *Biol. Med*. **2019**, 133, 3-10.

(7) Levine, M.; Padayatty, S. J.; Espey, M. G. *Advances in Nutrition*, **2011**, 2 (2), 78 – 88.

(8) Cotton, F. A., *Advanced Inorganic Chemistry, 6th Ed.*; Cotton, F. A., Eds.; Wiley: New York, **1999**.

(9) Rubin, D. L.; Muller H. H.; Young S. W. *Magnetic Resonance in Medicine*, **1992**, 154-165.

(10) Kivelitz, D.; Gehl, H.-B.; Heuck, A.; Krahe, T.; Taupitz, M.; Lodemann, K.-P.; Hamm, B. *Acta Radiol*. **1999**, 40 (4), 429–435.

(11) Hirohashi, S.; Uchida, H.; Yoshikawa, K.; Fujita, N.; Ohtomo, K.; Yuasa, Y.; Kawamura, Y.; Matsui, O. *Magn. Reson. Imaging*. **1994**, 12 (6), 837–846.

(12) Seibig, S.; van Eldik, R. *Inorganica Chimica Acta*, **1998**, 279 (1), 37-43.

(13) López-Alcalá, J. M.; Puerta-Vizcaíno, M. C.; González-Vílchez, F.; Duesler, E. N.; Tapscott, R. E. A. *Acta Crystallogr. C*, **1984**, 40 (6), 939-941.

(14) Richardson, N.; Davies, J. A.; Radüchel, B. *Polyhedron,* **1999**, 18 (19), 2457–2482.

(15) Krohling, C. A.; Eutrópio, F. J.; Bertolazi, A. A.; Dobbss, L. B.; Campostrini, E.; Dias, T.; Ramos, A. C. *Soil Sci. Plant Nutr.* **2016**, 62 (1), 39–47.

(16) Boehm-Sturm, P.; Haeckel, A.; Hauptmann, R.; Mueller, S.; Kuhl, C. K.; Schellenberger, E. A. *Radiology*, **2018**, 286 (2), 537–546.

(17) Martell, A. E.; Motekaitis, R. J.; Chen, D.; Hancock, R. D.; McManus, D. *Can. J. Chem.* **1996**, 74 (10), 1872–1879.

(18) Lauffer, R. B.; Greif, W. L.; Stark, D. D.; Vincent, A. C.; Saini, S.; Wedeen, V. J.; Brady, T. J. *Int. J. Rad. Appl. Instrum. B*, **1988**, 15 (1), 47–49.

(19) Frost, A. E.; Freedman, H. H.; Westerback, S. J.; Martell, A. E. *Nature*, **1957**, 80, 7, 1020-1021.

(20) Madsen, S. L.; Bannochie, C. J.; Martell, A. E.; Mathias, C. J.; Welch, M. J. *The Journal of Nuclear Medicine*, **1990**, 31 (10), 1662-1668.

(21) Larsen, S. K.; Jenkins, B. G.; Memon, N. G.; Lauffer, R. B. *Inorg. Chem.* **1990**, 29 (6), 1147–1152.

(22) Hoener, B.-A.; Engelstad, B. L.; Ramos, E. C.; Macapinlac, H. A.; Price, D. C.; Johnson, T. R.; White, D. L. *J. Magn. Reson. Imaging*, **1991**, 1 (3), 357–362.

(23) Gc, L.; Ym, W.; Ts, J.; Hm, C.; Rs, S. *J. Formos. Med. Assoc. Taiwan Yi Zhi*, **1993**, 92 (4), 359–366.

(24) Stark, D. D.; Elizondo, G.; Fretz, C. J. *Invest. Radiol*. **1990**, 25, S58.

(25) Lauffer, R. B.; Vincent, A. C.; Padmanabhan, S.; Villringer, A.; Saini, S.; Elmaleh, D. R.; Brady, T. J. *Magn. Reson. Med*. **1987**, 4 (6), 582–590.

(26) Jenkins, B. G.; Armstrong, E.; Lauffer, R. B. *Magn. Reson. Med*. **1991**, 17 (1), 164–178.

(27) Sheu, R. S.; Liu, G. C.; Wang, Y. M.; Jaw, T. S.; Chen, H. M.; Kuo, Y. T. *The Kaohsiung Journal of Medical Sciences*, **1997**, 13(2), 75-85.

(28) Martell, A. E.; Motekaitis, R. J.; Murase, I.; Sala, L. F.; Stoldt, R.; Ng, C. Y.; Rosenkrantz, H.; Metterville, J. J. *Inorganica Chim. Acta.* **1987**, 138 (3), 215–230.

(29) Kuźnik, N.; Szafraniec-Gorol, G.; Oczek, L.; Grucela, A.; Jewuła, P.; Kuźnik, A.; Zassowski, P.; Domagala, W. *J. Organomet. Chem*. **2014**, 769, 100–105.

(30) Bales, B. C.; Grimmond, B.; Johnson, B. F.; Luttrell, M. T.; Meyer, D. E.; Polyanskaya, T.; Rishel, M. J.; Roberts, J. *Contrast Media Mol. Imaging,* **2019**, 2019, 1–10.

(31) Wang, H.; Clavijo Jordan, V.; Ramsay, I. A.; Sojoodi, M.; Fuchs, B. C.; Tanabe, K. K.; Caravan, P.; Gale e. M. *J. Am. Chem. Soc*. **2019**, 141 (14), 5916–5925.

(32) Chang, C. A.; Francesconi, L. C.; Malley, M. F.; Kumar, K.; Gougoutas, J. Z.; Tweedle', M. F. *Inorg. Chem*. **1993**, 32 (16), 3501–3508.

(33) Snyder, E. M.; Asik, D.; Abozeid, S. M.; Burgio, A.; Bateman, G.; Turowski, S. G.; Spernyak, J. A.; Morrow, J. R. *Angew. Chem. Int. Ed*. **2020**, 59 (6), 2414–2419.

(34) Worah, D.; Berger, A. E.; Burnett, K. R.; Cockrill, H. H.; Kanal, E.; Kendall, C.; Leese, P. T.; Lyons, K. P.; Ross, E.; Wolf, G. L. *Investigative Radiology*. **1988**, 23, S281-S285.

(35) Duewell, S.; Wüthrich, R.; von Schulthess, G. K.; Jenny, H.B.; Muller, R. N.; Moerker, T.;, Fuchs, W. *Investigative Radiology*. **1991**, 26(1), 50-57.

(36) Krause, W. *Springer*. Vol. 221, **2003**

(37) Muetterties, K. A.; Hoener, B. A.; Engelstad, B. L.; Tongol, J. M., Wikstrom, M. G.; Wang, S. C.; Eason, R. G.; Moseley, M. E.; White, D. L. *Magnetic resonance in medicine*, **1991**, 22(1), 88-100.

(38) Kuźnik, N.; Wyskocka, M.; Jarosz, M.; Oczek, L.; Goraus, S.; Komor, R.; Krawczyk, T.; Kempka, M. *Arab. J. Chem*. **2019**, 12 (7), 1424–1435.

(39) Wilkinson, G.; Gillard, R. D.; McCleverty, J. A. Comprehensive Coordination Chemistry: The Synthesis, Reactions, Properties & Applications of Coordination Compounds. *Pergamon Press*, **1987**, Vol 4.

(40) Harris, W. R.; Carrano, C. J.; Raymond, K. N. *J. Am. Chem. Soc*. **1979**, 101 (8), 2213–2214.

(41) Turcot, I.; Stintzi, A.; Xu, J.; Raymond, K. N. *J. Biol. Inorg. Chem*. **2000**, 5 (5), 634–641.

(42) Cohen, S. M.; O'Sulliva, B.; Raymond, K. N. *Inorg. Chem*. **2000**, 39 (19), 4339–4346.

(43) Werner, E. J.; Kozhukh, J.; Botta, M.; Moore, E. G.; Avedano, S.; Aime, S.; Raymond, K. N. *Inorg. Chem*. **2009**, 48 (1), 277–286.

(44) Werner, E. J.; Avedano, S.; Botta, M.; Hay, B. P.; Moore, E. G.; Aime, S.; Raymond, K. N. *J. Am. Chem. Soc.* **2007**, 129 (7), 1870–1871.

(45) Pailloux, S. L.; Nguyen, S.; Zhou, S.; Hom, M. E.; Keyser, M. N.; Smiles, D.; Raymond, K. N *J. Heterocycl. Chem.* **2016**, 53 (4), 1065–1073.

(46) Pierre, V. C.; Botta, M.; Aime, S.; Raymond, K. N. *J. Am. Chem. Soc.* **2006**, 128 (29), 9272–9273.

(47) Cilibrizzi, A.; Abbate, V.; Chen, Y.-L.; Ma, Y.; Zhou, T.; Hider, R. C. *Chem. Rev.* **2018**, 118 (16), 7657–7701.

3 Materials and Methods

In this dissertation, a multi-technical approach was performed to characterize Fe(III)-based complexes as MRI probes. By combining NMR relaxometry at low and high resolution, UV-Vis spectrophotometry, potentiometry, cyclic voltammetry, and DFT calculations, we were able to provide a complete characterization of these systems. The following chapter presents the instruments and techniques that allowed us to perform this work.

3.1 Variable field relaxometer

This instrument allows to measure the relaxation rate in a range of magnetic field from 0.5 T to 3 T. The magnet (HTS 110) is built using a high temperature superconducting wire (35 K) and can operate without the use of cryogenic liquids. The magnetic field is varied by changing the current circulating within the system

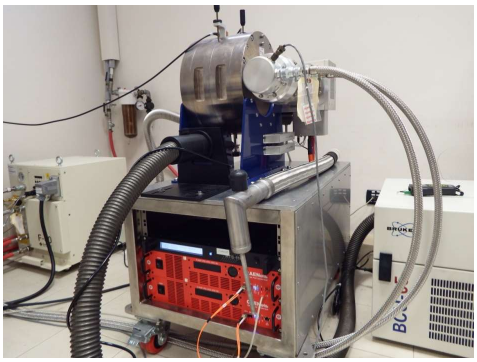

Figure 1. Variable field relaxometer with HTS 110 magnet.

At these magnetic field values the magnetization is strong enough to be observed directly. In addition, the high concentration of NMR active species in solution ([H_2O] ≈ 55.6 M) allows to evaluate the longitudinal proton relaxation time of the bulk water molecules. Once the magnetic field of interest has been set, the relaxation rate is measured thanks to the *inversion recovery* experiment.

This is basically a sequence of radio frequency pulses that allows to evaluate the component along the *z* axis of the magnetization.

A 180° pulse is sent to the sample, which consists in applying a B_1 field for a time twice that of the 90° pulse. In this way, the magnetization vector undergoes the precession of 180° and points in the *–z* direction (see Fig. 2).

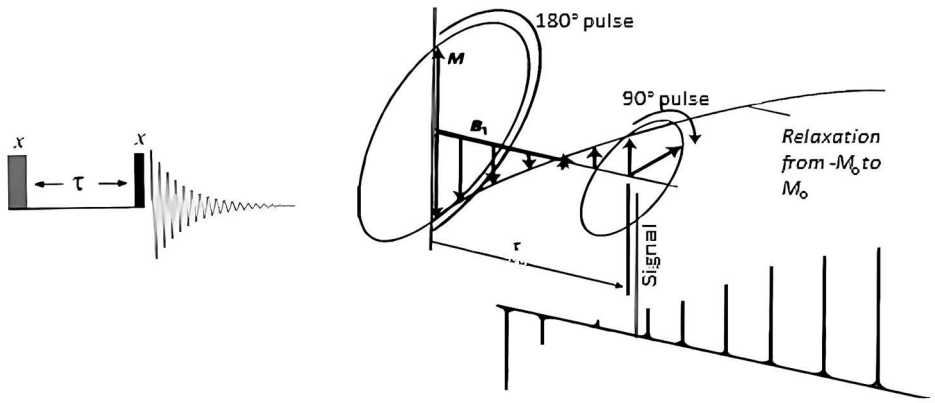

Figure 2. Inversion recovery sequence.

When the magnetization vector coincides with the *z* axis, no signal is detected, because on the *xy* plane, in which the detection coils are sensitive, there is no magnetization component. The magnetization vector contracts exponentially towards the thermal equilibrium value M_0. At a time τ, a 90° pulse is applied, which rotates the magnetization vector in the *xy* plane, where it begins to generate a

free induction decay signal (FID). From this point on, the signal is recorded and, through the Fourier transform, the spectrum is obtained in the frequency domain. The intensity of the spectrum obtained with this sequence of pulses depends on the length of the magnetization vector rotated in the *xy* plane. The length of this vector returns exponentially to its equilibrium value while the interval between the two pulses increases, so the intensity of the spectrum also varies in a similar way to an increase of τ.

The exponential decay of the magnetization is expressed as:

$$M_0 - M_z = AM_0 e^{-\frac{\tau}{T_1}} \qquad \text{(Eq. 1)}$$

Where M_0 is the length of the magnetization vector at equilibrium (before the 180° pulse), M_z is the length of the magnetization vector at time τ, T_1 is the longitudinal relaxation time. For τ = 0, M_z = - M_0. So by substituting we get $A = 2$:

$$M_0 - M_z = 2M_0 e^{-\frac{\tau}{T_1}} \qquad \text{(Eq. 2)}$$

Moving on to the natural logarithm:

$$\ln(M_0 - M_z) = \ln(2M_0) - \frac{\tau}{T_1} \qquad \text{(Eq. 3)}$$

By replacing the magnetizations with the intensities:

$$\ln(I_0 - I_z) = \ln(2I_0) - \frac{\tau}{T_1} \qquad \text{(Eq. 4)}$$

There is a value of $\tau = \tau_0$ whereby $I_0 = 0$, substituting we obtain $\tau_0 = T_1 ln2$. From the measure of τ_0 the sought T_1 value is easily obtained.

3.2 Fast field cycle (FFC) relaxometer

The variable field relaxometer, as described earlier, allows direct observation of magnetization in the field of interest. At magnetic field values below 0.5 T this is no longer possible because the magnetization is too weak to be observed directly. For this reason, a special instrument called *fast field cycle relaxometer* must be used. In particular, a SMARtracer relaxometer was used for data acquisition. The major advantage of using a Fast Field Cycle Relaxometer is that the field of a single magnet can be varied electronically within a few milliseconds while maintaining the high stability and homogeneity of the field required for NMR studies. The device shown schematically in Figure 8 has the following advantages:

- low operating costs (the use of liquid nitrogen to cool the magnet is not required);
- efficient temperature control (from 5 to 70 °C);
- Range of magnetic field values from 100 μT to 0.28 T (approximately from 10 kHz to 12 MHz in terms of proton Larmor frequency);
- Ease of use.

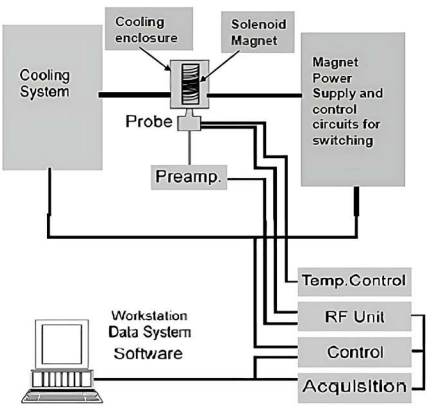

Figure 3. Block diagram of the SMARtracer relaxometer.

The relaxometer uses two types of sequences depending on the intensity of the measuring magnetic field: the pre-polarized sequence (PP) for low magnetic field values (0.01-4 MHz) and the non-polarized sequence (NP) for higher fields (4-10 MHz).

Figure 4. The SMARtracer FFC relaxometer.

3.2.1 Pre-Polarized sequence (PPS)

The sequence applied is as follows:

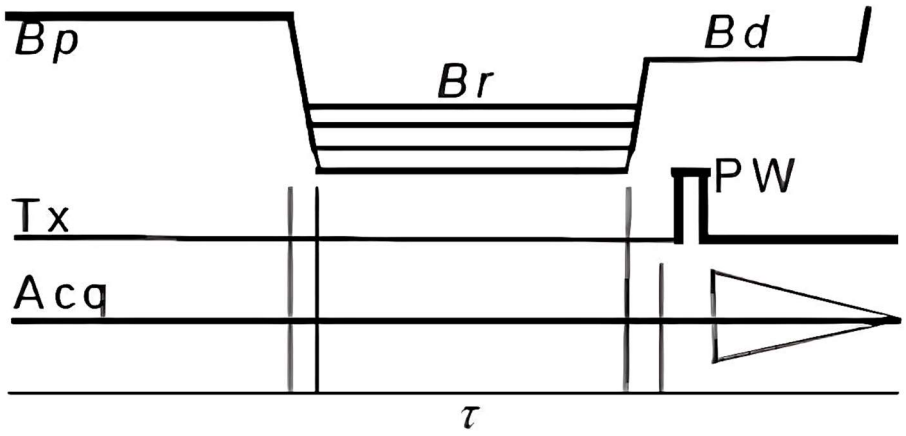

Figure 5. PPS scheme.

Where:

- B_p indicates the polarization field, fixed at 9 MHz;
- B_r is the variable relaxation field;
- B_d is the fixed acquisition range at 7.2 MHz.

The procedure involves the following basic operations:

1. the magnetic field is turned on at the value corresponding to the proton Larmor frequency of 9 MHz and it is kept for a certain time (*polarization time*) equal to at least 5 times the T_1 value of the sample at that field;
2. during this period, a magnetization vector is obtained on the *z* axis (M_z) due to the population difference imposed by the polarization magnetic field;
3. the field is then reduced to the relaxation value (field corresponding to the measurement frequency), for example 0.1 MHz, and it is kept for a certain variable time τ. During this interval, M_z decays towards its equilibrium value with a T_1 value relative to 0.1 MHz;
4. the field is quickly raised to a value corresponding to the fixed observation frequency (*acquisition field*), equal to 7.2 MHz, in a very short time called switch time;
5. as soon as the field reaches 7.2 MHz, a 90° pulse is applied, which brings the magnetization on the *y* axis and allows the measurement of the relative signal;
6. the field is then turned off to allow the magnetization to completely relax and the whole procedure is then repeated a number of times (generally 16), each time using a different value of τ.

The intensity of the signal obtained, which reflects the value of the magnetization, depends on the relaxation field and on the value of τ: by decreasing τ, the intensity of the signal increases, because the time available for the magnetization to return to its equilibrium value to the magnetic field B_r is lower.

By reporting the magnetization as a function of τ, an exponential is obtained whose time constant represents T_1 at the measuring range.

The advantage of the pre-polarized sequence is that of obtaining high magnetization values with magnetic fields in which these would be modest: T_1 at 0.1 MHz is measured at 7.2 MHz using the magnetization obtainable at 9 MHz.

Another positive aspect, also common to the NP sequence, is that since the acquisition field is constant, only one transmitter and receiver are needed.

3.2.2 Non-Polarized sequence (NPS)

The sequence can be represented as:

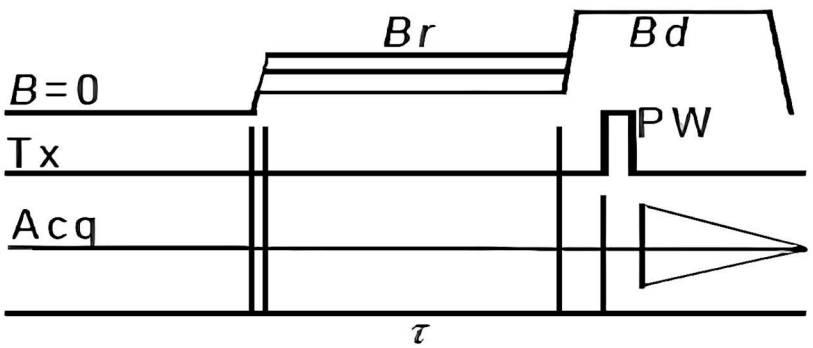

Figure 6. NP sequence scheme.

- B_r corresponds to the variable relaxation field (to which T_1 is measured);
- B_d is a fixed acquisition field (7.2 MHz).

A procedure similar to that of the previous sequence is followed, in which however the polarization magnetic field does not appear (at these field values it is not necessary):

1. the range is brought to the value corresponding to the measurement frequency (for example 10 MHz);
2. this field is maintained for a certain interval τ, during which the magnetization increases with a time constant T_1 relative to 10 MHz;
3. the field is brought to the acquisition value (7.2 MHz) very quickly, so that M_z does not have time to relax, and a 90° pulse is applied, which moves the magnetization on the *y* axis and allows its detection: the magnetization variation occurs according to T_1 at 10 MHz, but is determined at 7.2 MHz.

In this sequence the experiments are repeated 16 times, gradually varying the τ. In this case, for each field the signal intensity decreases by decreasing τ, because magnetization has less time to grow towards its maximum value.

3.3 Nuclear magnetic resonance (NMR)

In this work, nuclear magnetic resonance spectroscopy has been used for different purposes. In addition to being a fundamental technique for determining the structure and purity of the ligands, it allows the determination of the concentration of the paramagnetic

species (Bulk Magnetic Susceptibility method, BMS) and measurement of the transverse relaxation rate of the water oxygen atom as function of temperature (^{17}O NMR analysis). The NMR spectrometer used for these measurements is a Bruker Avance III with 11.74 T magnet.

Figure 7. Bruker Avance III spectrometer with 11.74 T magnet.

3.3.1 Concentration measurement: BMS method

To obtain an accurate estimate of a paramagnetic ion concentration in solution, we exploits the phenomenon whereby paramagnetic species cause a variation in the chemical shift ($\Delta\delta$) of interacting nuclei due to the effect of different factors[1-3]:

$$\Delta\delta = \Delta_d + \Delta_c + \Delta_p + \Delta_\chi \qquad \text{(Eq. 5)}$$

Among these contributions, Δ_d indicates the diamagnetic shift, which represents the contribution due to the bond with the metal

if it had no unpaired electrons. Given the presence of the paramagnetic ion, this contribution is often considered negligible. The hyperfine shift is due to two contributions, Δ_c, relative to the scalar contribution, and Δ_p, referred to the dipolar contribution, also called pseudo-contact term. Both contributions are observed when there is a direct interaction between the paramagnetic center and an atom or molecule with a nuclear spin, through chemical bonds (Δ_c) and/or space (Δ_p). These phenomena, however, can only be observed when the paramagnetic center has a chemical interaction with a molecule. The last contribution to the shift is given by magnetic susceptibility, Δ_χ. This is generated by the partial alignment of the magnetic moments of the paramagnetic species present in the solution and the applied magnetic field. To evaluate the effect on the chemical shift of an inert molecule (i.e. *tert*-butanol, dioxane, or any other substrate with which the paramagnetic species has no chemical interaction) therefore, only the effect due to magnetic susceptibility (Bulk Magnetic Susceptibility[4]) is considered, which can be calculated as:

$$\Delta_\chi = \frac{4\pi cs}{T}\left(\frac{\mu_{eff}}{2.84}\right)^2 \cdot 10^3 \qquad \text{(Eq. 6)}$$

where *c* indicates the millimolar concentration of the paramagnetic species, *s* depends on the shape of the tube and the position of the sample in the magnetic field (*s* = 1⁄3, -1⁄6 respectively for cylindrical tubes parallel or perpendicular to the field, *s* = 0 for spherical tubes), *T* is the absolute temperature at which the measurement is made and μ_{eff} is the actual magnetic moment, specific for the metal center. This method, also known as "Evans" method, allows

an extremely accurate measurement of the concentration of paramagnetic species. Experimentally, the concentration measurement is performed using a 3 mm tube, in which a solution prepared in the following way is inserted:

- 188 µl of the solution containing the paramagnetic complex;
- 22 µl of D_2O with 10% *tert*-butanol;
- 10 µl of H_2O milli-Q.

Through a ^1H NMR measurement, the chemical shift of the signals of the -CH_3 groups of the *tert*-butanol is obtained which is measured both in the presence and absence of the paramagnetic ion (Fig. 8).

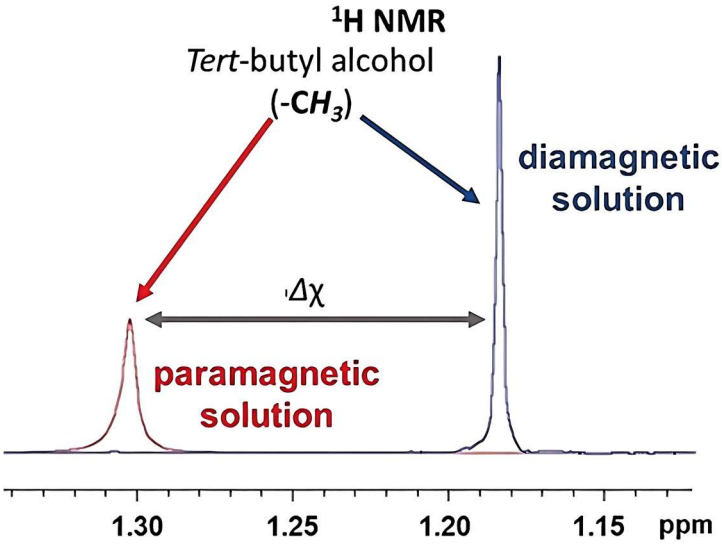

Figure 8. Shift of *tert*-butanol in the absence and presence of metal ion.[1]

Therefore, the concentration is calculated according to the following equation, taking into account the dilution factor (18/22):

$$C \cdot 10^3 = \Delta_\chi \frac{T}{4\pi\, {}^1/_3} \left(\frac{2.84}{\mu_{eff}}\right)^2 \qquad \text{(Eq. 7)}$$

3.3.2 ^{17}O NMR measurements

Since the exchange process has such a strong impact on aspects such as chemical shift and relaxation, NMR spectroscopy is a good method for understanding dynamic events. In the ^{17}O NMR measurements two important parameters are obtained for the characterization of the complexes, the transverse relaxation time T_2 of the water oxygen nucleus and the chemical shift difference ($\Delta\omega_r$) of the water signal both in the absence and presence of the paramagnetic ion.

The measurement of T_2 is quite simple to obtain, in fact the line width at half height of the water signal is measured on the ^{17}O NMR spectrum. The presence of a paramagnetic ion causes a decrease in T_2 and a consequent widening of the peak:

$$W_{1/2} = \frac{1}{T_2} \qquad \text{(Eq. 8)}$$

In reality, this measure does not allow to distinctly observe the peak of the water bound to the metal and that of the bulk water, but rather a single average peak (since these are in rapid exchange).

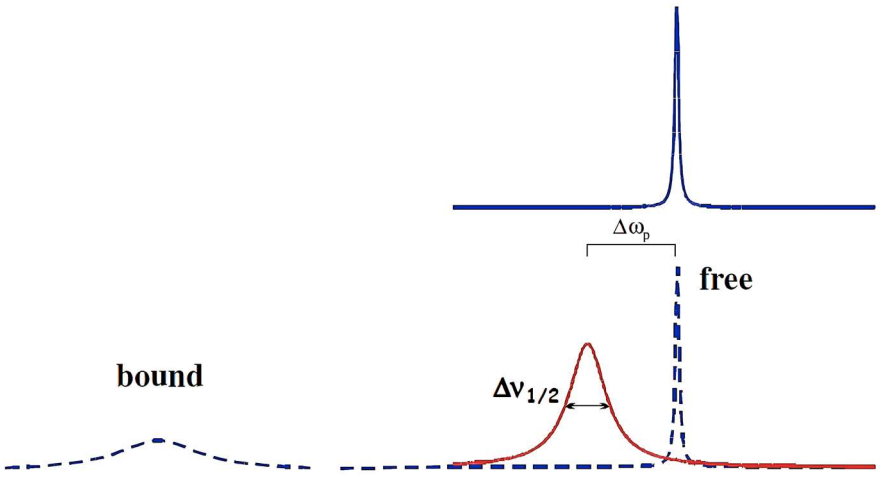

Figure 9. Representation of the ^{17}O NMR signal.

As for the measurement of $\Delta\omega_r$, the chemical shift difference of the water signal in the ^{17}O NMR spectrum in the absence and presence of the paramagnetic ion is detected. This is determined by the same factors already seen for the BMS method but, in this case, the two important contributions are Δ_c and Δ_p. The effect of magnetic susceptibility, assessed by the *tert*-butanol shift, is subtracted from the total value of the chemical displacement.

The water exchange between the paramagnetic metal site and the bulk is classified as exchange between two sites with distinct populations and relaxation times. The chemical shift of the solvent in a paramagnetic solution ω_p, relative to a diamagnetic reference ω_d, depends on τ_M as[1]:

$$\Delta\omega_p = \omega_p - \omega_d = \frac{p_m}{\tau_M^2}\frac{\Delta\omega_M}{(R_{2M} + \tau_M^{-1})^2 + (\Delta\omega_M)^2} + \Delta\omega_{OS} \qquad \text{(Eq. 9)}$$

$$\Delta\omega_M = \frac{g_L \mu_B S(S+1)B}{3k_B T} \frac{A_O}{\hbar} \quad \text{(Eq. 10)}$$

In Eq. 9, p_m is the molar fraction of bound water molecules, $\Delta\omega_M$ is the chemical shift difference between the paramagnetic and diamagnetic samples, while $\Delta\omega_{OS}$ corresponds to the outer sphere contribution, which typically is assumed to be proportional to $\Delta\omega_M$ through an empirical constant, $\Delta\omega_{OS} = C_{OS}\Delta\omega_M$. R_{2M} is the transverse relaxation rate of bound water ^{17}O. Unlike the interaction with proton nuclear spin previously discussed, where the dipolar contribution dominates the relaxation, for ^{17}O the dominant contribution in the transverse relaxation is the scalar term, R_2^{SC}, since oxygen is directly bonded to the metal and it can be expressed as:

$$R_{2M} = \frac{1}{T_{2M}} \cong R_2^{SC} = \frac{S(S+1)}{3}\left(\frac{A_O}{\hbar}\right)^2 \left(\tau_{c1}\frac{\tau_{e2}}{1+\omega_S^2\tau_{e2}^2}\right) \cong \frac{S(S+1)}{3}\left(\frac{A_O}{\hbar}\right)^2 \tau_{e1} \quad \text{(Eq. 11)}$$

In Eq. 11, S is the electron spin and $\frac{A_O}{\hbar}$ is the metal's hyperfine coupling constant with oxygen.

In analogy to the chemical shift, the relaxation rates of the solvent nuclei are increased when in the presence of a paramagnetic species. Specifically, the transverse relaxation increase is described by the equation:

$$R_{2p} = R_2^{obs} - R_2^d = \frac{p_M}{\tau_M} \frac{R_{2M}^2 + R_{2M}\tau_M^{-1} + (\Delta\omega_M)^2}{(R_{2M} + \tau_M^{-1})^2 + (\Delta\omega_M)^2} + R_{2OS} \quad \text{(Eq. 12)}$$

This set of equations, also known as the Swift-Connick equations, is the best method for accurate determination of parameters such as τ_M and $\frac{A_O}{\hbar}$.[5] Experimentally, the sample is prepared in a similar way to the

BMS method already reported, with the difference that instead of 10 µl of H_2O an equal amount of $H_2{}^{17}O$ (20% of ^{17}O) is added to increase the percentage of the active NMR nucleus at 1 %.

The measurements are carried out both on the sample containing the paramagnetic complex and in its absence at different temperatures:

- ^{17}O spectrum, with ^{1}H decoupling without NOE effect;
- ^{1}H NMR spectrum of the sample and the reference, similar to the BMS analysis.

The subsequent data processing allows to obtain the two parameters of interest: R_{2p}, obtained by calculating the difference between the row width obtained for the sample and that of the reference, multiplying it by π, and $\Delta\omega_r$, obtained from the subtracted $\Delta\delta$ of Δ_χ, multiplying by 2π.

The data are then scaled for the concentration of the paramagnetic center, using the molar fraction of the water directly bound.

3.4 Kinetic and thermodynamic studies

Kinetic and thermodynamic studies were carried out in collaboration with Prof. Zsolt Baranyai from Bracco Research Centre (Basovizza, Trieste, Italy). The protonation constants of the ligands and complexes were determined by pH potentiometric titration with 0.2 M NaOH at 25°C using a constant ionic strength (0.15 M $NaNO_3$) in 6 mL samples. The concentration of the ligands and the complexes were generally 0.002 M. The *Metrohm 888 Titrando* titration station with the combined electrode *Metrohm-6.0234.110* was used for pH measurements and titrations. The solutions were stirred and bubbled with N_2. Titrations were performed in a pH range of 1.7-12.0. KH

phthalate (pH=4.005) and borax buffers (pH=9.177) were used to calibrate the pH meter. For the calculation of $[H^+]$ from the measured pH values, the method proposed by Irving *et al.*[6] was applied as follows: 0.01 M HNO_3 solution was titrated with standardized NaOH solution at 0.15 M $NaNO_3$ ionic strength. The differences (A) between the measured (pH_{read}) and calculated pH (-log$[H^+]$), i.e., the average of the A values in the pH range of 1.75-2.20, were used to obtain the equilibrium H^+ concentration from the pH values measured in the titration experiments. The equilibrium calculations also required the stoichiometric water ion product (pK_w) to calculate the $[OH^-]$ values under basic conditions. The V_{NaOH}-pH_{read} data pairs from the HNO_3 - NaOH titration in the pH range of 10.8 to 12.0 were used to calculate the pK_w value. For calculation of the equilibrium constants, the program PSEQUAD was used.[7]

The kinetic inertness of the complexes was determined by the rates of ligand exchange reactions by spectrophotometry. Total concentration of the Fe(III) complexes was 0.1 mM, while the concentration of the transchelating ligand was 20 to 80 times higher, in order to guarantee pseudo-first-order conditions. The temperature was maintained at 25 °C and the ionic strength of the solutions was kept constant using 0.15 M $NaNO_3$. The pseudo-first-order rate constants (k_d) were calculated by fitting the absorbance data to the following equation:

$$A_t = (A_0 - A_p)e^{-k_d t} + A_p \qquad \text{(Eq. 13)}$$

where A_t, A_0 and A_p are the absorbance values at time t, the start of the reaction and at equilibrium, respectively. The calculation of the kinetic parameters were performed by the fitting of the absorbance - time

pairs with the *Micromath Scientist* computer program (version 2.0, Salt Lake City, UT, USA).

3.5 DFT Calculations

DFT calculations were carried out by Professor Platas-Iglesias from University of A Coruña. The geometries of the complexes were optimized using density functional theory (DFT) calculations with the TPSSh exchange correlation functional,[8] which belongs to the group of hybrid meta-GGA functionals, in conjunction with the Def2-TZVP basis set.[9] As demonstrated for Mn(II) complexes,[10] the inclusion of a few second-sphere water molecules is required for a better description of the distance between the metal ion and the coordinated water molecule, as well as the ^{17}O $A/\hbar$ values of coordinated water molecules. Geometry optimizations were followed by frequency calculations that confirmed the nature of the optimized structures are true energy minima on the potential energy surfaces. The calculation of hyperfine coupling constants was performed using the TPSSh functional, the aug-ccpVTZ-J[11] basis set for Fe and the EPR-III[12] basis set for all other atoms. The output of the calculations provided the isotropic hyperfine coupling constants A_{iso}, which are related to the $A/\hbar$ values obtained from NMR measurements by $A/\hbar = A_{iso}\times 2\pi$. Bulk solvent effects were considered throughout with the integral equation formalism of the polarized continuum model (IEF-PCM).[13] These calculations were performed with the Gaussian 09 program package (revision E.01).[14]

The geometries optimized as described above were used for state averaged complete active space self-consistent field (CASSCF) calculations,[15] which were carried out using the ORCA4 program

(version 4.2.0).[16] Solvent effects (water) were incorporated using the SMD solvation model.[17] The active space consisted in the five 3*d* electrons of Fe distributed over the five metal-based *d* orbitals [CAS(5,5)], using 1 sextet, 24 quartet and 75 doublet roots. These calculations used the Def2-TZVP basis set and were accelerated with the resolution of identity (RI) approximation[18] employing the Def2/JK[19] auxiliary basis set. Dynamic correlation was considered with the fully internally contracted variant of N-valence state perturbation theory (FIC-NEVPT2).[20] Spin-orbit coupling was considered in the framework of quasi-degenerate perturbation theory (QDPT).[21] Zero field splitting (ZFS) parameters were obtained within the effective Hamiltonian approximation. The axial (D) and rhombic (E) ZFS parameters are related to the energy of the ZFS Δ by the following expression:[22]

$$\Delta = \sqrt{\frac{2}{3}D^2 + 2E^2} \qquad \text{(Eq. 14)}$$

3.6 Cyclic Voltammetry

Electrochemical measurements were performed in collaboration with Prof. Mauro Ravera from University of Piemonte Orientale (Alessandria). The measurements were carried out by using an *Autolab PGSTAT12 electrochemical analyzer* (Eco Chemie, Utrecht, The Netherlands) connected to a personal computer running GPES 4.9 electrochemical software. A standard three-electrode cell was constructed so that the tip of the reference electrode (Ag/AgCl, 3M KCl) was close to the working electrode (a disk of glassy carbon (GC), diameter 0.1 cm, sealed in epoxy resin). The GC working electrode was

polished with alumina, rinsed with distilled water, and dried. This procedure resulted in an almost completely reproducible surface for all experiments. Measurements were performed under nitrogen in milliQ water containing 0.1 M KNO_3 as supporting electrolyte; the pH was set with nitric acid. The complex concentration was 1 mM. The temperature of the solution was kept constant (25±1 °C) by the circulation of a water/ethanol mixture through a jacketed cell. Positive feedback iR compensation was applied routinely. All peak potentials were measured at a scan rate of 0.2 V s^{-1} and reported vs. the reference electrode.

3.7 Notes and references

(1) Helm, L., Morrow, J. R., Bond, C. J., Carniato, F., Botta, M., Braun, M., Baranyai, M., Pujales-Paradela, Z., Regueiro-Figueroa, R., Esteban-Gómez, M., and Platas-Iglesias, C. *Contrast Agents for MRI*, 2017, 121-242.

(2) Peters, J. A., Huskens, J., & Raber, D. J. *Progress in Nuclear Magnetic Resonance Spectroscopy*, 1996, 28(3-4), 283-350.

(3) Aime, S., Botta, M., Fasano, M., & Terreno, E. *Chemical Exchange Saturation Transfer Imaging*, 2017

(4) Corsi, D. M.; Platas-Iglesias, C.; Bekkum, H. van; Peters, J. A. *Magn. Reson. Chem.* 2001, 39 (11), 723–726.

(5) Swift, T. J. & Connick, R. E., *The Journal of Chemical Physics*, 1962, 37(2), 307-320.

(6) Irving, H. M.; Miles, M. G. and Pettit, L. D. *Anal. Chim. Acta*, 1967, 38, 475–488.

(7) Zékány, L.; Nagypál I. *Ed. Legett D J, Plenum, New York*, **1985**, p. 291.

(8) Tao, J. M.; Perdew, J. P.; Staroverov, V. N.; Scuseria, G. E*. Phys. Rev. Lett.* **2003**, 91, 146401.

(9) Weigend, F.; Ahlrichs, R. *Phys. Chem. Chem. Phys.* **2005**, 7, 3297 – 3305.

(10) Patinec, V. ; Rolla, G. A.; Botta, M.; Tripier, R.; Esteban-Gómez, D.; Platas-Iglesias, C. *Inorg. Chem*. **2013**, 52, 11173 – 11184.

(11) Hedegard, E. D.; Kongsted, J.; Sauer, S. P. A. *J. Chem. Theory Comput*. **2011**, 7, 4077–4087.

(12) Rega, N.; Cossi, M.; Barone, V. *J. Chem. Phys.* **1996**, 105, 11060 – 11067.

(13) Tomasi, J.; Mennucci, B.; Cammi, R. *Chem. Rev.* **2005**, 105, 2999 – 3093.

(14) Gaussian 09, Revision E.01, Frisch, M. J.; Trucks, G. W.; Schlegel, H. B.; Scuseria, G. E.; Robb, M. A.; Cheeseman, J. R.; Scalmani, G.; Barone, V.; Petersson, G. A.; Nakatsuji, H.; Li, X.; Caricato, M.; Marenich, A.; Bloino, J.; Janesko, B. G.; Gomperts, R.; Mennucci, B.; Hratchian, H. P.; Ortiz, J. V.; Izmaylov, A. F.; Sonnenberg, J. L.; Williams-Young, D.; Ding, F.; Lipparini, F.; Egidi, F.; Goings, J.; Peng, B.; Petrone, A.; Henderson, T.; Ranasinghe, D.; Zakrzewski, V. G.; Gao, J.; Rega, N.; Zheng, G.; Liang, W.; Hada, M.; Ehara, M.; Toyota, K.; Fukuda, R.; Hasegawa, J.; Ishida, M.; Nakajima, T.; Honda, Y.; Kitao, O.; Nakai, H.; Vreven, T.; Throssell, K.; Montgomery, Jr., J. A.; Peralta, J. E.; Ogliaro, F.; Bearpark, M.; Heyd, J. J.; Brothers, E.; Kudin, K. N.; Staroverov, V. N.; Keith, T.; Kobayashi, R.; Normand, J.; Raghavachari, K.; Rendell, A.; Burant, J. C.; Iyengar, S. S.; Tomasi, J.; Cossi, M.; Millam, J. M.; Klene, M.; Adamo, C.; Cammi, R.;

Ochterski, J. W.; Martin, R. L.; Morokuma, K.; Farkas, O.; Foresman, J. B.; Fox, *D. J.* Gaussian, Inc., Wallingford CT, **2016**.

(15) (a) Roos, B. O.; Taylor, P. R.; Siegbahn, P. E. M. *Chem. Phys.* **1980**, 48(2), 157－173; (b) Siegbahn, P.; Heiberg, A.; Roos, B.; Levy, B.; *Phys. Scr.* **1980**, 21 (3－4), 323; (c) Siegbahn, P. E. M.; Almlöf, J.; Heiberg, A.; Roos, B. O. *J. Chem. Phys.* **1981**, 74 (4), 2384－2396.

(16) (a) Neese, F. Software Update: the ORCA Program System, Version 4.0. *Wiley Interdisciplinary Reviews: Computational Molecular Science* **2018**, 8 (1), e1327; (b) Neese, F. The ORCA Program System. *Wiley Interdisciplinary Reviews: Computational Molecular Science* **2012**, 2 (1), 73－78.

(17) Marenich, A. V.; Cramer, C. J.; Truhlar, D. G. *J. Phys. Chem. B*, **2009**, 113, 6378-6396.

(18) Kollmar, C.; Sivalingam, K.; Helmich - Paris, B.; Angeli, C.; Neese, F. *J. Comput. Chem*. **2019**, 40, 1463–1470.

(19) Weigend, F.; *J. Comput. Chem*. **2007**, 29, 167–175.

(20) (a) Angeli, C.; Cimiraglia, R.; Evangelisti, S.; Leininger, T.; Malrieu, J.-P. *J. Chem. Phys.* **2001**, 114 (23), 10252-10264; (b) Angeli, C.; Cimiraglia, R.; Malrieu, J.-P. *Chem. Phys. Lett.* **2001**, 350, 297-305; (c) Angeli, C.; Cimiraglia, R.; Malrieu, J.-P. *J. Chem. Phys.* **2002**, 117 (20), 9138-9153.

(21) Neese, F. *J. Chem. Phys*. **2005**, 122 (3), 034107.

(22) Khan, S.; Pollet, R.; Vuilleumier, R.; Kowalewski, J.; Odelius, M.; *J. Chem. Phys.* **2017**, 147, 244306.

4 Defining the conditions for the development of the emerging class of Fe(III)-based MRI contrast agents

Fe(III) complexes are attracting growing interest in chemists developing diagnostic probes for Magnetic Resonance Imaging because they leverage on an endogenous metal and show superior stability. However, in this case a detailed understanding of the relationship between chemical structure of the complexes, their magnetic, thermodynamic, kinetic and redox properties and the molecular parameters governing the efficacy (relaxivity) is still far from being available. We have carried out an integrated ^{1}H and ^{17}O NMR relaxometric study as a function of temperature and magnetic field, on the aqua ion and three complexes chosen as reference models, together with theoretical calculations, to obtain accurate values of the parameters that control their relaxivity. Moreover, thermodynamic stability and dissociation kinetics of the Fe(III) chelates, measured in association with the ascorbate reduction behaviour, highlight their role and mutual influence in achieving the stability required for use in vivo.

4.1 Introduction

The success and development of MRI as a diagnostic technique of primary importance has been accompanied and facilitated by the availability of metal-based contrast agents (CAs), which allow to achieve very important objectives: i) increase the signal intensity; ii) decrease image acquisition times; iii) improve image contrast and thus the diagnosis of different malignancies that could remain undetected using unenhanced procedures; iv) reduce artefacts and improve cost management. The CAs currently used in clinical practice are small and hydrophilic paramagnetic Gd(III) complexes that accelerate the relaxation rates (R_1 and R_2) of proximate tissue water protons in regions of agent accumulation.[1] In addition to these low molecular weight complexes, many other systems, from polynuclear complexes to sophisticated nanosized structures, supramolecular adducts or theranostic agents, have been designed and developed for bio-medical applications and pre-clinical research.[2]

The success of Gd-based contrast agents (GBCAs) was possible thanks to the detailed understanding of the correlation between the efficacy (relaxivity, r_1) and the structural and dynamic parameters that characterize these coordination compounds. In summary, the key parameters are the tumbling rate of the complex in solution ($1/\tau_R$), the exchange rate ($k_{ex} = 1/\tau_M$) of the water molecule in the inner sphere of coordination and its distance (r_{GdH}) from the metal centre, the electronic relaxation times ($T_{1,2e}$) of the paramagnetic ion and its hydration state (q).[1,3] Despite the fact that the clinically used Gd(III) chelates are generally very safe and very well tolerated by patients, there has been recently some concerns related to i) a new disease,

called nephrogenic systemic fibrosis, which was associated with the administration of GBCAs to patients with severely compromised kidney function[4] and ii) the retention of small amounts of Gd(III) in the tissues of patients exposed to multiple MRI scans, although without any evidence that this is associated with clinical harm.[5] This has given a boost to exploratory research activities focused on finding alternative contrast enhancer based on different chemical species. One obvious and effective approach is the development of contrast agents based on paramagnetic metal ions with improved tolerability. Among them, Mn(II) has received great attention over the past few years, with some of the complexes showing very promising properties.[6] However, while it has been demonstrated that Mn(II)-based MRI probes may have an efficacy quite comparable to that of GBCAs, the challenges remain open to achieving sufficient thermodynamic stability and kinetic inertness for clinical applications.[6] More recent reports have also considered the use of high-spin Fe(III) complexes,[7] which share the same d^5 configuration with the Mn(II) analogues, but with a superior safety profile, since iron is an essential element for life present in 3–5 g in the human body.[8] In particular, Schellenberger *et al.*[9] showed that low molecular weight Fe(III) complexes such as $[Fe(CDTA)]^-$ provide significant image contrast *in vivo* and present enhancement kinetics very similar to $[Gd(DTPA)]^{2-}$, (Magnevist®) a clinically used agent. Subsequently, Gale[10] and Morrow[11] reported Fe(III) complexes with relatively high relaxivities at the imaging fields. Alternatively, Fe(II/III) complexes have been used for redox-dependent paramagnetic chemical exchange saturation transfer (PARACEST) applications or ^{19}F MRI thermometers.[12,13] Overall, these recent results indicate a promising new way to design novel

contrast media for MRI, using an endogenous paramagnetic metal alternative to Gd(III). Despite these important initial contributions, the mechanisms responsible for water proton relaxation enhancement induced by Fe(III) complexes and the relationships between the molecular parameters that govern r_1 and the chemical structure have not been yet deciphered, preventing the development of systems with optimal properties through rational ligand design.

In this paper, we address some basic issues related to the relaxation of the solvent water protons by Fe(III) ions in some model systems, as a necessary initial step towards a detailed evaluation of the efficacy of Fe(III) complexes as diagnostic MRI probes. As stated by S. Koenig over 35 years ago, the Fe(III) ion has the potential to be particularly suitable as an MRI probe due to its relatively large magnetic moment and because it occurs *in vivo* in a variety of forms.[14] Thus, we report here the first detailed ^{1}H and ^{17}O NMR relaxometric analysis, combined with theoretical calculations of four representative Fe(III) complexes: $Fe(EDTA)^{-}$, $Fe(CDTA)^{-}$, $Fe(DTPA)^{2-}$ and the aqua ion $[Fe(H_2O)_6]^{3+}$. In addition, thermodynamic, kinetic and ascorbate reduction studies on $Fe(EDTA)^{-}$ and $Fe(CDTA)^{-}$ complexes are reported to assess the overall stability of the complexes.

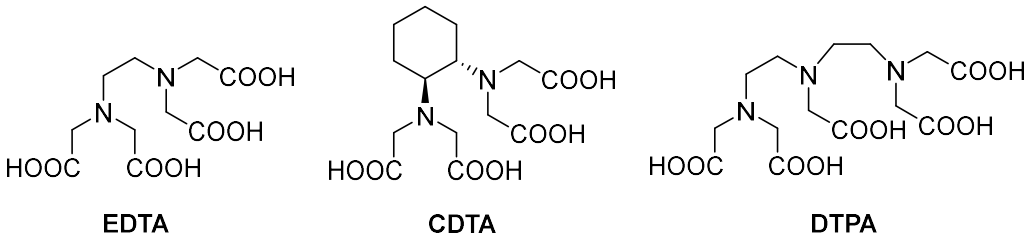

Scheme 1. Ligands discussed in the present work.

4.2 Results and discussion

The ^{1}H nuclear magnetic relaxation dispersion (NMRD) profiles recorded for the $[Fe(H_2O)_6]^{3+}$ complex, measured over an extended range of Larmor frequencies, are presented in Figure 1. Since water exchange is a key dynamic parameter that often affects the relaxivity of metal complexes, we also measured ^{17}O transverse relaxation rates and chemical shifts, which provide direct access to k_{ex}. These data were obtained at low pH (pH = 0-0.5) to avoid the hydrolysis of the cation and formation of hydroxo-species. ^{1}H NMRD and ^{17}O NMR data were reported several years ago in separate papers.[15,16] These studies provided markedly different $^{298}\tau_M$ values of 0.39 μs (^{1}H NMR) and 14.7 μs and 6.25 ms (^{17}O NMR). The ^{1}H NMRD profiles show a dispersion in the range 1-20 MHz, as typically observed for low-molecular Mn(II) and Gd(III) complexes. The relaxivity of $[Fe(H_2O)_6]^{3+}$ increases above 20 MHz until ca. 100 MHz, and then remains fairly constant up to 500 MHz. The ^{17}O transverse relaxation data are characteristic of a system in the slow exchange regime, where T_{2r} increases with increasing temperature.

Initial attempts to fit the ^{17}O NMR and ^{1}H NMRD data using the same exchange rate failed and provided evidence that proton exchange and the exchange of the whole water molecule occur in different timescales. We therefore carried on a simultaneous fit of the two data sets using the established equations for paramagnetic relaxation[17] and assuming two different residence times: $^{298}\tau_M{}^{H}$ (^{1}H) and $^{298}\tau_M{}^{O}$ (whole water).

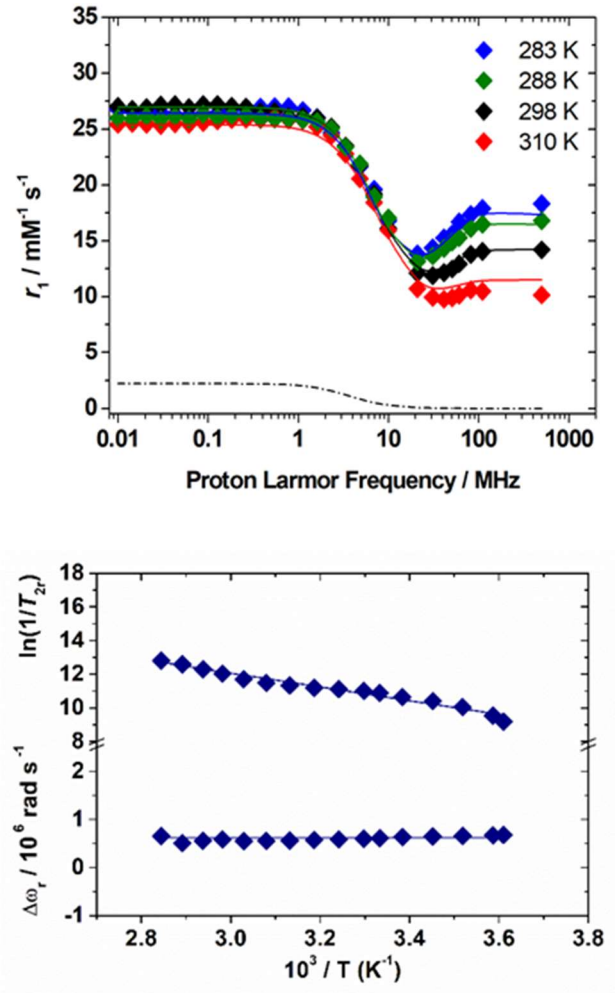

Figure 1. ^{1}H NMRD profiles at different temperatures (top) and ^{17}O NMR data (bottom) recorded for $[Fe(H_2O)_6]^{3+}$. The lines correspond to the fits of the data as described in the text. The dashed curve under the NMRD profiles represents the scalar contribution to r_1 at 298 K.

The ^{17}O NMR data were analysed using the Swift-Connick equations,[18] which depend on longitudinal (i = 1) and transverse (i = 2) relaxation times of the electron spin (T_{ie}) as well as $^{298}\tau_M^O$ and the hyperfine coupling constant $A_O/\hbar$. Given the large number of parameters that affect the ^{17}O NMR and NMRD data, we estimated some of them with

the use of DFT calculations, while some others were fixed to reasonable values. Following our previous work on Mn(II) complexes,[19] the ^{1}H and ^{17}O hyperfine coupling constants and the distances between the H atoms of the coordinated water molecules and the paramagnetic centre were estimated from DFT calculations (Table 1). These calculations were performed on $[Fe(H_2O)_6]^{3+}\cdot 12H_2O$, which includes 12 explicit second sphere water molecules. The fit of the data required including a scalar contribution to r_1, which depends on the hyperfine coupling constant $A_H/\hbar$. The scalar contribution was found to provide a small, but significant (~ 10%), contribution at low fields (< 1MHz).

The residence lifetime of the whole water molecule in the Fe(III) coordination sphere is rather long ($^{298}\tau_M^O$ = 25 μs). This can be ascribed to the high charge-to-radius ratio of the cation (cf. $^{298}\tau_M^O$ = 35 ns for Mn(II)).[20] Water exchange appears to be much faster however than estimated previously by Jordan ($^{298}\tau_M^O$ = 6.25 ms).[16] The residence lifetime of water protons obtained from ^{1}H NMRD measurements is much shorter ($^{298}\tau_M^H$ = 0.76 μs, Table 1), which indicates that ^{1}H exchange receives an important contribution from prototropic exchange under highly acidic conditions, as recently shown for Gd-complexes bearing amide ancillary groups.[21] Therefore, the observed exchange rate k can be expressed as $k = k_{ex}^{H2O} + k_H[H^+]$, where k_{ex}^{H2O} and k_H are the rate constants characterizing the exchange of the whole water molecule and the prototropic mechanism, respectively. Since $k_{ex}^{H2O} = 4.0\times10^4$ s^{-1} and $k_H = 9.06\times10^6$ s^{-1} M^{-1}, the prototropic exchange is expected to provide the main contribution at the acidic pH values required to avoid the hydrolysis of $[Fe(H_2O)_6]^{3+}$. These results explain the discrepancies between the data reported

earlier on by Merbach and Bertini,[15] and indicate that the $^{298}\tau_M^O$ value calculated by Jordan is very inaccurate. Finally, it is worth noting that the calculated k_H value is in good agreement with that calculated through a pH-dependent study on a cationic GdDOTA tetra amide derivative.[22]

Table 1. Parameters obtained from the simultaneous fit of ^{1}H NMRD and ^{17}O NMR data[a]

	$[Fe(H_2O)_6]^{3+}$ [d]	$Fe(EDTA)^-$	$Fe(CDTA)^-$
$^{298}r_1$ 20 MHz [mM^{-1} s^{-1}]	12.1	2.1	2.4
$^{298}\Delta^2$ [10^{20} s^{-2}]	4.2 ± 0.3	27.0 ± 1.4[e]	18.1 ± 1.3[e]
$^{298}\tau_V$ [ps]	5.3 ± 0.3	2.8 ± 0.1	3.4 ± 0.2
$A_O/\hbar$ [10^6 rad s^{-1}]	-99.3[b,c]	-64.8[b,c]	-62.8[b,c]
$^{298}\tau_M^O$ [ns]	25000 ± 3600	0.9 ± 0.9	36 ± 4.4
ΔH_M [kJ mol^{-1}]	31.4 ± 4.4	30.5 ± 1.4	51.5 ± 9.9
$^{298}\tau_R$ [ps]	60.7 ± 1.5	35.1 ± 1.7	48.4 ± 2.3
E_R [kJ mol^{-1}]	17.9 ± 1.0	25.2 ± 2.4	21.1 ± 2.3
q	6[b]	1[b]	1[b]
r_{FeH} [Å]	2.69[b,c]	2.69[b,c]	2.70[b,c]
a_{FeH} [Å]	3.5[a]	3.5[a]	3.5[a]

[a]Additional parameters fixed for fitting: E_V = 1 kJ mol^{-1}; ^{298}D = 2.24×10^5 cm^2 s^{-1}; E_D = 20 kJ mol^{-1}. [b]Parameters fixed during the fitting procedure. [c]Values obtained with DFT calculations. [d]A scalar contribution to relaxivity was included, with $A_H/\hbar$ fixed to the DFT value of 8.6×10^6 rad s^{-1}. An outer-sphere contribution to the chemical shifts with C_{OS} = 0.038 + 0.007 was considered. Proton exchange is characterized by $^{298}\tau_M^H$ = 756 + 129 ns and ΔH_M^H = 28.2 + 4.1 kJ mol^{-1}. [e]The activation energy for the modulation of the ZFS E_Δ = 7.8 + 0.5 and 9.8 + 0.5 kJ mol^{-1} for $Fe(EDTA)^-$ and $Fe(CDTA)^-$.

The inner-sphere contribution to relaxivity is given by Equation (1), where q is the number of coordinated water molecules, T_{1M} is the relaxation time of a coordinated water molecule.

$$r_1^{IS} = \frac{q}{55.55}\frac{1}{T_{1M} + \tau_M} \quad (1)$$

At high magnetic fields (> 20 MHz), T_{1M} can be approximated by eqs. (2-3):

$$\frac{\mathbf{1}}{\boldsymbol{T_{1M}}} \cong \frac{\mathbf{2}}{\mathbf{15}}\boldsymbol{\gamma_I}^{\mathbf{2}}\boldsymbol{g_e}^{\mathbf{2}}\boldsymbol{\mu_B}^{\mathbf{2}}\boldsymbol{S(S+1)r_{FeH}}^{\mathbf{-6}}\left[\frac{\mathbf{3\tau_{c1}}}{\mathbf{1+\omega_I}^{\mathbf{2}}\boldsymbol{\tau_{c1}}^{\mathbf{2}}}\right] \quad (2)$$

$$\frac{\mathbf{1}}{\boldsymbol{\tau_{c1}}} = \frac{\mathbf{1}}{\boldsymbol{\tau_M}} + \frac{\mathbf{1}}{\boldsymbol{\tau_R}} + \frac{\mathbf{1}}{\boldsymbol{T_{1e}}} \quad (3)$$

In the case of low molecular weight Mn(II) and Gd(III) complexes τ_M and T_{1e} are generally in the ns timescale, while τ_R is in the ps timescale, so that $\tau_{c1} \cong \tau_R$.[1] For $[Fe(H_2O)_6]^{3+}$ the relaxation of the electron spin is faster and $^{298}\tau_M^H$ is also relatively long, and thus τ_{c1} receives significant contributions from both T_{1e} and τ_R at high magnetic fields, explaining the different shapes of the ^{1}H NMRD profiles of Fe(III), Gd(III) and Mn(II) complexes (Figure 2). In detail, the NMRD profile simulated for Mn(II) shows a dispersion in the range 0.01 to 0.1 MHz related to the scalar contribution to relaxivity. The relaxivity decreases above 1 MHz, reaching a value of ca. 2 mM^{-1} s^{-1} above 100 MHz. The lower relaxivity of Mn(II) at high fields is due to the lower value of S(S+1) compared with Gd(III), an effect partially balanced by a shorter metal-proton distance of the coordinated water molecule (r_{GdH} and r_{MnH} were estimated to be 3.1 and 2.83 Å, respectively).[6] The relaxivity simulated for Fe(III) is relatively low at low fields, as a result of a faster electron relaxation. However, r_1 calculated at high fields is comparable, or higher, to that of Gd(III), which is explained by the contribution of T_{1e} to τ_{c1}, as well as by the short r_{FeH} distance (2.69 Å, as estimated using

DFT). From these results we can draw the following important conclusion: small Fe(III) complexes may provide relaxivities quite comparable to those of GBCAs with the same number of coordinated water molecules at the magnetic fields commonly used in MRI.

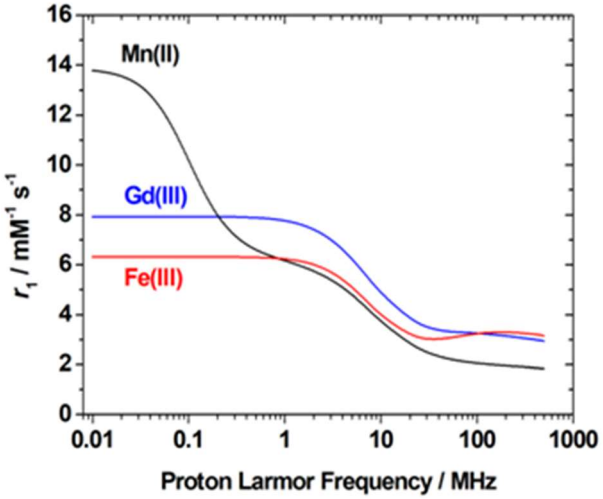

Figure 2. ^{1}H NMRD profiles simulated for q=1 complexes of Fe(III), Mn(II) and Gd(III) using the parameters determined for the corresponding aqua-ions.

Once the relaxometric properties of the $[Fe(H_2O)_6]^{3+}$ complex were deciphered, we turned our attention to the complexes with $EDTA^{4-}$ and $CDTA^{4-}$, which are known to contain a water molecule coordinated to the Fe(III) ion.[23] $Fe(EDTA)^{-}$ represents the prototype and model system of monohydrate iron(III) complexes (q = 1), but although some relaxometric data were published in the mid-1980s,[24] a complete and in-depth relaxometric study is yet missing. In particular, it is known that at neutral pH the Fe(III) ion is heptacoordinate with a water molecule in its first coordination sphere characterized by a relatively fast exchange rate. We decided to carry

out a complete study of this complex, together with the corresponding iron chelates of DTPA and CDTA, combining ^{1}H e ^{17}O NMR relaxometric measurements. Both metal chelates have a well-known pH-dependent chemical speciation (Figs. 3-4), which is reflected in the corresponding dependence of r_1 on pH, as shown in Figure 5. Relaxivity is constant in the acidic zone and up to pH ca. 6.5 for $Fe(EDTA)^-$ and 8.5 for $Fe(CDTA)^-$, where deprotonation of the bound water occurs followed by hydrolysis and formation of more complex species.

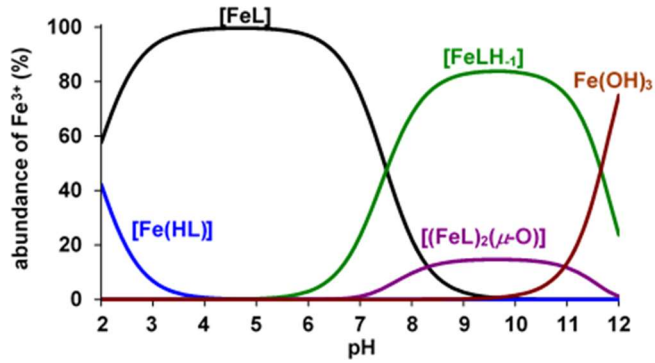

Figure 3. Species distribution of $[Fe(EDTA)]^-$ system ($[Fe^{3+}]=[CDTA]=1.0$ mM, 298 K, 0.15 M $NaNO_3$).

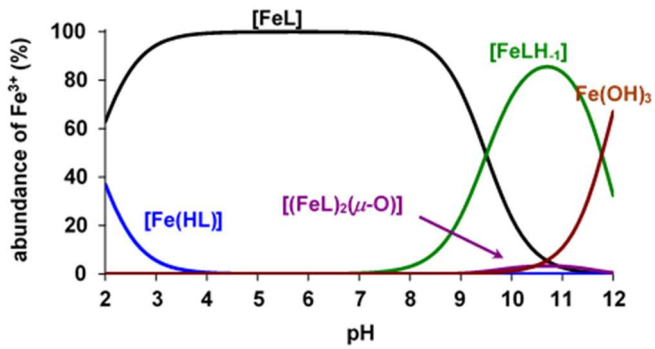

Figure 4. Species distribution of $[Fe(CDTA)]^-$ system ($[Fe^{3+}]=[CDTA]=1.0$ mM, 298 K, 0.15 M $NaNO_3$).

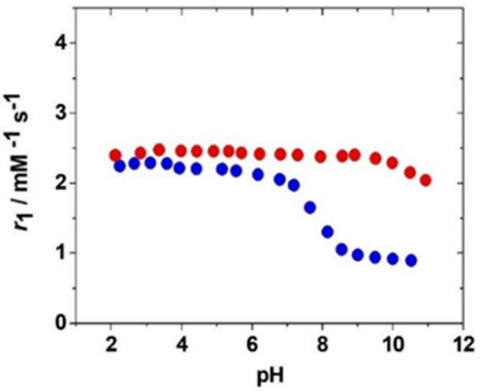

Figure 5. pH dependency of the relaxivity, r_1, at 298 K and 20 MHz for the complexes $Fe(EDTA)^-$ (blue symbols) and $Fe(CDTA)^-$ (red symbols).

Therefore, the relaxometric data were measured at pH = 5.3 where only the species $[FeL(H_2O)]^-$ is present in solution. To gain insight into the molecular parameters that control the relaxivity of the Fe(III) species, ^1H $1/T_1$ NMRD profiles were recorded at three different temperatures (283, 298 and 310 K) over a range of magnetic field strengths of 2.3×10^{-4} to 3.0 T, which correspond to proton Larmor frequencies of 0.01-127 MHz (Figure 6). An additional value at 500 MHz was measured using a high-resolution NMR spectrometer.

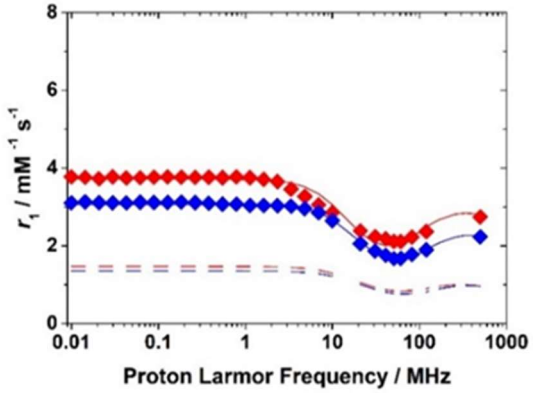

Figure 6. ^1H NMRD profiles at 298 K for the complexes $Fe(EDTA)^-$ (blue symbols) and $Fe(CDTA)^-$ (red symbols).

The profiles of the two complexes reproduce the characteristic properties observed for the aqua ion, i.e.: a plateau at low fields, a dispersion around 10 MHz, a minimum around 50-70 MHz followed by a marked increase with the observation frequency to give a large hump centred around 300 MHz. The amplitude of the NMRD profiles (Figure 7) decreases with increasing temperature across the entire range of observed frequencies (0.01-500 MHz). This shows that the residency time of the coordinated water molecule does not influence r_1, which implies that the systems are in the condition of fast exchange. This agrees with the conclusions of a previous ^{17}O NMR study.[25] Thus, the shape of the profiles confirms that, at magnetic field values of clinical MRI relevance, both molecular tumbling and electron relaxation influence relaxivity. The latter increases with the increase of the applied magnetic field and is therefore responsible for the r_1 increase at frequency values greater than 50 MHz.

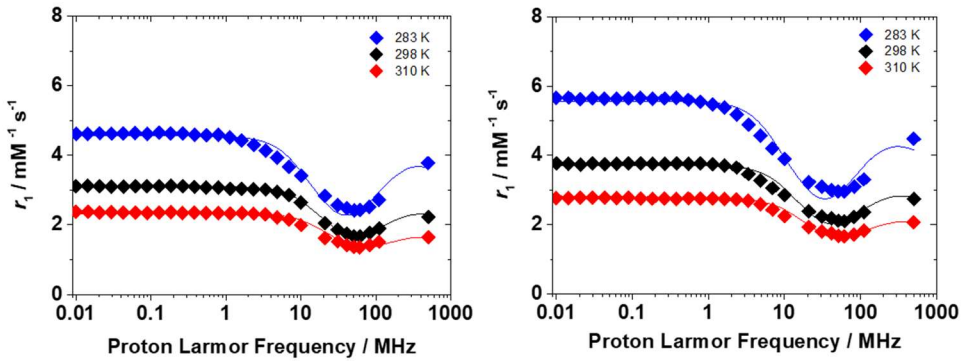

Figure 7. ^1H NMRD profiles at 283 (♦), 298 (♦) and 310 K (♦) of $Fe(EDTA)^-$ (left, $[Fe^{3+}]$ = 8.98 mM, pH = 5.3) and $Fe(CDTA)^-$ (right, $[Fe^{3+}]$ = 4.87 mM, pH = 6.98).

This in an interesting and clearly distinct behaviour from that of the small complexes of Gd(III) and Mn(II). The effect of molecular tumbling appears to be relevant in explaining the differences in the profiles of the iron complexes with EDTA and CDTA.

The lower dashed curves (Figure 6) show the calculated outer-sphere contribution. In fact, while the molecular mass of $Fe(CDTA)^-$ is about 15% greater than that of the EDTA complex, its relaxivity values are about 20-25% higher (at 60 and 120 MHz).

Although there is no clear evidence of an influence of the water exchange rate, k_{ex}, in the NMRD profiles, determining the value of this parameter is very important, as it can become a key factor in the development of neutral complexes or macromolecular systems. An estimate of the k_{ex} values for the two Fe(III) chelates were obtained about twenty years ago by measuring the temperature dependence of the ^{17}O line broadening over a wide temperature range (273 to 388 K).[23] A more accurate assessment is obtained by measuring the temperature dependence of the solvent ^{17}O NMR transverse relaxation rates, R_2, and shifts, $\Delta\omega$, of concentrated solutions of the complexes and by performing a simultaneous global fit of the ^1H and ^{17}O NMR data. We collected the data on 4.5 mM solutions of the complexes at pH = 5.5 and 11.75 T (Figure 8).

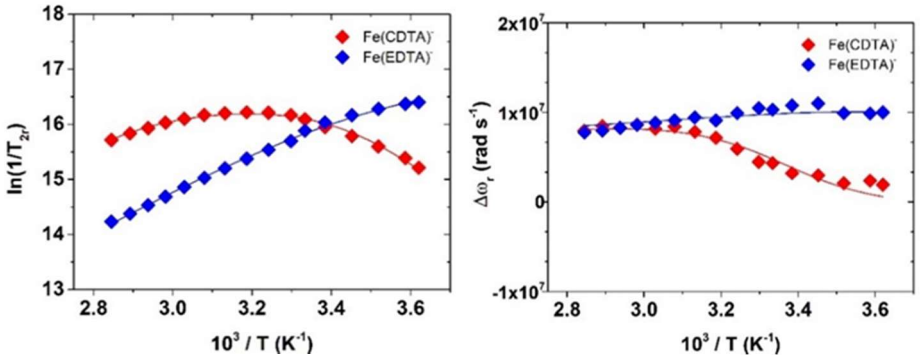

Figure 8. Temperature dependence of the reduced water ^{17}O NMR transverse relaxation rates (left) and chemical shifts (right) for the complexes $Fe(EDTA)^-$ (♦) and $Fe(CDTA)^-$(♦). Data measured at 67.78 MHz (11.74 T).

The quantitative analysis of the ^1H NMRD and ^{17}O NMR data of $Fe(CDTA)^-$ and $Fe(EDTA)^-$ was performed in a similar way than for $[Fe(H_2O)_6]^{3+}$. The parameters characterizing the outer-sphere contribution (^{298}D, E_D and a_{FeH}) were fixed, while the values of $A_O/\hbar$ and r_{FeH} were estimated with DFT calculations (Table 1). Seven-coordinate complexes with EDTA-like ligands can give rise to two diastereoisomeric forms with capped trigonal prismatic [CTP, $\Delta(\delta)/\Lambda(\lambda)$ enantiomeric pair] and pentagonal bipyramidal [PB, $\Delta(\lambda)/\Lambda(\delta)$ enantiomeric pair] coordination environments.[26] Our calculations show that for $Fe(CDTA)^-$ the CTP geometry is more stable than the PB one by a Gibbs free energy difference of 23.6 kJ mol^{-1}. However, the two diastereoisomers are virtually isoenergetic in the case of $Fe(EDTA)^-$, with the PB isomer being favoured by only 0.1 kJ mol^{-1}. Thus, the CTP diastereoisomer is likely the only one present in solution for $Fe(CDTA)^-$, while in the case of $Fe(EDTA)^-$ both the CTP and PB isomers present significant populations in solution.

Nevertheless, the two isomers are characterized by similar $A_O/\hbar$ and r_{FeH} values (Table 2).

Table 2. Calculated r_{FeO} and r_{FeH} distances and hyperfine coupling constants ($A_O/\hbar$ and $A_H/\hbar$) obtained with DFT calculations and ZFS parameters obtained with CASSF/NEVPT2 calculations.[a]

	$[Fe(H_2O)_6]^{3+}\cdot 12H_2O$	$Fe(EDTA)^-$		$Fe(CDTA)^-$	
Isomer		CTP	PB	CTP	PB
r_{FeH} [Å]	2.688	2.690	2.714	2.704	2.719
r_{FeO} [Å]	2.031	2.173	2.204	2.192	2.212
$A_O/\hbar$ [10^6 rad s^{-1}]	-99.2	-64.8	-59.4	-62.9	-58.5
$A_H/\hbar$ [10^6 rad s^{-1}]	8.69	0.43	-0.52	-0.05	-0.66
D [cm^{-1}]	0.01466	-0.1354	0.1446	-0.1415	0.1471
E [cm^{-1}]	1.14×10^{-4}	-0.0279	0.0407	0.0339	0.0426
Δ [cm^{-1}]	0.036	0.117	0.131	0.125	0.134
Δ^2 [$10^{20} s^{-2}$]	0.051	4.89	6.1	5.6	6.4

[a] CTP and PB denote the capped trigonal prismatic and pentagonal bipyramidal isomers, respectively.

The analysis of the NMRD data did not require including a scalar contribution to relaxivity, which is likely related to low $A_O/\hbar$ values of the proton nuclei of coordinated water molecules, as suggested by DFT. Finally, the temperature dependence of relaxivity could be well reproduced by allowing the zero-field splitting energy Δ to vary with temperature, following an Arrhenius behaviour with activation energy E_Δ. It is well established that relaxation of the electron spin may be the result of both transient and static ZFS contributions. For highly symmetrical complexes such as $[Fe(H_2O)_6]^{3+}$, the ZFS energy is very small (CASSCF/NEVPT2 calculations based on a CAS(5,5) active space provide Δ = 0.036 cm^{-1}, Table 2). In this case electron spin relaxation originates from the transient ZFS, which is associated with transient

distortions of the metal coordination environment occurring in solution. The static ZFS corresponds to the averaged value of all configurations existing in solution. The values of Δ^2 obtained from the fits of the data correspond to Δ = 0.28 and 0.23 cm^{-1} for $[Fe(EDTA)(H_2O)]^-$ and $[Fe(CDTA)(H_2O)]^-$, respectively. CASSCF/NEVPT2 calculations give very similar Δ values for the two complexes (~0.13 cm^{-1}). The calculated values are reasonably close to the experimental ones, taking into account that dynamic effects were not considered in this study. The values of the rotational correlation times $^{298}\tau_R$ are quite consistent with the size of the complexes. The longer $^{298}\tau_R$ value obtained for $[Fe(H_2O)_6]^{3+}$ is probably associated with the presence of a well-defined second coordination sphere promoted by the high positive charge density of the metal ion. Water exchange is several orders of magnitude faster in $Fe(EDTA)^-$ and $Fe(CDTA)^-$ than in the aqua-ion. Water exchange is also considerably faster for $Fe(EDTA)^-$ (k_{ex}^{298} = 104×10^7 s ^{1}) than for $Fe(CDTA)^-$ (k_{ex}^{298} = 2.8×10^7 s ^{1}). The k_{ex}^{298} value obtained for $Fe(CDTA)^-$ is in reasonably good agreement with previous estimates (1.3-1.7×10^7 s^{-1}), while previous works only based on ^{17}O NMR data reported much lower k_{ex}^{298} values for $Fe(EDTA)^-$ (6.0-7.2×10^7 s^{-1}).[22] The k_{ex}^{298} value determined for $Fe(EDTA)^-$ is endowed with a rather large error, as k_{ex} provides a significant contribution to T_{2r} only at low temperatures. Nevertheless, our combined ^1H and ^{17}O NMR data suggests that previous works underestimated the water exchange rate in $Fe(EDTA)^-$. The lower water exchange rate determined for $Fe(CDTA)^-$ can be attributed to the rigidifying effect of the cyclohexyl backbone, which increases the energy cost required to reach the transition state.[27]

The Fe(III) ion forms with the octadentate ligand DTPA a purely outer sphere (OS) complex (q = 0), hence it represents an effective model to compare the measured r_1 values with those calculated for the OS contribution. The NMRD profiles of $Fe(DTPA)^{2-}$ were measured in the Larmor frequency range 0.01 to 500 MHz and at temperatures of 283, 298 and 310 K, at neutral pH (Figure 9). The experimental and calculated OS profiles are completely similar in shape, while small differences in amplitude are associated with small differences in a_{FeH} and in the parameters of the electron relaxation (Table 3).

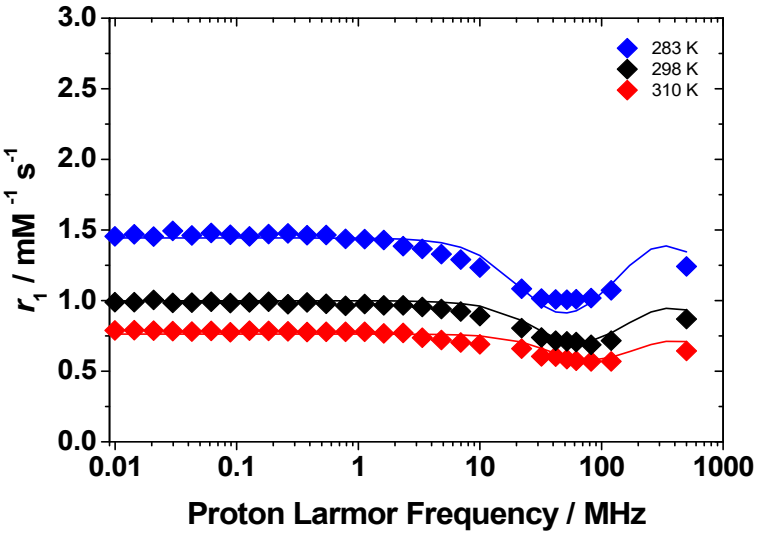

Figure 7. ^1H NMRD profiles at 283 (♦), 298 (♦) and 310 K (♦) of $Fe(DTPA)^{2-}$ (left, $[Fe^{3+}]$ = 5.31 mM, pH = 7.08).

Table 3. Parameters obtained from the simultaneous fit of ^{1}H NMRD data.[a]

	$Fe(DTPA)^{2-}$
$^{298}r_1$ 20 MHz [mM^{-1} s^{-1}]	0.81
$^{298}\Delta^2$ [10^{20} s^{-2}]	3.9 ± 0.1
E_Δ [kJ mol^{-1}]	8.1 ± 2.5
$^{298}\tau_V$ [ps]	3.4 ± 0.9
E_v [kJ mol^{-1}]	1.0[a]
^{298}D [10^5 cm^2 s^{-1}]	2.24[a]
E_D [kJ mol^{-1}]	20.0[a]
q	0[a]
a_{FeH} [Å]	3.5[a]

[a] parameters fixed during the fitting procedure.

The assessment of the thermodynamic stability and kinetic inertness of the metal-based contrast agents is important to avoid the transmetallation and transchelation reactions with the challenging endogenous components. In particular, Fe(III) complexes can hydrolyse forming hydroxo and oxo complexes at high pH values and can be transchelated by transferrins. In fact, transferrins, like serum transferrin (sTf), ovotransferrin (OTf) or lactoferrin (LTf), are strong Fe(III)-binding proteins with one Fe(III)-binding site in each lobe.[28] The human sTf and LTf are known to bind Fe(III) with high affinity ($\log K_{FeTf}$ = 22.8, $\log K_{Fe2Tf}$ = 21.5), which requires the concomitant binding of a synergistic bicarbonate anion.[29] Since serum transferrin is normally only 30% saturated with Fe(III), it retains a relatively high capacity to compete with Fe(III)-complexes. Thus, we conducted potentiometric titrations to determine the protonation constants of the ligands (Table

4), while spectrophotometric experiments were performed to determine the equilibrium constants that describe solution speciation of the Fe(III)-EDTA and Fe(III)-CDTA systems. The protonation constants of EDTA and CDTA ligands, defined by Eq. (4), were determined by pH-potentiometry.

$$K_i^{\boldsymbol{H}} = \frac{[H_i L]}{[H_{i-1}][H^+]} \tag{4}$$

where i=1, 2…6. The $\log K_i^H$ values obtained by pH-potentiometry are listed in Table 4. Standard deviations (3σ) are shown in parentheses. The stability and protonation constants of Fe(III) complexes formed with EDTA and CDTA, defined by Eqs. (5) and (6), were investigated by pH-potentiometry and spectrophotometry at 298 K in 0.15 M $NaNO_3$ solution.

$$\boldsymbol{K_{ML}} = \frac{[ML]}{[M][L]} \tag{5}$$

$$\boldsymbol{K_{MHL}} = \frac{[MHL]}{[ML][H^+]} \tag{6}$$

The stability constants of $Fe(EDTA)^-$ and $Fe(CDTA)^-$ were determined by spectrophotometry. The equilibrium reaction (Eq. (7)) was studied in the $[H^+]$ range of 0.02 – 5.6 M (the ionic strength was constant $I=[Na^+]+[H^+]=0.15$ M in the samples $[H^+]\leq 0.15$ M), where the formation of Fe^{3+}, FeHL, FeL and H_xL species was assumed (x=4 and 5; y=3, 4 and 5). Some characteristic absorption spectra are shown in Figures 8 and 9.

$$Fe^{3+} + H_xL \rightleftharpoons [Fe(H_{x-y}L)] + yH^+ \quad (7)$$

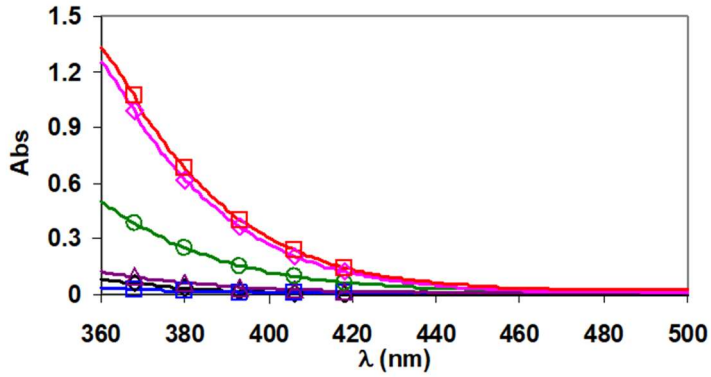

Figure 8. Absorption spectra of Fe^{3+}-EDTA systems. Solid lines and open symbols represent the measured and calculated absorbance values ([Fe^{3+}]=1.974 mM, [EDTA]=1.996 mM, [H^+]=5.686 M, 3.000 M, 1.498 M, 0.997 M, 0.329 M and 0.100 M, [H^+]≤0.15 M → [HNO_3]+[$NaNO_3$]=0,15 M, 298 K).

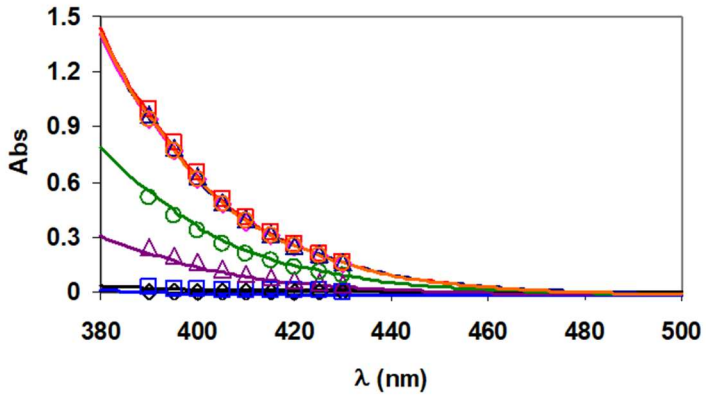

Figure 9. Absorption spectra of Fe^{3+}-CDTA systems. Solid lines and open symbols represent the measured and calculated absorbance values ([Fe^{3+}]=1.989 mM, [CDTA]=2.011 mM, [H^+]=5.687 M, 3.006 M, 1.496 M, 0.999 M, 0.332 M, 0.100 M, 0.030 M and 0.017 M [H^+]≤0.15 M → [HNO_3]+[$NaNO_3$]=0,15 M, 298 K).

Since the molar absorptivities of Fe^{3+} is significantly lower than that of $Fe(EDTA)^-$ and $Fe(CDTA)^-$ complexes in the wavelength range of 360 – 440 nm, the increase of the absorbance values of the Fe^{3+}-EDTA and Fe^{3+}-CDTA systems can be explained by the formation of FeL and FeHL species dominating at $[H^+]<1.5$ M.

The protonation constants of $Fe(EDTA)^-$ and $Fe(CDTA)^-$ complexes were determined by pH-potentiometric titrations of the complexes in the pH range 1.7 – 12.0 ([FeL]=10 mM). At pH>6.0 the titrations curves indicate the base consumption process which can be interpreted by the hydrolysis of the Fe(III) ion with the coordination of OH^- ion (Eq. (8)) and by the dimerization of the FeL (Eq. (9)) $FeLH_{-1}$ species (Eq. (10)) via the formation of μ-oxo dimers.

$$FeLH_{-1} + H^+ \rightleftharpoons FeL \tag{8}$$

$$\boldsymbol{K_{FeLH_{-1}}} = \frac{[FeL]}{[FeLH_{-1}][H^+]}$$

$$2FeL \rightleftharpoons [(FeL)_2(\mu\text{-}O)] + H^+ \tag{9}$$

$$\boldsymbol{K_D} = \frac{[(FeL)_2(\mu - O)][H^+]}{[FeL]^2}$$

$$2FeLH_{-1} \rightleftharpoons [(FeL)_2(\mu\text{-}O)] \tag{9}$$

$$\boldsymbol{K_d} = \frac{[(FeL)_2(\mu - O)]}{[FeLH_{-1}]^2}$$

According to the method proposed by Gustafson and Martell,[29] the protonation and dimerization constant of FeL and $FeLH_{-1}$ species were calculated from the pH potentiometric titration data ($[FeL]_{tot}$, $[NaOH]_{tot}$, pH, pA and pK_w) obtained in the pH ranges 4.0 – 9.0 for $Fe(EDTA)^-$ and 7.5 – 10.5 for $Fe(CDTA)^-$. The stability and protonation constants of the Fe(III)-complexes formed with EDTA and CDTA ligands are reported in Table 4.

Table 4. Protonation constants of EDTA and CDTA, stability and protonation constants of $Fe(EDTA)^-$ and $Fe(CDTA)^-$ complexes (298 K).

	CDTA		**EDTA**	
I	0.15 M $NaNO_3$	0.1 M KNO_3[a]	0.15 M $NaNO_3$	0.1 M KNO_3[b]
log K_1^H	9.54 ± 0.02	12.30	9.40 ± 0.01	10.22
log K_2^H	6.08 ± 0.02	6.12	6.10 ± 0.01	6.18
log K_3^H	3.65 ± 0.03	3.49	2.72 ± 0.01	2.70
log K_4^H	2.69 ± 0.03	2.40	2.08 ± 0.01	2.00
log K_5^H	1.14 ± 0.04	1.60	1.23 ± 0.01	–
$\Sigma \log K_i^H$	**23.11**	**25.91**	**20.29 ($-\log K_5^H$)**	**21.10**
	$Fe(CDTA)^-$		**$Fe(EDTA)^-$**	
I	0.15 M $NaNO_3$	0.1 M KNO_3[c]	0.15 M $NaNO_3$	0.1 M KNO_3[c]
$\log K_{FeL}$	**24.36 ± 0.02**	**29.05**	**22.14 ± 0.04**	**24.95**
$\log K_{FeHL}$	1.77 ± 0.02	–	1.12 ± 0.02	–
$\log K_{FeLH-1}$	9.50 ± 0.02	9.54	7.51 ± 0.01	7.52
$-\log K_D$	17.64 ± 0.04	18.03	13.00 ± 0.03	12.40
$\log K_d$	1.40 ± 0.03	1.07	2.02 ± 0.02	2.64

[a] Ref.[31]; [b]Ref.[32]; [c] Ref.[33].

It is well known that the equilibrium constants are generally determined in the presence of the constant ionic background (some salts like KCl, NaCl, etc.) which should be selected with the necessary care since its cation can react with the donor atoms of the ligand (determination of the protonation constants) or its counter ion may interact with the metal ion (determination of the stability and protonation constant). The $\log K_i^H$ and $\log K_{ML}$ values, published in

literature were most frequently determined in 0.1 M KCl or 0.1 M Me_4NCl.[34] The protonation constants of ligands, particularly the $\log K_1^H$ values determined in the presence of Na^+ ion are generally lower than those obtained in solutions, where the constant ionic strength was controlled by K^+ or Me_4N^+ salts. The $\log K_i^H$ values obtained in NaCl, $NaNO_3$ or $NaClO_4$ solutions are lower because the interaction between the smaller Na^+ ion and the fully deprotonated ligands is stronger than that of the larger K^+ or Me_4N^+ ions. The difference is particularly high for CDTA ligand which form relatively stable complexes with Na^+ ($\log K_{Na(CDTA)}$=4.66; 0.5 M Me_4NCl, 298 K;[35] $\log K_{Na(EDTA)}$=1.82; 0.1 M Me_4NCl, 298 K).[36] Moreover, the Cl^- as a counter ion of the ionic background might interact with Fe^{3+} ion via the formation of $FeCl_x$ complexes (x=1, 2, 3 and 4). Therefore, all the equilibrium studies were performed at 298 K in 0.15 M $NaNO_3$ solution. Thus, background electrolyte $NaNO_3$ (0.15 M) was used to mimic the high Na^+ concentrations present in vivo (~0.15 M in blood plasma). Therefore, the $\log K_1^H$ values of EDTA and CDTA are lower by 0.8 and 2.8 $\log K$ units than in the presence of 0.1 M KNO_3 ionic background, as a result of the formation of $Na(EDTA)^{3-}$ and $Na(CDTA)^{3-}$ complexes. Also the stability constant of the $Fe(EDTA)^-$ and $Fe(CDTA)^-$ complexes are lower by 2.8 and 4.7 $\log K$ units than the $\log K_{FeL}$ values previously measured in 0.15 M KNO_3 (Table 4).[33] These results show that the high Na^+ concentrations present *in vivo* have a significant impact in the stability of the complexes. The equilibrium constants characterizing the formation of $FeLH_{-1}$ ($\log K_{FeLH-1}$, Eq. (7)) and the dimeric [$(FeL)_2(\mu$-O)] species by the dimerization of FeL ($-\log K_D$, Eq. (8)) and $FeLH_{-1}$ species ($\log K_d$, Eq. (9)) of $Fe(EDTA)^-$ and $Fe(CDTA)^-$ are very similar in 0.15 M $NaNO_3$ and 0.1 M KNO_3 solutions.

In accordance with previous studies,[30,33] the K_D and K_d values confirm the lower tendency of $Fe(CDTA)^-$ to form the oxo-bridged dimer than $Fe(EDTA)^-$. The speciation diagrams obtained with the equilibrium constants (Figure 3 and 4) evidence that $Fe(CDTA)^-$ does not hydrolyze significantly at physiological pH, while the EDTA complex presents significant populations of the hydroxo-complex and μ–oxo dimer at pH 7.4.

The stability constants (I = 0.15 M $NaNO_3$, Table 5) show that the $Fe(CDTA)^-$ complex is significantly more stable than $Fe(EDTA)^-$. The stability constants are significantly lower than those determined in 0.1 M KNO_3 ($\log K_{FeL}$ = 29.05 and 24.95 for $Fe(CDTA)^-$ and $Fe(EDTA)^-$, respectively).[25] This indicates that the Na^+ ion reduces the stability of Fe(III)-complexes due to its interaction with the ligands. The equilibrium constants characterizing the deprotonation of the coordinated water molecule ($\log K_{FeLH-1}$) confirm that the hydrolysis does not occur at physiological pH for $Fe(CDTA)^-$, in perfect agreement with the relaxivity pH dependency showed above (see Figures 3-4). At higher pH, complexes form an oxo-bridged dimer. The equilibrium constants characterizing dimer formation (K_D and K_d, Table 4) confirm previous results that pointed to a lower tendency of $Fe(CDTA)^-$ to form the oxo-bridged dimer than $Fe(EDTA)^-$.[25]

The kinetic inertness of $Fe(EDTA)^-$ and $Fe(CDTA)^-$ was assessed by transchelation reactions with the HBED ligand, which provided the rates characterizing the spontaneous dissociation k_0 and first and second order hydroxide-assisted dissociation rates (k_{OH} and k_{OH}^2, respectively, Table 5).[37] The rates of the transchelation reactions (Eq. (10)) between FeL complexes and HBED were studied by spectrophotometry.

$$A_t = (A_0 - A_p)e^{-k_d t} + A_p \quad (10)$$

where A_t, A_0 and A_p are the absorbance values at time t, the start of the reaction and at equilibrium, respectively. Some characteristic absorption spectra are shown in Figures 10 and 11.

$$FeL + HBED \rightleftharpoons Fe(HBED) + L \qquad (L=EDTA, CDTA) \quad (11)$$

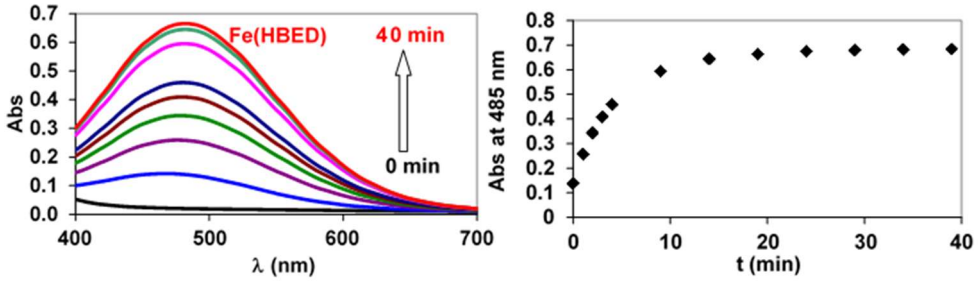

Figure 10. Absorption spectra of $Fe(EDTA)^-$ – HBED reacting system [$Fe(EDTA)^-$]=2.0×10^{-4} M, [HBED]=2.0×10^{-3} M, pH=11.05, [Na_2HPO_4]=0.01 M, 0.15 M $NaNO_3$, 298 K).

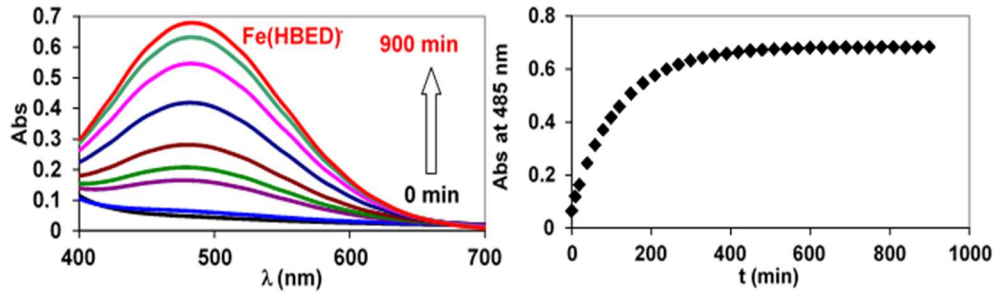

Figure 11. Absorption spectra of $Fe(CDTA)^-$ – HBED reacting system [$Fe(CDTA)^-$]=2.0×10^{-4} M, [HBED]=2.0×10^{-3} M, pH=11.94, [Na_2HPO_4]=0.01 M, 0.15 M $NaNO_3$, 298 K).

In the presence of excess exchanging HBED ligand the transchelation can be treated as a pseudo-first-order process and the rate of the reactions can be expressed with the Eq. (12), where k_d is a pseudo-first-order rate constant and $[FeL]_t$ is the total concentration of the complex.

$$-\frac{d[FeL]_t}{dt} = k_d[FeL]_t \quad (12)$$

The rates of the transmetallation reactions were studied at different concentrations of the HBED ligand in the pH range 7.4 – 12.5. The obtained pseudo-first order rate constants k_d are presented in Figure 12 as a function of pH.

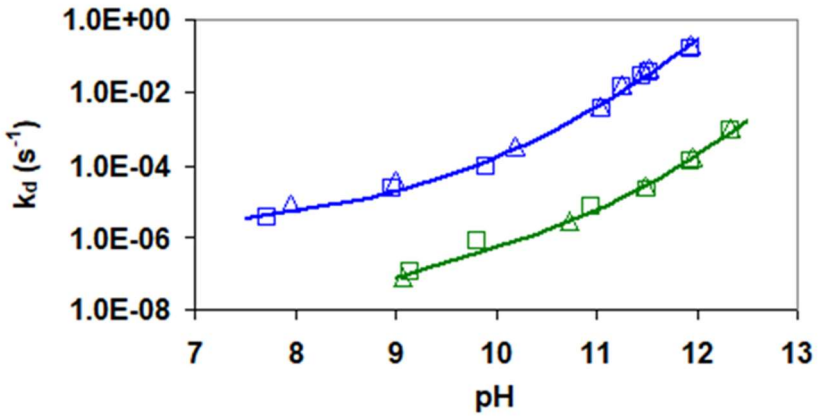

Figure 12. k_d pseudo-first-order rate constant characterizing the transchelation reactions of $Fe(EDTA)^-$ and $Fe(CDTA)^-$ with HBED ligand. Solid lines and the open symbols represent the calculated and measured k_d rate constants. ($[Fe(EDTA)^-]=[Fe(CDTA)^-]=2.0\times10^{-4}$ M, [HBED]=2.0 (□,□) and 4.0 mM (△,△), [HEPES]=[piperazine]=[Na_2HPO_4]=0.01 M, 0.15 M $NaNO_3$, 298 K).

The kinetic data presented in Figure 12 show that the k_d values are independent on [HBED] and increase with pH, indicating that the rate-determining step of the transchelation reactions is the dissociation of the $Fe(EDTA)^-$ and $Fe(CDTA)^-$ complexes, followed by the fast reaction between the free Fe^{3+} ion and the exchanging HBED ligand. By considering the species distribution of Fe^{3+}-EDTA and Fe^{3+}-CDTA systems, the dependence of the k_d values on pH can be interpreted as spontaneous dissociation (k_0, Eq. (11)) and OH^--ion assisted dissociation (k_{OH}, Eq. (13) and k_{OH}^2, Eq. (14)) of the $FeLH_{-1}$ species dominates in the investigated pH ranges.

$$FeLH_{-1} \xrightarrow{k_0} Fe^{3+} + L + OH^- \quad (13)$$

$$FeLH_{-1} + OH^- \xrightarrow{k_{OH}} Fe^{3+} + L + OH^- \quad (14)$$

$$FeLH_{-1} + 2OH^- \xrightarrow{k_{OH}^2} Fe^{3+} + L + 2OH^- \quad (15)$$

By taking into account all possible pathways and Eq. (12), the rate of the dissociation of $Fe(EDTA)^-$ and $Fe(CDTA)^-$ can be expressed by Eq. (16).

$$-\frac{d[FeL]_t}{dt} = k_d[FeL]_t = k_0[FeLH_{-1}] + k_{OH}[FeLH_{-1}][OH^-] + k_{OH}^2[FeLH_{-1}][OH^-]^2 \quad (16)$$

Considering the total concentration of the $Fe(EDTA)^-$ and $Fe(CDTA)^-$ complexes ($[FeL]_t=[FeL]+[FeLH_{-1}]$) and the protonation constant of $FeLH_{-1}$ (K_{FeLH-1}, Eq. (8)), the k_d pseudo-first-order rate constants

presented can be expressed by Eq. (15). Based on the species distribution of the Fe^{3+}-EDTA and Fe^{3+}-CDTA systems at $[Fe^{3+}]=[EDTA]=[CDTA]=0.2$ mM, the formation of the dimeric $[(FeL)_2(\mu\text{-}O)]$ species can be neglected in our experimental conditions.

$$k_d = \frac{k_0 + k_{OH}\left(\frac{K_W}{[H^+]}\right) + k_{OH}^2\left(\frac{K_W}{[H^+]}\right)^2}{1 + K_{FeLH_{-1}}[H^+]} \quad (17)$$

where k_0, k_{OH} and k_{OH}^2 are the rate constants characterizing the spontaneous and OH^- assisted dissociation of $FeLH_{-1}$ species, K_w is the stoichiometric water ionic product, whereas $K_{FeLH\text{-}1}$ is the protonation constant of the $FeLH_{-1}$ species. The rate and protonation constants characterizing the transchelation reactions of $Fe(EDTA)^-$ and $Fe(CDTA)^-$ complexes with HBED were calculated by fitting the k_d values presented in Figure 12 to the Eq. (17).

The comparison of the rate constants reported in Table 5 reveals that the spontaneous and the first and second order OH^- assisted dissociations of $Fe(EDTA)^-$ are about 15, 280 and 1200 times faster than those of $Fe(CDTA)^-$. The significantly slower dissociation of the $Fe(CDTA)^-$ is explained by the structural rigidity of the CDTA ligand due to the presence of the cyclohexyl moiety on the ligand backbone,[27] as observed for the Mn(II) analogues.[38] The dissociation rate constant (k_d) of $Fe(CDTA)^-$ calculated near to physiological condition (pH=7.4, 25°C), is approximately 1000 times lower than that of $Fe(EDTA)^-$, i.e. the former complex is more inert.

Table 5. Equilibrium and rate (k_i) constants, and half-lives ($t_{1/2}$=ln2/k_d) characterizing the stability and dissociation reactions of Fe(EDTA)$^-$ and Fe(CDTA)$^-$ complexes (0.15 M $NaNO_3$, 25°C).

	Fe(EDTA)$^-$	Fe(CDTA)$^-$
$\log K_{FeL}$	22.14± 0.04	24.36 ± 0.02
$\log K_{FeLH-1}$	7.51(1)[b] / 7.41 (2)[c]	9.50(2)[b] / 9.58(4)[c]
k_0 (s^{-1})	$(5 \pm 1) \times 10^{-6}$	$(3.2 \pm 0.5) \times 10^{-7}$
k_{OH} ($M^{-1}s^{-1}$)	1.0 ± 0.2	$(3.6 \pm 0.8) \times 10^{-3}$
k_{OH}^2 ($M^{-2}s^{-1}$)	$(1.4 \pm 0.2) \times 10^3$	1.2 ± 0.1
k_d (s^{-1}) at pH=7.4	2.9×10^{-6}	2.1×10^{-9}
$t_{1/2}$ (h) at pH=7.4	66	8.9×10^4
$E_{1/2}$ [mV vs SCE] [d]	-132.5	-150.5

[b] From spectrophotometric titrations; [c] From dissociation experiments; [d] From Ref [24] (E(NHE)=E(SCE)+0.242V).

It is worth highlighting that for Mn(II) complexes the kinetic inertness is a crucial issue to achieve and typically they follow an acid-assisted dissociation pathway. In general, they tend to form less stable and inert complexes than Fe(III) ($\log k_{MnEDTA}$ = 12.46; $\log k_{MnCDTA}$=14.32; $t_{1/2}$MnEDTA=0.076 h; $t_{1/2}$MnCDTA=12.3 h (pH 7.4).[30]

Importantly, Fe(III)-based compounds may participate in the redox cycle by taking the electron from the reducing agent, which is followed by its reduction and the concomitant electron transfer to H_2O_2 (Fenton reaction). According to the concentration and the redox properties of the possible reducing agents in human blood plasma, ascorbic acid is the most relevant candidate to involve Fe(III)-complexes into the Fenton reaction.[31] The redox stability of Fe(EDTA)$^-$ and Fe(CDTA)$^-$ was investigated via the reduction of the Fe(III)-

complexes with ascorbic acid monitored by spectrophotometry (pH=7.4, 25°C in 0.15 M $NaNO_3$).

Some characteristic absorption spectra are shown in Figures 13 and 14.

$$2Fe^{III}L + HA^- \longrightarrow 2Fe^{II}L + A + H^+ \quad (L=EDTA, CDTA) \qquad (18)$$

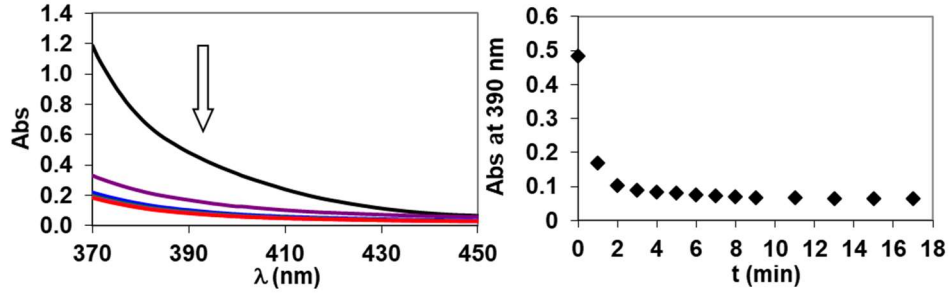

Figure 13. Absorption spectra and absorbance values of the $Fe(EDTA)^-$–ascorbic acid reacting system ($[Fe(EDTA)^-]=2.0\times10^{-3}$ M, [ascorbic acid]=0.02 M, pH=7.40, [HEPES]=0.01 M, 0.15 M $NaNO_3$, 298 K).

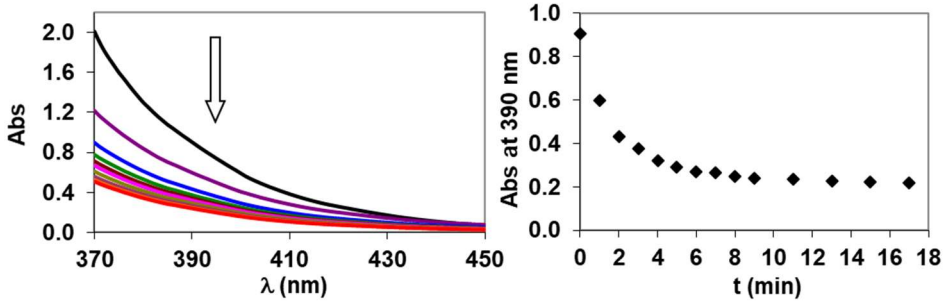

Figure 14. Absorption spectra and absorbance values of the $Fe(CDTA)^-$–ascorbic acid reacting system ($[Fe(CDTA)^-]=2.0\times10^{-3}$ M, [ascorbic acid]=0.02 M, pH=7.40, [HEPES]=0.01 M, 0.15 M $NaNO_3$, 298 K).

In the presence of excess ascorbic acid the reduction of the Fe(III)-complexes can be treated as a pseudo-first-order process and the rate of reactions can be expressed with Eq. (19), where k_{obs} is a pseudo-

first-order rate constant and $[FeL]_t$ is the total concentration of the Fe(III)-complexes.

$$-\frac{d[FeL]_t}{dt} = k_{obs}[FeL]_t \quad (19)$$

Rates of the reduction of the Fe(III)-complexes were studied at pH=7.4 and at different concentrations of ascorbic acid. The obtained pseudo-first order rate constants k_{obs} as a function of $[Fe^{III}L]$ are presented in Figure 15.

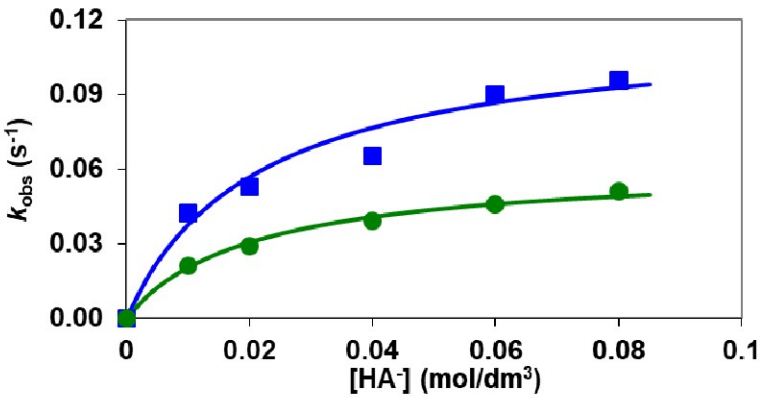

Figure 15. k_{obs} pseudo-first-order rate constant characterizing the reduction of $Fe(EDTA)^-$ (■) and $Fe(CDTA)^-$ (●) by ascorbic acid. Solid lines and the open symbols represent the calculated and measured k_d rate constants. ($[Fe^{III}L]=2.0\times10^{-3}$ M, [HEPES]=0.01 M, 0.15 M NaNO3, 298 K).

The kinetic data in Figure 15 indicates that the k_{obs} shows a saturation curve as a function of $[HA^-]$, which might be interpreted by the formation of the reaction intermediate and the rate determining transformation of the intermediate to the final product. By taking into account the protonation constants of ascorbic acid ($\log K_1^H$=11.34,

$\log K_2^H$=4.04, 0.1 M KNO_3, 298 K)[39], the monohydrogenascorbate HA^- species dominates in our experimental conditions (pH=7.4, 298 K, 0.15 M $NaNO_3$). According to the kinetic data, the electron-transfer might occur by the formation of the ternary $Fe^{III}L$-HA intermediate between the ascorbate anion (HA^-) and the $Fe^{III}L$ complex (Eq. (21)) replacing the inner-sphere water molecule ({$Fe^{III}L$-HA}, Eq. (20)). The $Fe^{III}L$ might also react rapidly with the radical (Eq. (22)) formed in the previous step. The presence of free radicals in the oxidation of ascorbic acid was confirmed by EPR measurements.[40]

$$Fe^{III}L + HA^- \overset{K_{FeL\text{-}HA}}{\rightleftharpoons} \{Fe^{III}L\text{-}HA^-\} \quad (20)$$

$$\boldsymbol{K_{FeL-HA} = \frac{[\{Fe^{III}L - HA^-\}]}{[Fe^{III}L][HA^-]}}$$

$$\{Fe^{III}L\text{-}HA^-\} \xrightarrow{k_{HA}} Fe^{II}L + \text{radical} \quad (21)$$

$$Fe^{III}L + \text{radical} \xrightarrow{fast} Fe^{II}L + A + H^+ \quad (22)$$

By taking into account all possible pathways and Eq. (19), the rate of the reduction of $Fe(EDTA)^-$ and $Fe(CDTA)^-$ with ascorbic acid can be expressed by Eq. (23).

$$\boldsymbol{-\frac{d[FeL]_t}{dt} = k_{obs}[FeL]_t = k_{HA}[Fe^{III}L - HA]} \quad (23)$$

Considering the total concentration of the $Fe^{III}L$ ($[FeL]_t=[FeL]+[FeLH_{-1}]+[Fe^{III}L\text{-}HA]$), the formation of $FeLH_{-1}$ species (Eq. (8)) and the ternary $Fe^{III}L$-HA intermediate (Eq. (20)), the k_{obs} pseudo-first-order rate constants presented can be expressed by Eq. (24).

$$\boldsymbol{k_{obs} = \frac{k[HA^-]}{1 + K_{FeL-HA}[HA^-] + \left(K_{FeLH_{-1}}[H^+]\right)^{-1}}} \qquad (24)$$

where $k=k_{HA}K_{FeL\text{-}HA}$ and $K_{FeL\text{-}HA}$ are the rate and the equilibrium constants characterize the ascorbate anion assisted reduction of the Fe(III)-complexes and the formation of the ternary $Fe^{III}L$-HA intermediate, respectively. The k and $K_{FeL\text{-}HA}$ values of $Fe(EDTA)^-$ and $Fe(CDTA)^-$ complexes have been calculated by fitting of the kinetic data (Figure 15) to Eq. (24).

According to the kinetic data, the electron-transfer occurs by the formation of the ternary $Fe^{III}L$-HA intermediate between the ascorbate anion (HA^-) and the $Fe^{III}L$ complex, likely through the substitution of the inner-sphere water molecule. The formation of a similar ternary $Fe(EDTA)^-$-oxalate complex was identified by the pH-potentiometric studies of the $Fe(EDTA)^-$–oxalate system ($Fe^{III}(EDTA)^-$-Ox: $K_{FeL\text{-}Ox}$=275 M^{-1}).[41] The k_{HA} rate constants characterizing the ascorbate anion assisted reduction of the $Fe(EDTA)^-$ and $Fe(CDTA)^-$ were found to be 8 ± 2 and 3.0 ± 0.2 $M^{-1}s^{-1}$ at pH=7.4. By taking into account the stability of the ternary $Fe^{III}L$-HA intermediates ($Fe^{III}(EDTA)^-$-HA: $K_{FeL\text{-}HA} = 75 \pm 15$ M^{-1}; $Fe^{III}(CDTA)^-$-HA: $K_{FeL\text{-}HA} = 40 \pm 5$ M^{-1}) and the *in vivo* concentration of the ascorbate anion ($[HA^-]$=43 μM),[42] the ascorbate-assisted reduction rate (k_{obs}) and half-lives ($t_{1/2}$ = ln2/k_{obs}) of $Fe(EDTA)^-$ and $Fe(CDTA)^-$ are 2.4×10^{-4} and 1.3×10^{-4} s^{-1}, (0.8 and 1.5 hours, respectively).

Thus, the half-lives of the complexes near physiological condition are about 83 ($Fe(EDTA)^-$) and 59000 ($Fe(CDTA)^-$) times faster upon reduction than in the absence of the reducing agent.

Based on previous studies[43,44] the ascorbate-assisted reduction rate constant of $Fe^{III}L$ complexes is expected to decrease with the electrode potential of $Fe^{III}L$, as confirmed by the 1.8 times slower reduction of $Fe(CDTA)^-$ with respect to $Fe(EDTA)^-$. Since the electrode potential is correlated to the thermodynamic stability constant of $Fe^{III}L$, we emphasize that the thermodynamic properties of the Fe(III)-complexes play a very important role together to the kinetic ones for their in vivo applications. Ascorbic acid is a strong reducing agent ($H_2A \rightarrow A + 2H^+ + 2e^-$ $E^0 = 0.39$ V vs. NHE),[45] however, the reduction potential is strongly influenced by the pH and the formation of the HA· and $A^{\cdot -}$ radicals as intermediates. Thus, at physiological condition, the electrode potential of the Fe^{III}/Fe^{II}-complex redox couple should be lower than –0.2 V vs. NHE to avoid the formation of Fe(II)-complexes and the occurrence of the Fenton reactions.[46]

4.3 Conclusions

We have shown here that monohydrated Fe(III) complexes are very attractive candidates for the design of efficient MRI contrast agents, in particular at the high magnetic fields of modern clinical scanners and of those used in animal studies. The detailed multinuclear relaxometric analysis over a wide range of proton Larmor frequencies, performed for the first time for Fe(III) complexes, revealed some key differences as compared to related Mn(II) and Gd(III) complexes. The relaxivity of Fe(III) complexes at high fields receives contributions from

both τ_R and T_{1e}, which assume values of the same order of magnitude between ca 1.5 and 3 T (Figure 16).

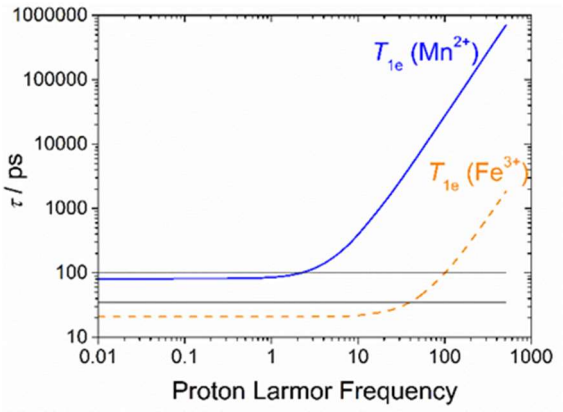

Figure 16. Values of T_{1e} calculated with the parameters obtained from the relaxometric data of Mn(II) and Fe(III) complexes with EDTA. The horizontal lines indicate the range of τ_R values typical of small complexes (35 to 100 ps).

On the other hand, T_{1e} is considerably longer for Mn(II) and Gd(III) complexes, hence T_{1e} affects relaxivity only below ~10 MHz. We anticipate that optimization of both T_{1e} and τ_R will allow obtaining Fe(III) complexes with effectiveness (relaxivity) even higher than that of the commercially available and clinically used agents. Another important conclusion of the present work is that the properties of Fe(III) contrast agent candidates must be tuned to: i) increase the pK_a of the coordinated water molecule well above physiological pH, ii) obtain kinetically inert complexes, for example by ligand rigidification, and iii) shift the reduction potential of the complex out of the biological window (E^0 < –0.2 V vs. NHE), to avoid complex dissociation upon reduction and also triggering the Fenton reaction. In this perspective, coordination chemistry appears to be able to play an

important role as two structurally very similar compounds such as the iron(III) complexes of EDTA and CDTA have markedly different pK_a values of bound water. The small structural differences between the two chelates also result in significantly different k_{ex} values and suggests the possibility of modulating this parameter through a suitable chemical design, as successfully happened in the case of Gd(III) complexes. Even the kinetic inertia seems significantly depend on structural aspects seemingly minor. Then, the CDTA scaffold is clearly better suited for the design of Fe(III)-based MRI contrast agents than it is EDTA.

It will be necessary to understand, at least from an empirical point of view through the collection of a large number of new data, if it is conceivable to optimize the electronic relaxation time with an appropriate design of the ligand as this would allow to increase the relaxation and tune the frequency value corresponding at its maximum value. So, while much remains to be done, we hope that these results may represent useful guidelines for the development of metal-diagnostic probes of improved safety, biotolerability and efficacy.

4.4 Notes and References

Author contribution: the author carried out all the relaxometric measurements. The relaxometric data were analysed under the supervision of Professor Mauro Botta and Professor Carlos Platas-Iglesias. The work proposed in this chapter has been published as a scientific paper: Baranyai, Z.; Carniato, F.; Nucera, A.; Horváth, D.; Tei, L.; Platas-Iglesias, C.; Botta, *Chem. Sci.* **2021**, 12 (33), 11138–11145.

(1) (a) A. E. Merbach, L. Helm and E. Toth, The Chemistry of Contrast Agents in Medical Magnetic Resonance Imaging, *John Wiley & Sons Ltd, 2nd edn*, **2013**; (b) J. Wahsner, E. M. Gale, A. Rodríguez-Rodríguez, P. Caravan, *Chem. Rev.,* **2019**, 119, 957-1057.

(2) (a) E. A. Akam, E. Abston, N. J. Rotile, H. R. Slattery, I. Y. Zhou, M. Lanuti and P. Caravan, *Chem. Sci.*, **2020**, 11, 224-231. (b) M. Botta, L. Tei, *Eur. J. Inorg. Chem.*, **2012**, 1945-1960; (c) A. J. L. Villaraza, A. Bumb, M. W. Brechbiel, *Chem. Rev.*, **2010**, 110, 2921–2959; (d) M. C. Heffern, L. M. Matosziuk and T. J. Meade, *Chem. Rev.*, **2014**, 114, 4496-4539; (e) E. Di Gregorio, L. Lattuada, A. Maiocchi, S. Aime, G. Ferrauto and El. Gianolio, *Chem. Sci.,* **2021**, 12, 1368-1377; (f) C. J. Adams and T. J. Meade, *Chem. Sci.*, **2020**, 11, 2524-2530.

(3) S. Aime, M. Botta, D. Esteban-Gómez, C. Platas-Iglesias, *Mol. Phys.*, **2019**, 117, 898-909.

(4) (a) J. M. Hazelton, M. K. Chiu, H. H. Abujudeh, *Curr. Radiol. Rep.*, **2019**, 7, 5; (b) J. Endrikat, S. Dohanish, N. Schleyer, S. Schwenke, S. Agarwal, T. Balzer, *Invest. Radiol.*, **2018**, 53, 541-550.

(5) (a) E. Gianolio, E. Di Gregorio, S. Aime, *Eur. J. Inorg. Chem.*, **2019**, 137–151; (b) M. Le Fur, P. Caravan, Metallomics, 2019, 11, 240-254.

(6) M. Botta, F. Carniato, D. Esteban-Gomez, C. Platas-Iglesias, L. Tei, *Future Med. Chem.*, **2019**, 11, 1461 – 1483.

(7) (a) N. Kuznik, M. Wyskocka, *Eur. J. Inorg. Chem.*, **2015**, 445–458; (b) M. F. Tweedle, *Radiology*, **2018**, 286, 409–411.

(8) G. J Anderson, D. M. Frazer, *Am. J. Clin. Nutr.*, **2017**, 106, 1559S-1566S.

(9) (a) P. Boehm-Sturm, A. Haeckel, R. Hauptmann, S. Mueller, C. K. Kuhl, E. Schellenberger, *Radiology*, **2018**, 286, 537–546; (b) J. Xie,

A. Haeckel, R. Hauptmann, I. P. Ray, C. Limberg, N. Kulak, B. Hamm, E. Schellenberger, *Magn. Res. Med.,* **2021**, 85, 3370-3382.

(10) H. Wang, V. Clavijo Jordan, I. A. Ramsay, M. Sojoodi, B. C. Fuchs, K. K. Tanabe, P. Caravan, E. M Gale, *J. Am. Chem. Soc.*, **2019**, 141, 5916–5925.

(11) (a) E. M. Snyder, D. Asik, S. M. Abozeid, A. Burgio, G. Bateman, S. G. Turowski, J. A. Spernyak, J. R. Morrow, *Angew. Chem. Int. Ed.*, **2020**, 59, 2414–2419; (b) D. Asik, R. Smolinski, S. M. Abozeid, T. B. Mitchell, S. G. Turowski, J. A. Spernyak, J. R. Morrow, *Molecules*, **2020**, 25, 2291; (c) A. Patel, D. Asik, E. M. Snyder, A. E. Dilillo, P. J. Cullen, J. R. Morrow, *ChemMedChem*, **2020**, 15, 1050-1057.

(12) a) S. J. Dorazio, J. R. Morrow, *Eur. J. Inorg. Chem.* **2012**, 2006-2014; b) K. Du, E. A. Waters, T. D. Harris, *Chem. Sci.* **2017**, 8, 4424–4430; c) I.-R. Jeon, J. G. Park, C. R. Haney, T. D. Harris, *Chem Sci.* **2014**, 5, 2461-2465.

(13) A. E. Thorarinsdottir, A. I. Gaudette and T. D. Harris, *Chem. Sci.,* **2017**, 8, 2448–2456.

(14) S. H. Koenig, C. M. Baglin, R. D. Brown III, *Magn. Reson. Med.*, **1985**, 2, 283-288.

(15) (a) T. W. Swaddle, A. E. Merbach, *Inorg. Chem.*, **1981**, 20, 4212-4216; (b) I. Bertini, F. Capozzi, C. Luchinat, Z. Xia, *J. Phys. Chem.*, **1993**, 97, 1134-1137.

(16) M. Grant, R. B. Jordan, *Inorg. Chem.*, **1981**, 20, 55-60.

(17) (a) I. Solomon, *Phys. Rev.*, **1955**, 99, 559-565; (b) N. Bloembergen, L. O. Morgan, *J. Chem. Phys.*, **1961**, 34, 842-850; (c) J. H. Freed, *J. Chem. Phys.,* **1978**, 68, 4034-4037.

(18) T. J. Swift and R. E. Connick, *J. Chem. Phys.*, **1962**, 37, 307-312.

(19) G. A. Rolla, C. Platas-Iglesias, M. Botta, L. Tei and L. Helm, *Inorg. Chem.*, **2013**, 52, 3268–3279.

(20) D. Esteban-Gómez, C. Cassino, M. Botta and C. Platas-Iglesias, *RSC Adv.,* **2014**, 4, 7094–7103.

(21) L. Leone, M. Boccalon, G. Ferrauto, I. Fabian, Z. Baranyai, L. Tei, *Chem. Sci.*, **2020**, 11, 7829-7835.

(22) S. Aime, A. Barge, M. Botta, D. Parker and A. S. De Sousa. *J. Am. Chem. Soc*. **1997**, 119, 4767-4768

(23) T. Schneppensieper, S. Seibig, A. Zahl, P. Tregloan, R. van Eldik, *Inorg. Chem.*, **2001**, 40, 3670 – 3676.

(24) J. Bloch, G. Navon*, J. Inorg. Nucl. Chem.*, **1980**, 42, 693-699.

(25) A. Brausam, J. Maigut, R. Meier, P. A. Szilágyi, H.-J. Buschmann, W. Massa, Z. Homonnay, R. van Eldik, *Inorg. Chem.*, **2009**, 48, 7864–7884.

(26) J. Maigut, R. Meier, A. Zahl, R. van Eldik, *Inorg. Chem.*, **2008**, 47, 5702-5719.

(27) (a) E. Balogh, M. Mato-Iglesias, C. Platas-Iglesias, E. Tóth, K. Djanashvili, J. A. Peters, A. de Blas, T. Rodríguez-Blas, *Inorg. Chem.*, **2006**, 45, 8719-8728; (b) G. Tircsó, M. Regueiro-Figueroa, V. Nagy, Z. Garda, T. Garai, F. K. Kalman,, D. Esteban-Gómez, E. Tóth, C. Platas-Iglesias, *Chem. Eur. J.*, **2016**, 22, 896 – 901.

(28) Y. Li, B. Liu, Z. Ge, B. Yang, *J. Photochem. and Photobiol. B*, **2008**, 91, 137 – 142.

(29) W. R. Harris, V. L. Pecoraro, *Biochemistry*, **1983**, 22, 292 – 299.

(30) R. L. Gustafson, A. E. Martell, *J. Phys. Chem.* **1963**, 67, 576–582

(31) J. Felcman, J. da Silva, *Talanta*, **1983**, 30, 565

(32) R. Delgado, et al, *Talanta*, **1997**, 45, 451

(33) A. Brausam, J. Maigut, R. Meier, P. A. Szilágyi, H.-J. Buschmann, W. Massa, Z. Homonnay, R. van Eldik, *Inorg. Chem.* **2009**, 48, 7864–7884.

(34) A. E. Martell, S. M. Smith, Critical stability constants Vol 1-5. *New York: Plenum Press*, **1974-1982**

(35) J. Carr, DG. Swartzfager. *Anal. Chem*. **1971**, 43, 1520-1522

(36) J. Watters. O.E. Schupp, *J. Inorg. Nucl. Chem*. **1968**, 30, 3359-3362

(37) A. Vágner, A. Forgács, E. Brücher, I. Tóth, A. Maiocchi, A. Wurzer, H.-J. Wester, J. Notni, Z. Baranyai, *Front. Chem.*, **2018**, 6, 170.

(38) (a) F. K. Kalman, G. Tircso, *Inorg. Chem.*, **2012**, 51, 10065 − 10067; (b) K. Pota, Z. Garda, F. K. Kalman, J. L. Barriada, D. Esteban-Gomez, C. Platas-Iglesias, I. Toth, E. Brucher, G. Tircso, *New J. Chem.*, **2018**, 42, 8001—8011.

(39) M. Taqui-Khan and A. E. Martell, *J. Am. Chem. Soc.* **1968**, 90, 3386

(40) (a) C. Lagercrantz*, Acta Chem. Scand.,* **1964**, 18, 562; (b) H. Dahn, L, Loewe, C. A. Bunton, *Helv. Chim. Acta*, **1960**, 43, 320; (c) Y. Kirino, P. L. Southwick, and R. H. Schuler, *J. Am. Chem. Soc.*, **1974**, 96, 673

(41) (a) W. H. Koppenol, R. H. Hider, *Free Radic. Biol. Med.*, **2019**, 133, 3-10; (b) Y. Turyan, R. Kohen, *J. Electroanal. Chem.*, **1995**, 380, 273-277.

(42) D. Pyreu, E. Kozlovskii, *Zh. Neorg. Khim.*, **2000**, 45, 459-464.

(43) P. M. May, P. W. Linder, D. R. Williams, *J. Chem. Soc. Dalton Trans.*, **1977**, 588-595.

(44) M. Taqui-Khan, A. E. Martell, *J. Am. Chem. Soc.*, **1968**, 90, 3386-3389.

(45) (a) E. Pelizzetti, E. Mentasti, E. Pramauro, *Inorg. Chem.*, **1976**, 15, 2898 – 2900; (b) E. Pelizzetti, E. Mentasti, E. Pramauro, *Inorg. Chem.*, **1978**, 17, 1181 – 1186.

(46) J. C. Joyner, J. Reichfield, J. A. Cowan, *J. Am. Chem. Soc.,* **2011**, 133, 15613-15626.

5 Investigating the interaction of Fe(III) complexes with macromolecules: the $[Fe(EDTA\text{-}BOM_x)]^-$ case

A necessary prerequisite to take full advantage of the PRE effect is to have a thorough knowledge of specific model systems. The case of Fe(III)-based metal probes is a clear example of how this lack of basic knowledge represented a serious obstacle to their development. For example, just very few papers analysing the interaction of these complexes with macromolecular structures have been published. This may be a key element because these interactions have been exploited in the past to achieve very high relaxivity values. For this very reason, we decided to investigate Fe(III) complexes of EDTA-derived ligands containing lipophilic chains that allow the formation of supramolecular adducts. The combination of relaxometric, voltammetric, potentiometric and spectrophotometric data for these Fe(III)-based systems allowed us to obtain a thorough characterization that can help to better understand phenomena hitherto largely neglected or investigated in a non-systematic and in-depth way.

5.1 Introduction

In the last 40 years the Magnetic Resonance Imaging has firmly established itself as one of the most performing diagnostic techniques. The success of MRI has also been strongly supported by the use of metal-based contrast agents, which allow achieving a better contrast resolution and shortening the time of examination. Their importance and extensive applications have always been a strong stimulus for worldwide research. Until now, these studies have been mainly focused on Gd(III)- and Mn(II)-based complexes, which helped to generate a huge database of the characteristics of many compounds, so as to be able to help chemists in the design of the metal probes with optimal characteristics.[1,2] However, although Fe(III)-based probes had also been partially studied in the early days of MRI contrast agent development, these have been neglected in recent years, which has not allowed for an equally extensive data set on this type of complex. This is critical because it is the first step that can enable the development of metal probes optimized by rational design. Our preliminary studies have let us define the conditions for the development of new Fe(III)-based paramagnetic probes by investigating model systems such as the aquaion, $[Fe(EDTA)]^-$, and $[Fe(CDTA)]^-$.[3] Another aspect we wanted to evaluate relates to the effect that specific structural modifications can have. For this reason, the study of a series of ligands sharing a common basic structure, ethylenediaminetetraacetic acid (EDTA), will be dealt with in the following chapter. We have previously discussed how $Fe(EDTA)^-$ can be used as a model to represent monohydrate complexes of Fe(III)

and its characteristics have been deeply described. We hereby propose the ^{1}H NMRD and ^{17}O NMR characterization of derivatives of EDTA, EDTA-BOM and EDTA-BOM_2, which bear respectively one and two benzyloxymethyl (BOM) functionalities. Works related to these or similar ligands have already been proposed in the past for complexes based on both Gd(III)[4,5] and Mn(II)[6,7]. We expect the presence of these new substituents to have a dual effect. First, the paramagnetic relaxation theory predicts that an increase in the molecular weight of the complex is also associated with an increase in the value of relaxivity at high magnetic fields (≥ 20 MHz).[8] Secondly, the lipophilic nature of the BOM functionalities can promote a non-covalent interaction with human serum albumin (HSA), which will be further explored. The formation of these macromolecular adducts should lead to a strong increase in relaxation enhancement.[9] Furthermore, in order to investigate the behavior of these complexes in supramolecular adducts, we also studied the interaction with β-cyclodextrin and poly-β-cyclodextrin. For each complex, we combined relaxometric, potentiometric, spectrophotometric and voltammetric data to obtain an in-depth characterization of them. In the case of the adducts with HSA, we also studied their kinetic inertness by UV-Vis spectrophotometric measurements.

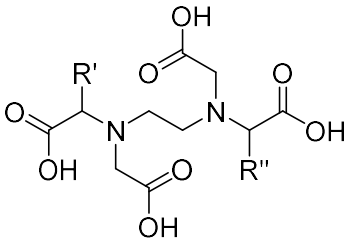

EDTA: R'=R''=H

EDTA-BOM: R'=H, R''=BOM

EDTA-BOM_2:R'=R''=BOM

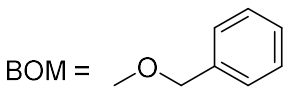

Scheme 1. Schematic representation of the discussed ligands.

5.2 Results and discussion

Chemicals. 2,2'-((2-((2-(benzyloxy)-1-carboxyethyl)-(carboxymethyl)-amino)-ethyl)-azanediyl)diacetic acid (EDTA-BOM) and 2,2'-(4,9-dicarboxy-1,12-diphenyl-2,11-dioxa-5,8-diazadodecane-5,8-diyl)diacetic acid (EDTA-BOM_2) were provided by Bracco Imaging S.p.A. A stock solutions of Fe^{3+} was prepared from $Fe(NO_3)_3 \cdot 9H_2O$ (reagent grade, Carlo Erba, Milano, Italy). HSA (crystallized and lyophilized) and β-cyclodextrin were purchased from Sigma (St. Luis, Mo., USA) and were used without any further purification. The poly-β-ciclodextrin was purchased from Cyclolab (Budapest, Hungary).

Complexation of Iron(III)

$[Fe(EDTA\text{-}BOM)]^-$ and $[Fe(EDTA\text{-}BOM_2)]^-$ were synthetized by adding 1 equiv. of the $Fe(NO_3)_3$ stock solution to the solution of the ligands (1.05 equiv.) at pH = 2. After the addition, the pH was set to 2.7 with NaOH 0.1 M and the samples were left under stirring for 2 hours at room temperature (r.t.). Then, the samples are brought to pH 7.08 with NaOH and left under stirring for 1 hour, slowing down the stirring

for the last 15 minutes. The samples were then filtered on a syringe. Their purities are checked through HPLC-MS chromatography and the concentrations of the solutions are determined by the Evans method. $[Fe(EDTA\text{-}BOM)]^-$: MS (ESI+): m/z calcd for $C_{18}H_{20}FeN_2O_9$: 464.21; found: 466.45 ($M+2H^+$); $[Fe(EDTA\text{-}BOM_2)]^-$. MS (ESI+): m/z calcd for $C_{26}H_{28}FeN_2O_{10}$: 584.36; found: 586.66 ($M+2H^+$), 608.62 ($M+H^++Na^+$), 630.64 ($M+2Na^+$).

Relaxometric characterization.

We initially investigated the pH-dependency of relaxivity at 120 MHz and 298 K. This allows us to verify the stability of the complexes throughout the pH range as well as the presence of phenomena such as hydrolysis or dimerization (Fig. 1).

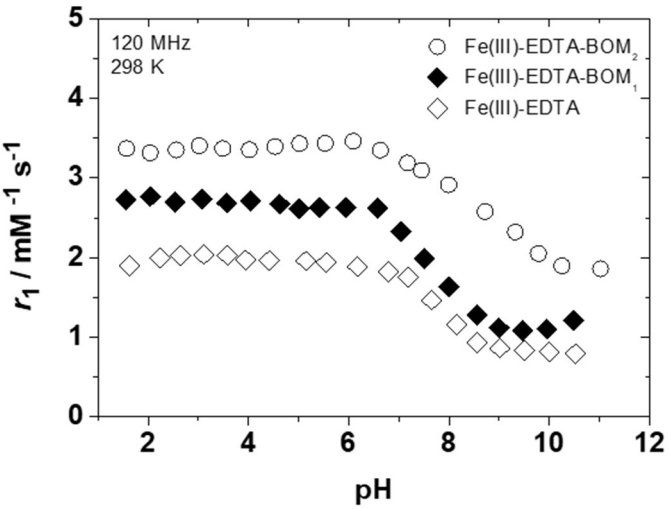

Figure 1. pH-dependency of r_1 for the $[Fe(EDTA\text{-}BOM_2)]^-$ (○), $[Fe(EDTA\text{-}BOM)]^-$ (◆) and $[Fe(EDTA)]^-$ (◇) (120 MHz and 298 K).

The relaxivity of these complexes appear to have a trend comparable to $[Fe(EDTA)]^-$, which is reasonable considering that the coordination

of the complex does not change. The values are slightly higher as the presence of one or two BOM groups leads to an increase in the molecular weight, which is associated with an increase in the rotational correlation time. As in the case of $[Fe(EDTA)]^-$, the complexes are stable up to pH = 6.5, in which the relaxivity values suggest the presence of complexes with $q = 1$. A decrease in relaxivity is progressively noted, attributable to the formation of an OH^- group bound to the ferric ion.[3,10] The measurements of the complexes were carried out at pH = 5.4, so as to be sure of the presence of 100% of the monohydrate species. For both complexes ^1H NMRD profiles were measured at four different temperatures.

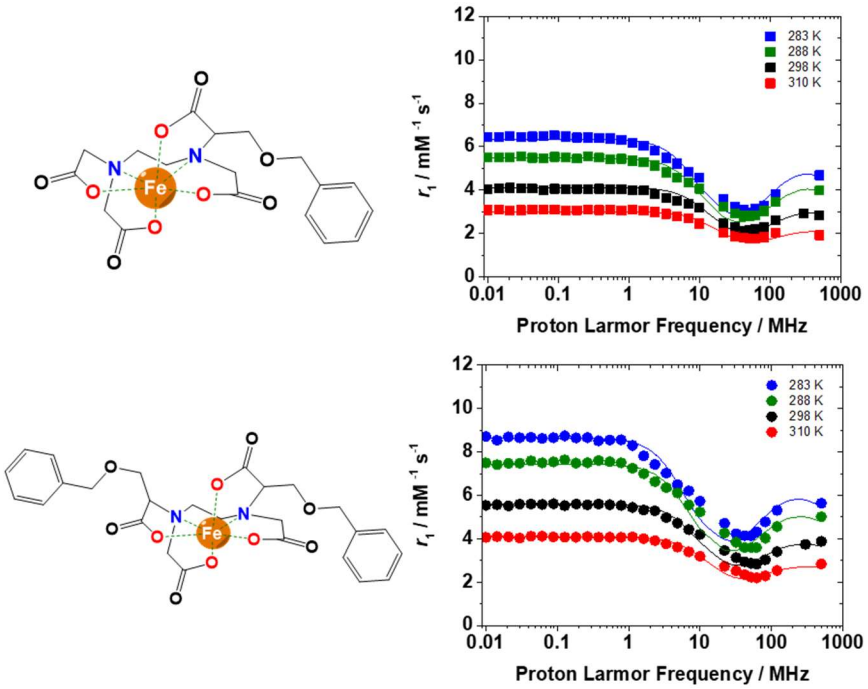

Figure 2. Structures and ^1H NMRD profiles (pH = 5.4) at different temperatures (283 (blue), 288 (green), 298 (black) and 310 K (red)) of $[Fe(EDTA)(BOM)]^-$ (■, $[Fe^{3+}]$ = 2.98 mM) and $Fe(EDTA\text{-}BOM_2)]^-$ (●, $[Fe^{3+}]$ = 2.82 mM).

NMRD profiles are a fundamental tool for determining parameters that influence ^{1}H relaxation. However, a detailed study of water exchange dynamics also requires the implementation of high-resolution studies, especially in the cases proposed here. Indeed, considering that relaxivity increases as temperature decreases, we can estimate that the complexes are in a fast exchange regime. This could lead to an inaccurate measurement of the mean residence lifetime of the bound water molecule (τ_M), as it would not be a limiting factor in NMRD profiles. On the other hand, variable-temperature ^{17}O NMR measurements allow us to quantitatively measure parameters such as τ_M, the hyperfine coupling constant ($A_o/\hbar$), and can also be used to confirm the hydration state of the complex. The differences between ^{17}O transverse relaxation rate (R_{2p}^{O}) values between monohydrate and non-hydrate complexes are generally more pronounced than those estimated from r_1. Thus, the ^{17}O reduced transverse relaxation rates and chemical shifts collected at different temperatures for the presented complexes are shown in Figure 3.

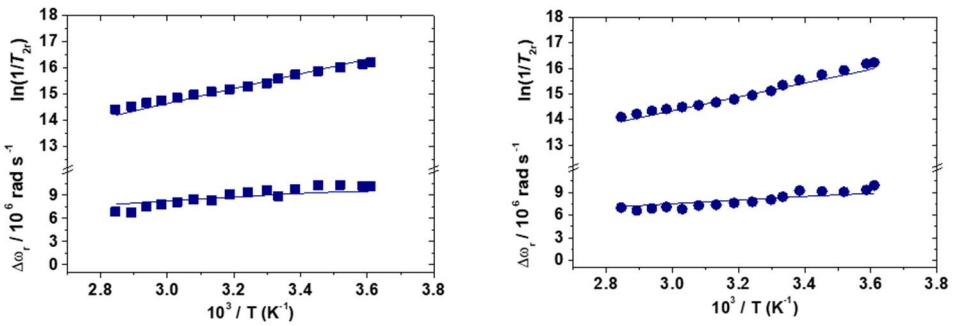

Figure 3. Reduced ^{17}O NMR transverse relaxation rates and chemical shifts of [Fe(EDTA-BOM)]$^{-}$ (■, pH = 5.4, [Fe^{3+}] = 9.30 mM) and [Fe(EDTA-BOM_2)]$^{-}$ (●, pH = 5.4, [Fe^{3+}] = 6.18 mM), measured at 11.74 T.

The data were fitted simultaneously, using the SBM equations [11–13] for the NMRD profiles (introducing the Freed model for the outer-sphere contribution [14]) and the Swift-Connick equations for the ^{17}O NMR data.[15]

We have already discussed how the paramagnetic relaxation mechanism is influenced by multiple factors. Consequently, the congruence of our fits can be increased by fixing some of the parameters. Considering the structural similarities that these complexes share with their parent ligand (EDTA), we assumed that the parameters defining the outer sphere contribution are the same. Regarding water molecule exchange, the complexes are all affectively in the fast exchange regime, with a τ_M value of 1 ns. This confirms how ^{17}O NMR analysis is of great relevance since we would not have been able to accurately measure this value from NMRD profiles alone.

The values of the rotational correlation times are also very important in explaining the trend and values of relaxivity as a function of magnetic field and temperature, and as highlighted in Figure 4, the values we determined adequately follow the linear trend with respect to the molecular weight of the complex. Finally, one of the most critical aspects concerns the parameters defining the electronic relaxation times (Δ^2 and τ_V). Indeed, we have shown how, unlike Gd(III) and Mn(II)-based complexes, these are a limiting factor for Fe(III)-based complexes. In this case, the fit of Δ^2 required once again the integration of the dependence on temperature according to an Arrhenius-like behaviour.[3] Interestingly, the changes in the mean-squared energy associated to the ZFS are quite marked. We have already discussed in the comparison between $Fe(EDTA)^-$ and $Fe(CDTA)^-$ that variations in the ligand backbone can also heavily

influence these parameters. This effect might also be enhanced by the presence of one or two aromatic rings, which act as electron-withdrawer groups.

All the parameter obtained from the fit of our data are reported in Table 1.

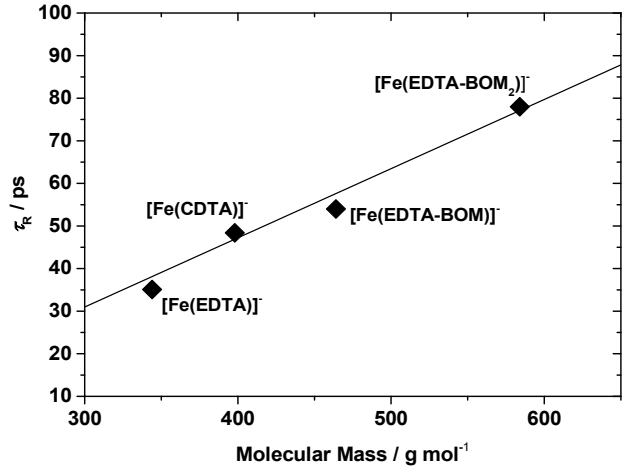

Figure 4. Values of τ_R as a function of molecular weight of different Fe(III) complexes.

Table 1. Data obtained from the simultaneous fit of ^{1}H NMRD and ^{17}O NMR data.

Parameters	$[Fe(EDTA-(BOM)_2)]^-$ (MW = 584 g/mol)	$[Fe(EDTA-BOM)]^-$ (MW = 464 g/mol)	$[Fe(EDTA)]^-$ (MW = 344 g/mol)
$^{298}r_1$ 60 MHz / mM^{-1} s^{-1}	2.9	2.2	1.7
$^{298}r_1$ 120 MHz / mM^{-1} s^{-1}	3.4	2.6	1.9
$^{298}\Delta^2$ / 10^{20} s^{-2}	9.0 ± 0.5	19.1 ± 0.1	27.0 ± 1.4
E_Δ / *kJ mol*$^{-1}$	10.2 ± 1.3	9.5 ± 1.5	7.8 ± 0.5
$^{298}\tau_V$ / ps	3.9 ± 0.3	2.8 ± 0.3	2.8 ± 0.1
E_V / *kJ mol*$^{-1}$	1.0 [a]	1.0 [a]	1.0 [a]
$A_O/\hbar/10^6$ *rad* s^{-1}	-54.5 ± 0.6	-56.8 ± 0.5	-64.8 [a]
$^{298}\tau_M^O$ / ns	1 ± 1	1 ± 1	1 ± 1
ΔH_M / *kJ mol*$^{-1}$	23.0 ± 2.7	25.0 ± 2.5	30.5 ± 1.4
$^{298}\tau_R$ / ps	78.0 ± 5.9	54.0 ± 6.7	35.1 ± 1.7
E_R / *kJ mol*$^{-1}$	26.0 ± 1.4	25.5 ± 6.6	25.2 ± 2.4
q	1 [a]	1 [a]	1 [a]
r / Å	2.69 [a]	2.69 [a]	2.69 [a]
a / Å	3.5 [a]	3.5 [a]	3.5 [a]
^{298}D / 10^5 cm^2 s^{-1}	2.24 [a]	2.24 [a]	2.24 [a]
E_D / *kJ mol*$^{-1}$	20.0 [a]	20.0 [a]	20.0 [a]

[a] = fixed parameters

Study of the interaction with human serum albumin (HSA)

The history of MRI probe research has led to several works related to the interaction of Gd(III) or Mn(II) complexes with human serum albumin. However, fewer paper have been published regarding this topic for Fe(III)-based complexes.[16–18] The interaction with HSA has always been the subject of great interest and this is because, being the most abundant protein in the body, it can be exploited to our advantage. In fact, the non-covalent interaction of the complex with albumin has a dual effect: in terms of relaxation, the formation of a supramolecular adduct leads to a sharp increase in the rotational correlation time, which consequently increases relaxivity values (at high magnetic fields). Furthermore, for small-sized molecules, the interaction with this protein limits extravasation, thus allowing a prolongation of the lifetime in the bloodstream of a contrast agent. Therefore we investigated the interaction of the $[Fe(EDTA\text{-}BOM_x)]^-$ (x = 1,2) complexes with HSA. This interaction and the binding parameters that define it were studied through a titration performed at 298 K and pH = 5.4 (value for which the complexes are monohydrated), evaluating the longitudinal relaxation rate at 120 MHz after increasing the HSA concentration (the concentration of the complex is kept constant). These titrations are shown in Fig. 5. The binding parameters were obtained by considering the equilibrium:

$$Fe(EDTA\text{-}BOM_x)^- + HSA \rightleftharpoons Fe(EDTA\text{-}BOM_x)^-\text{-}HSA \qquad (x=1,2)$$

from which it is possible to obtain the expression of the association constant K_A according to the equation:

$$K_A = \frac{[Fe(EDTA - BOM_x)^- - HSA]}{[Fe(EDTA - BOM_x)^-][HSA]} \quad (1)$$

Every value of R_1^{obs} can be described by considering the relaxivity of the free chelate (r_1^f) and the relaxivity of the HSA-bound complex (r_1^b) as follows:

$$R_1^{obs} = (r_1^f[Fe(EDTA - BOM_x)^-] + r_1^b[Fe(EDTA - BOM_x)^- - HSA])1000 + R_1^{HSA} \quad (2)$$

Hence, by combining Eq. 1 and 2, we were able to obtain the binding parameters reported in Tab. 2.

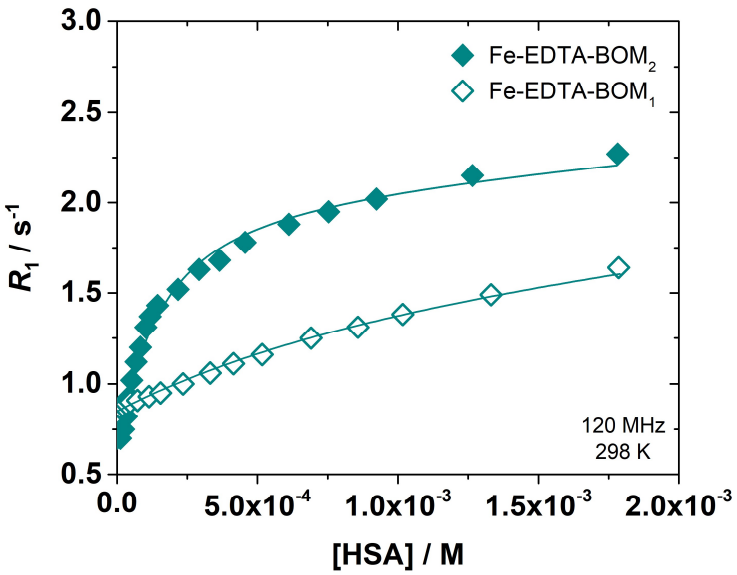

Figure 5. Water proton relaxation rate of the aqueous solution of [Fe(EDTA-BOM$_2$)]$^-$ (full, [Fe^{3+}]=0.094 mM, pH = 5.4) and [Fe(EDTA-BOM)]$^-$ (empty, [Fe^{3+}]=0.18 mM, pH = 5.4) as a function of increasing amounts of HSA, measured at 120 MHz and 298 K.

Table 2. Fit parameters of Fig. 5.

Parameters	[Fe(EDTA-BOM)]$^-$- HSA	[Fe(EDTA-(BOM)$_2$)]$^-$- HSA
K_A / M^{-1}	$(8.7 \pm 0.2)\cdot 10^2$	$(9.3 \pm 1.1)\cdot 10^3$
n	1[a]	1[a]
r_1^{bound} / mM^{-1} s^{-1}	7.6 ± 0.2	18.0 ± 0.4

[a]Fixed parameters.

From Figure 5 it is immediately noticeable that the presence of two benzyloxymethyl arms leads to a better interaction with HSA. This is also confirmed by two other aspects. The affinity constant for [Fe(EDTA-BOM$_2$)]$^-$ is more than a tenfold of that of [Fe(EDTA-BOM)]$^-$. Additionally, at the maximum concentration of albumin (1.78 mM), we have 40% of free iron(III) chelate for [Fe(EDTA-BOM)]$^-$, while only 1% for [Fe(EDTA-BOM$_2$)]$^-$. The affinity constants values are also comparable to those of the Mn(II) analogues.[6] Consequently, we have collected the ^{1}H NMRD profiles of the two adducts, which are reported and compared to the profiles of the free complexes in Fig. 6. Unlike what has been seen in the past for adducts of complexes based on Gd(III)[5] or Mn(II)[6], for which the peak of relaxivity was between 20-80 MHz, in the case of Fe(III) this peak is shifted to higher proton Larmor frequencies values (≈ 300 MHz). This is mainly attributable to the fact that the contribution of the electronic relaxation times is different: its influence is important even at high magnetic fields, while for Mn(II) and Gd(III) its effect is mainly detectable in the low fields region due their longer T_{ie} (i = 1,2) values. This is a particularly relevant property because it confirms that this complexes can be studied to optimize

magnetic probes suitable for the magnetic field of clinical scanners that will be used in the next decade (≥ 3 T).

From Fig. 6 we have determined that the formation of a supramolecular adduct allows a discrete gain in terms of relaxivity at 298 K. While for the $[Fe(EDTA\text{-}BOM)]^-$ r_1 goes from 2.6 $mM^{-1}\ s^{-1}$ to 7.6 $mM^{-1}\ s^{-1}$, $[Fe(EDTA\text{-}BOM_2)]^-$ has an increase of almost 600% (at 120 MHz and 298 K, r_1^{bound} = 18.0 $mM^{-1}\ s^{-1}$ v. r_1^{free} = 3.4 $mM^{-1}\ s^{-1}$).

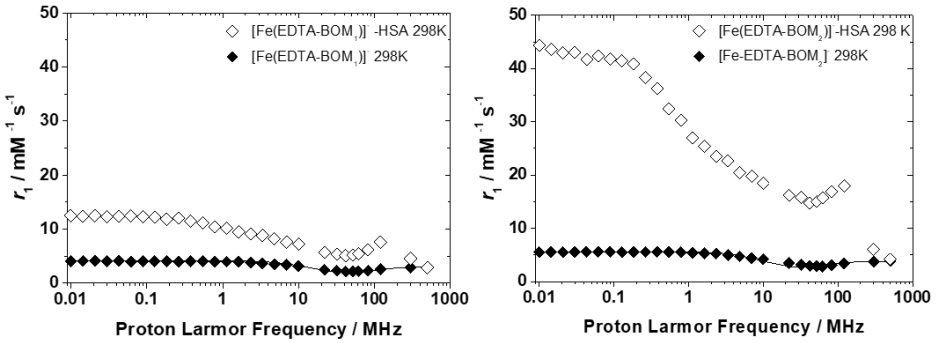

Figure 6. ^1H NMRD profiles (298 K) of $[Fe(EDTA\text{-}BOM)]^-$ (left) and $[Fe(EDTA\text{-}(BOM)_2)]^-$ (right) (free complex (black) and bound to HSA (empty)).

Study of the interaction with β-cyclodextrin (β-CD) and poly-β-cyclodextrin (poly-β-CD)

It is well known that the hydrophobic nature of aromatic rings such as those of the BOM functionalities allow the formation of inclusion compounds with β-cyclodextrin (β-CD) and its oligomers.[19] Hence, we have also investigated the formation of supramolecular adducts with these other host molecules, following a similar procedure. In particular, it is interesting to assess the effects on the relaxivity of the formation of supramolecular adducts with substrate of medium

molecular size, as this parameter might influence the value of frequency at which r_1 achieves its maximum value. In the case of many Gd(III) complexes there are several studies concerning the interaction with β-cyclodextrin (β-CD) and its oligomers.[19–21] We determined the values of the binding constant and r_1^{bound} in the case of the interaction between $[Fe(EDTA\text{-}BOM_2)]^-$, β-CD and poly-β–cyclodextrin (poly-β–CD). The experimental approach followed is the same utilized above and the parameters evaluated are reported in Tab. 3.

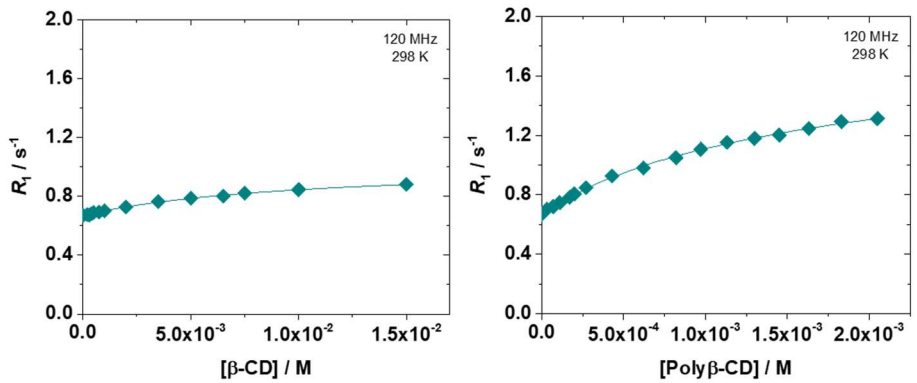

Figure 7. Water proton relaxation rate of the aqueous solution of $[Fe(EDTA\text{-}BOM_2)]^-$, (0.085 mM, pH = 5.40) as a function of increasing amounts of β-CD (left) and poly-β-CD (right), measured at 120 MHz and 298 K.

Table 3. Fit parameters of Fig. 8 ([a]Fixed parameters).

Parameters	**[Fe(EDTA-(BOM)$_2$)]$^-$-β-CD**	**[Fe(EDTA-(BOM)$_2$)]$^-$-poly-β-CD**
K_A / M^{-1}	101 ± 7	134 ± 7
n	1[a]	5[a]
r_1^{bound} / mM^{-1} s^{-1}	7.5 ± 0.2	16.5 ± 0.4

From the titrations reported in Fig. 7 and the fit of the curves, it is evident that the non-covalent binding of the complex with both of the host molecules is much weaker than that with HSA. At the maximum concentration of the titrants, in both cases we have found that around 40 % of the complex is not bound. In order to obtain the binding parameters (Tab. 3) we fitted the curves by using a modified version of equations 1 and 2. In the case of poly-β-CD, the titration curve is well fitted by assuming that the complex binds to the polymer following a 1:2 binding model thanks to the presence of the two BOM functionalities. The number of binding sites (n = 5) arises from the fact that poly-β-CD is made up of an average of 10-11 units of β-CD.

Finally, considering the increase of relaxivity in the supramolecular adducts, for [Fe(EDTA-BOM_2)]$^-$-β-CD, r_1^{bound} is almost twice of that of the free complex, while from the interaction with poly-β-CD, relaxivity is increased by a factor of 4.85.

Finally, we collected their NMRD profiles at 25°C, shown in Figure 8. As can be seen, for all the adducts the sharp increase in relaxivity can be seen around 300 MHz. This suggests that, for this system, the size of the host molecule does not markedly influence the frequency at which relaxivity reaches its maximum.

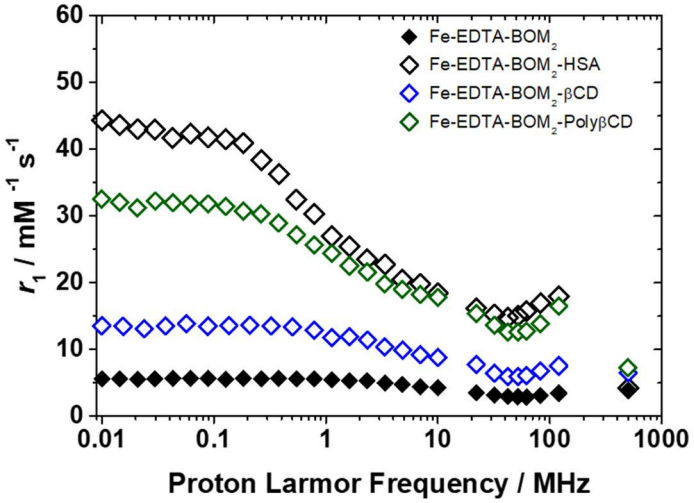

Figure 8. ^{1}H NMRD profiles (298 K) of $[Fe(EDTA\text{-}BOM_2)]^-$ free (black), bound to HSA (empty, black), to poly-β-CD (empty, green) and to β-CD (empty, blue).

Study of the redox behavior

The evaluation of the efficacy and safety of a metal-based complex to be used *in vivo* must necessarily consider also the redox behavior. The biological matrix is extremely complex and rich in both oxidizing and reducing agents. If the probe can participate in redox reactions, there are two main effects that can be generated:

1. *Formation of reactive oxygen species* (ROS): especially in the case of iron(III), it is possible that the redox potential of the complex may allow the establishment of a redox equilibrium capable of leading to the formation of toxic radical species (*Fenton reaction*). An ideal metal complex should have a reduction potential both lower than molecular oxygen and higher than antioxidant agents (thiols, etc...);

2. *Loss of efficacy*: contrast enhancement is directly associated with the paramagnetism of the metal ion, which therefore must be in the highest spin multiplicity. If the metal ion is reduced, a very important decrease of the signal would be detected, signaling the decreased efficiency of the probe. This phenomena, however, can be exploited. Works have been reported where redox-responsive iron complexes were used as contrast agents for acute inflammations (characterized by elevated levels of ROS).[22]

Regarding Fe(III) complexes, it has recently been shown that these should have a reduction potential of less than 0.1 V or greater than 0.9 V vs. NHE, to avoid problems for *in vivo* applications.[23] Within this window, in fact, they could give redox cyclization by reacting with molecules in the body such as peroxides (for oxidation) or ascorbate (for reduction). The study of redox behavior therefore is another key element in the study of these probes.
Our complexes were analyzed by cyclic voltammetry and the data are reported in Table 4.

Table 4. CV data of the three complexes.

Parameters	**[Fe(EDTA)]$^-$**	**-BOM$_1$**	**-BOM$_2$**
$E^{0'}$ / V	-0.126 ± 0.002	-0.123 ± 0.001	-0.114 ± 0.001
ΔE / mV	352	109	115

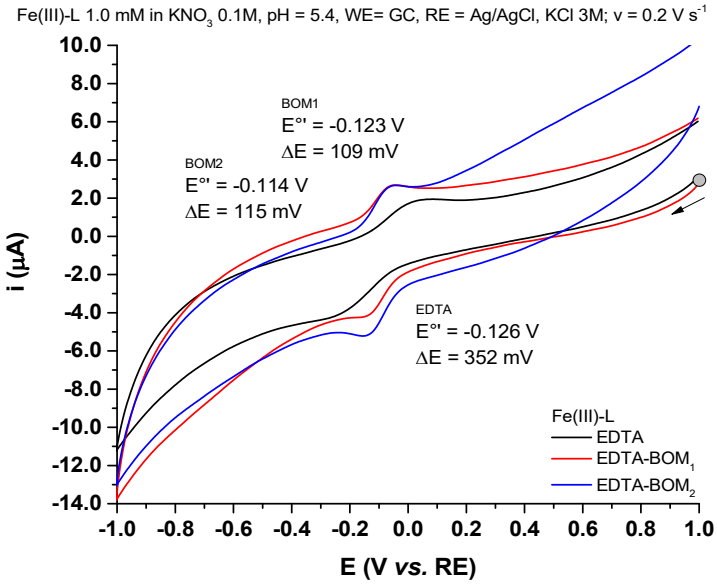

Figure 9. CV of the different Fe(III) complexes measured at 298 K. The arrow indicates the position from which scans were initiated.

The formal reduction potential values for all complexes are approximately -0.1 V and the differences are negligible. This is in agreement with the expectations since the coordination cage of the metal ion is identical in all three cases. The half-wave potential (ΔE) is correlated with the structural rearrangement of the complexes due to reduction. The reported values suggest that this process is disadvantaged for all the complexes investigated, in particular for $[Fe(EDTA)]^-$. The presence of one or two benzyloxymethyl groups does not affect significantly the redox behavior.

Thermodynamic, kinetic and redox studies.

Equilibrium, kinetic and redox properties of the $[Fe(EDTA\text{-}BOM_x)]^-$ (x = 1, 2) series have been investigated.

The protonation constants were obtained following the equation:

$$K_{H_iL} = \frac{[H_iL]}{[H_{i-1}L][H^+]} \quad (3)$$

According to the values we calculated, the incorporation of the BOM unit on the acetate pendants reduces the $\log K_1^H$ value of the EDTA-BOM_1 and EDTA-BOM_2 due to the electron withdrawal properties of the aromatic moiety. Similar behavior has been explored by comparing the related $\log K_i^H$ values of DTPA with those of BOPTA.[24] The data we obtained from our calculations are reported in Table 5.

Table 5. Protonation constants of the EDTA-BOM_1, EDTA-BOM_2 and EDTA ligands (25°C).

	EDTA-BOM$_1$	**EDTA-BOM$_2$**	**EDTA^3**
I	0.15 M $NaNO_3$		
$\log K_1^H$	**9.18 ± 0.01**	**8.91 ± 0.01**	**9.40**
$\log K_2^H$	**5.84 ± 0.02**	**6.04 ± 0.01**	**6.10**
$\log K_3^H$	2.81 ± 0.02	2.85 ± 0.02	2.72
$\log K_4^H$	2.16 ± 0.02	2.36 ± 0.02	2.08
$\log K_5^H$	1.15 ± 0.05	–	1.23
$\Sigma \log K_i^H$	**21.14**	**20.16**	**21.52**

Stability constants of the Fe(III) complexes were determined by two different experimental methods: pH-potentiometry and spectrophotometry. The stability constants of the Fe(III) complexes were calculated from the absorbance-pH data pairs obtained in the $Fe(Bha)_3$–EDTA-BOM_1 and the $Fe(Bha)_3$–EDTA-BOM_2 systems at pH around 6-7. (Bha: benzohydroxamic acid). The complexes show a low redox stability and the Fe(III)/Fe(II) reduction results in the oxidation

of the competition partners (e.g. Bha). Based on the $\Sigma \log K_i^H$ values of the ligands, the stability constants (K_{FeL}, Eq. (4)) of the [Fe(EDTA-BOM$_1$)]$^-$ and [Fe(EDTA-BOM$_2$)]$^-$ complexes were estimated.

$$K_{FeL} = \frac{[FeL]}{[Fe^{3+}][L]} \quad (4)$$

Since the formation of both Fe(III) complexes takes place at pH<2, the stability constants cannot be accurately calculated from the pH-potentiometric data. The protonation and dimerization constants ($\log K_{FeLH-1}$, $-\log K_D$ and $\log K_d$, Eqs. (5-7)) of the Fe(III) complexes were evaluated from the pH-potentiometric data.

$$FeLH_{-1} + H^+ \rightleftharpoons FeL$$
$$K_{FeLH_{-1}} = \frac{[FeL]}{[FeLH_{-1}][H^+]} \quad (5)$$

$$2FeL \rightleftharpoons [(FeL)_2(\mu\text{-}O)] + 2H^+$$
$$K_D = \frac{[(FeL)_2(\mu - 0)][H^+]^2}{[FeL]^2} \quad (6)$$

$$2FeLH_{-1} \rightleftharpoons [(FeL)_2(\mu\text{-}O)]$$
$$K_d = \frac{[(FeL)_2(\mu - 0)]}{[FeLH_{-1}]^2} \quad (7)$$

The protonation and dimerization constant of the [Fe(EDTA-BOM$_1$)]$^-$ can be calculated from the spectrophotometric titration of the complex (Figure 10). The protonation and the dimerization constants of [Fe(EDTA-BOM$_1$)]$^-$ obtained by pH-potentiometry and spectrophotometry are in a good agreement. According to the pH-potentiometric and spectrophotometric titrations the dimerization of

$[Fe(EDTA\text{-}BOM_2)]^-$ is the preferred process and the dimer has a relatively low solubility. Moreover, the dimerization takes place by the hydrolysis of the Fe(III) ion via the formation of $Fe(OH)_3$ precipitate (Figure 11). Based on this evidences, the dimerization of the $[Fe(EDTA\text{-}BOM_2)]^-$ was considered without the formation of the monomeric FeL(OH) species in our model for the evaluation of the equilibrium data. The protonation, stability and dimerization constants of the complexes we investigated are shown in Table 6.

Table 6. Protonation, stability and dimerization constants of the $[Fe(EDTA\text{-}BOM_1)]^-$, $[Fe(EDTA\text{-}BOM_2)]^-$ and $[Fe(EDTA)]^-$ (25°C).

	EDTA-BOM$_1$	**EDTA-BOM$_2$**	**EDTA**[3]
I		0.15 M $NaNO_3$	
FeL	**~22**	**~21**	**22.14**
FeHL	–	–	1.12
FeLH$_{-1}$	7.56 ± 0.01	–	7.51
-logK_D	12.92 ± 0.04	12.72 ± 0.06	13.00
logK_d	2.21 ± 0.03	–	2.02

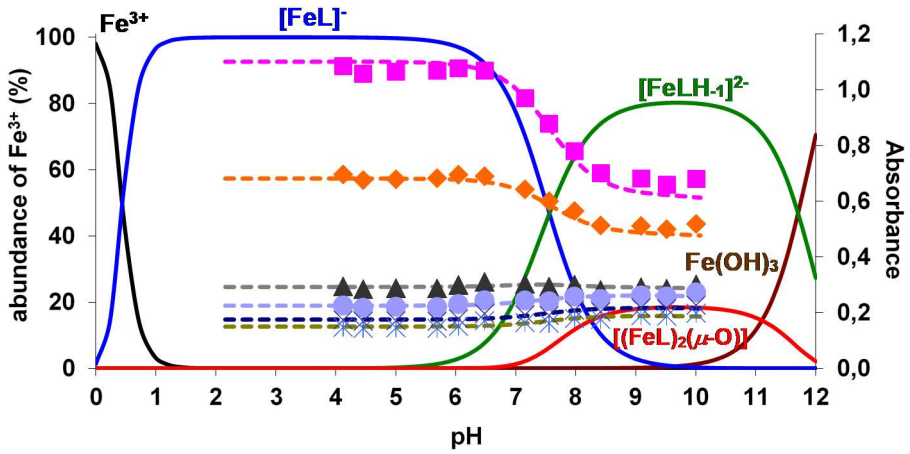

Figure 10. Species distribution and absorbance values of Fe^{3+}-EDTA-BOM_1 system as a function of pH. Symbols and dashed lines represent the experimental and calculated absorbance values. ([Fe^{3+}]=2.0 mM, [EDTA-BOM_1]=2.1 mM; λ = 395 (■), 410 (◆), 450 (▲), 470 (●), 500 (×) and 520 nm (✳) l=1.0 cm, 0.15 M $NaNO_3$, 25°C).

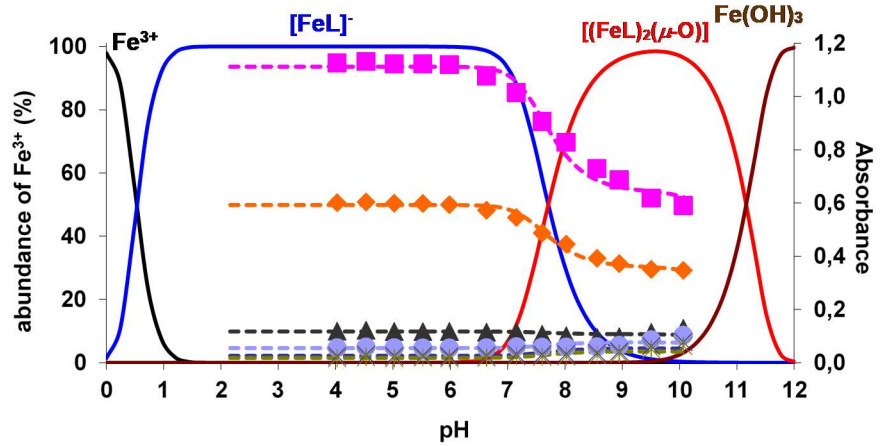

Figure 11. Species distribution and absorbance values of Fe^{3+}-EDTA-BOM_1 system as a function of pH. Symbols and dashed lines represent the experimental and calculated absorbance values. ([Fe^{3+}]=2.0 mM, [EDTA-BOM_2]=2.1 mM; λ = 395 (■), 410 (◆), 450 (▲), 470 (●), 500 (×) and 520 nm (✳) l=1.0 cm, 0.15 M $NaNO_3$, 25°C).

The kinetic inertness of both Fe(III) complexes was determined by following the transchelation reactions with the HBED ligand (Eq. (8)) in the presence and absence of 0.6 mM human serum albumin (HSA) in the pH range 8 – 12. Rates of the transchelation reactions were investigated in the presence of large HBED excess in order to guarantee the pseudo-first-order kinetic condition. The description of the experiment is reported in *Chapter 3* and the values of the pseudo-first-order rate constant (k_d) as a function of [OH^-] are reported in Figure 12. The transchelation reactions take place by the rate determining dissociation of the Fe(III)-complexes followed by the fast reaction between the free Fe^{III}-ion and the exchanging HBED ligand. Mechanism of the dissociation reactions is shown in Scheme 2. Rate and equilibrium constants characterizing the dissociation reactions of the Fe(III)-complexes are reported in Table 7.

$$FeL + HBED \rightleftharpoons Fe(HBED) + L \quad (L = EDTA\text{-}BOM_1,\ EDTA\text{-}BOM_2) \quad (8)$$

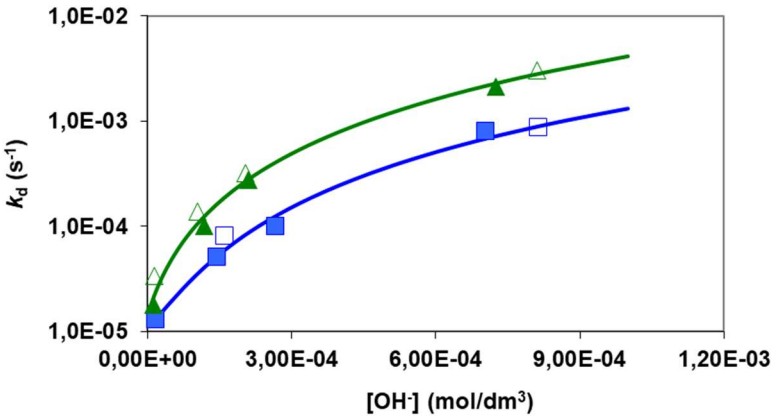

Figure 12. k_d pseudo-first-order rate constant characterizing the transchelation reactions of $[Fe(EDTA\text{-}BOM_1)]^-$ and $[Fe(EDTA\text{-}BOM_2)]^-$ with HBED ligand. Solid lines and the open symbols represent the calculated and measured k_d rate constants. ($[Fe(EDTA\text{-}BOM_1)]^- = [Fe(EDTA\text{-}BOM_2)]^- = 2.0\times10^{-4}$ M, [HBED]=2.0 (■,▲) and 4.0 mM (□,△), [piperazine]=$[Na_2HPO_4]$=0.01 M, 0.15 M $NaNO_3$, 25°C).

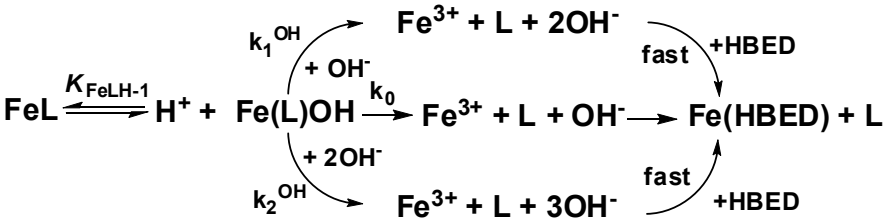

Scheme 2. Dissociation mechanism of the Fe(III)-complexes.

Table 7. Rate (k_i) and equilibrium constants (K_{FeLH-1}) and half-lives ($t_{1/2}$=ln2/k_d) characterizing the dissociation reactions of [Fe(EDTA-BOM$_1$)]$^-$, [Fe(EDTA-BOM$_2$)]$^-$ and [Fe(EDTA)]$^-$ complexes (0.15 M $NaNO_3$, 25°C).

	[Fe(EDTA-BOM$_1$)]$^-$	**[Fe(EDTA-BOM$_2$)]$^-$**	**[Fe(EDTA)]$^{-3}$**
k_0 **(s^{-1})**	$(6 \pm 1) \times 10^{-6}$	$(1.4 \pm 0.5) \times 10^{-5}$	5×10^{-6}
k_1^{OH} **(M^{-1}s^{-1})**	0.2 ± 0.03	0.5 ± 0.05	1.0
k_2^{OH} **(M^{-2}s^{-1})**	$(1.0 \pm 0.2) \times 10^3$	$(3.6 \pm 0.4) \times 10^3$	1.4×10^3
logK_{FeLH-1}	**7.56**	**>7.0**	**7.41**
k_d **(s^{-1}) at pH=7.4**	6.1×10^{-6}	1.5×10^{-5}	2.9×10^{-6}
$t_{1/2}$ **(h) at pH=7.4**	31.6	13.2	66
k_d **(s^{-1}) at pH=7.4 in 0.6 mM HSA**	2.8×10^{-6}	3.4×10^{-6}	–
$t_{1/2}$ **(h) at pH=7.4 in 0.6 mM HSA**	68	56	–

Kinetic inertness of [Fe(EDTA-BOM$_1$)]$^-$ and [Fe(EDTA-BOM$_2$)]$^-$ complexes are lower than that of the parent [Fe(EDTA)]$^-$ due to the the faster spontaneous and -OH$^-$ assisted dissociation of the Fe(L)OH species. It is well known that the BOM unit of [Gd(BOPTA)]$^{2-}$ (Multihance®) can interact with HSA via the formation of "host-guest" adduct [25] The formation of similar "host-guest" interaction is assumed between the BOM unit/s of the Fe(III)-complexes and HSA, which might be influence the dissociation rate of [Fe(EDTA-BOM$_1$)]$^-$ and [Fe(EDTA-BOM$_2$)]$^-$. The dissociation rate of [Fe(EDTA-BOM$_1$)]$^-$ and [Fe(EDTA-BOM$_2$)]$^-$ are about 2 and 4 times slower in the presence of 0.6 mM HSA and very similar to that of the parent [Fe(EDTA)]$^-$ close to physiological condition (0.15 M $NaNO_3$, 25°C). Since the p/value of

HSA is 4.7,[26] the "host-guest" adducts formed between the Fe(III)-complexes and HSA are highly negatively charged, which might hinder the -OH^- assisted dissociation of the Fe(III) complexes. As it was shown in our previous studies the $[Fe(EDTA)]^-$ complex can take place in a redox reaction with ascorbic acid.[3] The rate of the redox reactions between these Fe(III)-complexes and monohydrogenascorbate (HA^-) have been determined by spectrophotometric measurements in the presence of large HA^- excess in order to guarantee the pseudo-first-order kinetic condition (Eq. (11). By taking into account the protonation constants of the ascorbic acid ($\log K_1^H$=11.34, $\log K_2^H$=4.04, 0.1 M KNO_3 25°C),[27] the monohydrogenascorbate HA^- species dominates in our experimental condition (pH=7.4, 25°C, 0.15 M $NaNO_3$). The description of the experiment is reported in *Chapter 3* and the values of the pseudo-first-order rate constant (k_{obs}) as a function of $[HA^-]$ are reported in Figure 13. According to the kinetic data in Figure 13, the electron-transfer (k_{HA}, Eq. (10)) can occur by the formation of the ternary Fe(III)L-HA intermediate between the ascorbate anion (HA^-) and the Fe(III)L complex through the substitution of the inner-sphere water molecule (Fe(III)L-HA, Eq. (9)).

$$Fe^{III}L + HA^- \overset{K_{FeL\text{-}HA}}{\rightleftharpoons} \{Fe^{III}L\text{-}HA^-\} \qquad K_{FeL-HA} = \frac{[\{Fe^{III}L - HA^-\}]}{[Fe^{III}L][HA^-]} \tag{9}$$

$$\{Fe^{III}L\text{-}HA^-\} \xrightarrow{k_{HA}} Fe^{II}L + \text{radical} \tag{10}$$

$$Fe^{III}L + \text{radical} \xrightarrow{fast} Fe^{II}L + A + H^+ \tag{11}$$

The Fe(III)L-HA can also react rapidly with the radical formed in the previous step (Eq. (11)). Rate and equilibrium constants characterizing the reduction of the Fe(III)-complexes are reported in Table 8.

$2Fe^{III}L + HA^{-} \longrightarrow 2Fe^{II}L + A + H^{+}$ (L=EDTA-BOM$_1$, EDTA-BOM$_2$) (11)

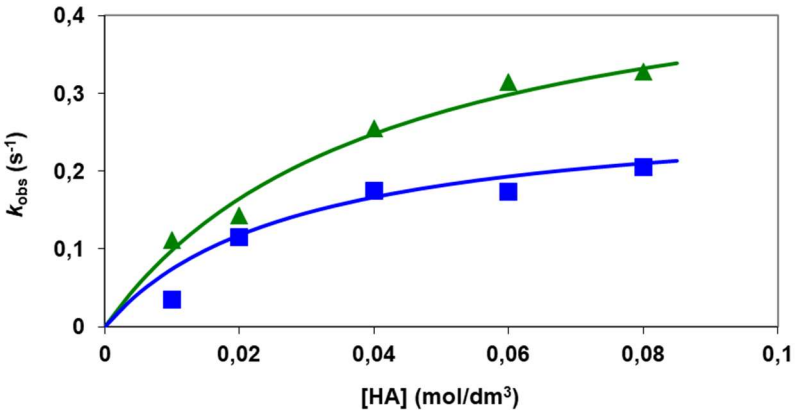

Figure 13. k_{obs} pseudo-first-order rate constant characterizing the reduction of [Fe(EDTA-BOM$_1$)]$^-$ (■) and [Fe(EDTA-BOM$_2$)]$^-$ (▲) by ascorbic acid. Solid lines and the open symbols represent the calculated and measured k_{obs} rate constants. ([FeL]=2.0×10^{-3} M, [HEPES]=0.01 M, 0.15 M $NaNO_3$, 25°C).

Table 8. Rate (k_i) and equilibrium constants (K_{FeL-HA}) and half-lives ($t_{1/2}$=ln2/k_d) characterizing the reduction of $[Fe(EDTA\text{-}BOM_1)]^-$, $[Fe(EDTA\text{-}BOM_2)]^-$ and $[Fe(EDTA)]^-$ complexes (0.15 M $NaNO_3$, 25°C).

	$[Fe(EDTA\text{-}BOM_1)]^-$	**$[Fe(EDTA\text{-}BOM_2)]^-$**	**$[Fe(EDTA)]^{-3}$**
k ($M^{-1}s^{-1}$)	20 ± 3	32 ± 5	8
K_{FeL-HA} (M^{-1})	71 ± 17	63 ± 19	75
$\log K_{FeLH-1}$	7.2 ± 0.2	7.4 ± 0.1	7.51
k_{obs} (s^{-1}) at phys. cond.	4.3×10^{-4}	5.3×10^{-4}	2.4×10^{-4}
$t_{1/2}$ (h) at phys. cond.	0.5	0.4	0.8

The reduction rate (k) of $[Fe(EDTA\text{-}BOM_1)]^-$ and $[Fe(EDTA\text{-}BOM_2)]^-$ by ascorbate are about 2 and 4 times higher than that of $[Fe(EDTA)]^-$. According to the previous studies of the Fe(III)-complex assisted oxidation of the ascorbic acid, the rate of the reactions decreases with the decrease of the electrode potential of the Fe(III)-complexes.[27–29] The slower ascorbate anion assisted reduction of the $[Fe(EDTA)]^-$ can be explained by the higher stability constant results in the lower Fe(III)/Fe(II) electrode potential value ($[Fe(EDTA)]^-$: $E_{1/2}$ = –132.5 mV vs SCE).[30]

By taking into account the stability of the ternary Fe(III)L-HA intermediates (K_{FeL-HA}, Table 8) and the *in vivo* concentration of the ascorbate anion ([HA-]=43 μM), [31] the ascorbate anion assisted reduction rate (k_{obs}) and half-lives ($t_{1/2}$=ln2/k_{obs}) of the $[Fe(EDTA\text{-}BOM_1)]^-$ and $[Fe(EDTA\text{-}BOM_2)]^-$ are 4.3×10^{-4} and 5.3×10^{-4} s^{-1}, and 0.5 and 0.4 hours which are about 63 and 33 times higher than those of the dissociation half-lives of the Fe(III)-complexes obtained from the

transchelation reactions with HBED near physiological condition (pH=7.4, 25°C, 0.15 M $NaNO_3$).

5.3 Conclusions

In this work we presented the study of Fe(III) complexes obtained starting from derivatives of the historically famous EDTA. In particular, the presence of lipophilic functionality has allowed us to study the interactions with biological macromolecules, thus also expanding the knowledge on the effect that the molecular tumbling can have on water proton relaxation enhancement. Among the studied complexes, the case of $[Fe(EDTA\text{-}(BOM)_2)]^-$ turned out to be the most fascinating, thus suggesting that a higher lipophilic character could have an important beneficial effect in terms of contrast enhancement, provided that this does not affect other main aspects such as the solubility. In conclusion, although our thermodynamic and kinetic studies suggest that the Fe(III) complexes of the EDTA-BOM_x series cannot be considered as potential candidates for clinical *in vivo* applications, they might represent an initial platform for the future design of complexes able to combine high efficacy, enhanced stability and inertness and non-covalent binding capability.

5.4 Notes and References

Author contribution: the author carried out the relaxometric measurements and analysed the data under the supervision of Professor Mauro Botta. Furthermore, the author carried out the

thermodynamic end kinetic experiments and their critical analysis under the supervision of Doctor Zsolt Baranyai.

(1) Eldik, R. van. *Advances in Inorganic Chemistry: Relaxometry of Water-Metal Ion Interactions*; Elsevier, 2005.

(2) Botta, M.; Carniato, F.; Esteban-Gómez, D.; Platas-Iglesias, C.; Tei, L. *Future Med. Chem.* **2019**, *11* (12), 1461–1483.

(3) Baranyai, Z.; Carniato, F.; Nucera, A.; Horváth, D.; Tei, L.; Platas-Iglesias, C.; Botta, *Chem. Sci.* **2021**, *12* (33), 11138–11145.

(4) Aime, S.; Chiaussa, M.; Digilio, G.; Gianolio, E.; Terreno, E. *JBIC J. Biol. Inorg. Chem.* **1999**, *4* (6), 766–774.

(5) Aime, S.; Botta, M.; Fasano, M.; Crich, S. G.; Terreno, E.. *JBIC J. Biol. Inorg. Chem.* **1996**, *1* (4), 312–319.

(6) Aime, S.; Anelli, P.; Botta, M.; Brocchetta, M.; Canton, S.; Fedeli, F.; Gianolio, E.; Terreno, E. *JBIC J. Biol. Inorg. Chem.* **2002**, *7* (1–2), 58–67.

(7) Kruk, D.; Kowalewski, J. *JBIC J. Biol. Inorg. Chem.* **2003**, *8* (5), 512–518.

(8) Aime, S.; Botta, M.; Esteban-Gómez, D.; Platas-Iglesias, C. *Mol. Phys.* **2019**, *117* (7–8), 898–909.

(9) Lauffer, R. B. *Chem. Rev.* **1987**, *87* (5), 901–927.

(10) Krohling, C. A.; Eutrópio, F. J.; Bertolazi, A. A.; Dobbss, L. B.; Campostrini, E.; Dias, T.; Ramos, A. C. *Soil Sci. Plant Nutr.* **2016**, *62* (1), 39–47.

(11) Koenig, S. H.; Brown, R. D. *Prog. Nucl. Magn. Reson. Spectrosc.* **1990**, *22* (6), 487–567.

(12) Solomon, I. *Phys. Rev.* **1955**, *99* (2), 559–565.

(13) Bloembergen, N.; Morgan, L. O. *J. Chem. Phys.* **1961**, *34* (3), 842–850.

(14) Freed, J. H. *J. Chem. Phys.* **1978**, *68* (9), 4034–4037.

(15) Swift, T. J.; Connick, R. E. *J. Chem. Phys.* **1962**, *37* (2), 307–320.

(16) Larsen, S. K.; Jenkins, B. G.; Memon, N. G.; Lauffer, R. B. *Inorg. Chem.* **1990**, *29* (6), 1147–1152.

(17) Snyder, E. M.; Asik, D.; Abozeid, S. M.; Burgio, A.; Bateman, G.; Turowski, S. G.; Spernyak, J. A.; Morrow, J. R. *Angew. Chem. Int. Ed.* **2020**, *59* (6), 2414–2419.

(18) Sokolow, G. E.; Crawley, M. R.; Morphet, D. R.; Asik, D.; Spernyak, J. A.; McGray, A. J. R.; Cook, T. R.; Morrow, J. R. *Inorg. Chem.* **2022**, *61* (5), 2603–2611.

(19) Avedano, S.; Botta, M.; Haigh, J. S.; L. Longo, D.; Woods, M. *Inorg. Chem.* **2013**, *52* (15), 8436–8450..

(20) Aime, S.; Botta, M.; Frullano, L.; Crich, S. G.; Giovenzana, G. B.; Pagliarin, R.; Palmisano, G.; Sisti, M. C. *Chem. – Eur. J.* **1999**, *5* (4), 1253–1260.

(21) Aime, S.; Botta, M.; Panero, M.; Grandi, M.; Uggeri, F. *Magn. Reson. Chem.* **1991**, *29* (9), 923–927.

(22) Wang, H.; Jordan, V. C.; Ramsay, I. A.; Sojoodi, M.; Fuchs, B. C.; Tanabe, K. K.; Caravan, P.; Gale, E. M. *J. Am. Chem. Soc.* **2019**, *141* (14), 5916–5925.

(23) Koppenol, W. H.; Hider, R. H. *Free Radic. Biol. Med.* **2019**, *133*, 3–10.

(24) Baranyai, Z.; Pálinkás, Z.; Uggeri, F.; Brücher, E.. *Eur. J. Inorg. Chem.* **2010**, *2010* (13), 1948–1956.

(25) Aime, S.; Botta, M.; Fasano, M.; Terreno, E. *Acc. Chem. Res.* **1999**, *32* (11), 941–949.

(26) Vlasova, I. M.; Saletsky, A. M. *J. Appl. Spectrosc.* **2009**, *76* (4), 536–541.

(27) Taqui-Khan, M.; Martell, A. E. *J. Am. Chem. Soc.* **1968**, 90, 3386

(28) Pelizzetti, E.; Mentasti, E.; Pramauro, E. *Inorg. Chem.* **1976**, *15* (11), 2898–2900.

(29) Pelizzetti, E.; Mentasti, E.; Pramauro, E. *Inorg. Chem.* **1978**, *17* (5), 1181–1186.

(30) Brausam, A.; Maigut, J.; Meier, R.; Szilágyi, P. Á.; Buschmann, H.-J.; Massa, W.; Homonnay, Z.; van Eldik, R. *Inorg. Chem.* **2009**, *48* (16), 7864–7884.

(31) May, P. M.; Linder, P. W.; Williams, D. R. *J. Chem. Soc. Dalton Trans.* **1977**, No. 6, 588–595.

6 Catechol-based ligands for Fe(III) complexation

The investigations reported so far have represented a key step in laying the groundwork for the development of new Fe(III)-based paramagnetic probes. In particular, we have succeeded in precisely defining the mechanisms affecting the paramagnetic relaxation enhancement effect of these complexes. Other very important aspects concern their thermodynamic stability and kinetic inertia. As an example from nature, in the last section of this dissertation we propose the study of systems based on siderophores, i.e., ligands with a high affinity toward Fe(III). In particular, we will address the study of catechol-based ligands. First, the analysis of a well-defined type of iron-catecholate, the Fe(III)-Tiron system, is proposed. In this way, we will be able both to verify the actual ability to form Fe(III)-complexes with high stability and to renew the fragmentary and now outdated literature data. From here, the first examples of novel catechol-based ligands for Fe(III) complexation are proposed. For each of these ligands, the synthesis, characterization and finally relaxometric studies of the corresponding Fe(III) complexes are shown.

6.1 Characterization of the Fe(III)-*Tiron* system in solution through an integrated approach combining NMR relaxometric, thermodynamic and kinetic data

6.1.1 Introduction

It has long been known that chelators containing catechol functional groups play an important biological role. For example, the presence of this chemical moiety characterizes the siderophores, compounds involved in the cellular transport of iron. In fact, the ability of catechol ligands to coordinate stably various metal ions has been used in a number of therapies. In general, catechol chelators show a remarkable affinity towards metal ions in high oxidation states. In particular, *Tiron*® (disodium 4,5-dihydroxy-1,3-benzendisulfonate) is a water-soluble and non-toxic ligand capable of strongly coordinating different metal ions and therefore of potential interest for use in chelation therapy. In the chemical field, *Tiron* is known for analytical applications, primarily as a chelating agent used in the determination of trace metals. For example, *Tiron* is used as a colorimetric reagent of various metal ions, among which Fe, Al and Ti, for the sequestration of Pb(II), the spectrofluorimetric determination of Cu(II) and the spectrophotometric detection of Th(IV) and Bi(III).[1–3]More recently, it has been proposed for uses in electrochemistry concerning the preparation of redox flow batteries or modified glass electrodes.[4,5]

However, *Tiron* is best known for its ability to form very stable Fe(III) complexes. This characteristic explains its widespread use as a complexometric indicator for the spectrophotometric detection of

Fe(III) ions.[6–8] The solution chemistry of the Fe(III)-*Tiron* system is quite complex and it is strongly affected by pH and ligand-to-metal molar ratios. As shown by UV-Vis spectrophotometric data, three distinct coordination complexes can be identified in aqueous solution in the different pH zones.[9,10] Each species is characterized by a well-defined stoichiometry, which determines its state of hydration and therefore its reactivity, stability and color. At pH values below 2, the turquoise-green solution is due to the presence of a complex in which only one unit of *Tiron* is coordinated to the metal center, which completes its coordination sphere with four water molecules (q = 4): $[Fe(Tiron)(H_2O)_4]^-$. In the pH range 4 - 5, the solution turns purple indicating the coordination of a second *Tiron* with displacement of two Fe^{III}-bound water molecules and the formation of the bishydrated complex (q = 2): $[Fe(Tiron)_2(H_2O)_2]^{5-}$. Finally, above pH 7 the coordination sphere of the ferric ion is occupied by three bidentate *Tiron* ligands and therefore the complex q = 0 is present in the bright red solution: $[Fe(Tiron)_3]^{9-}$ (Scheme 1).

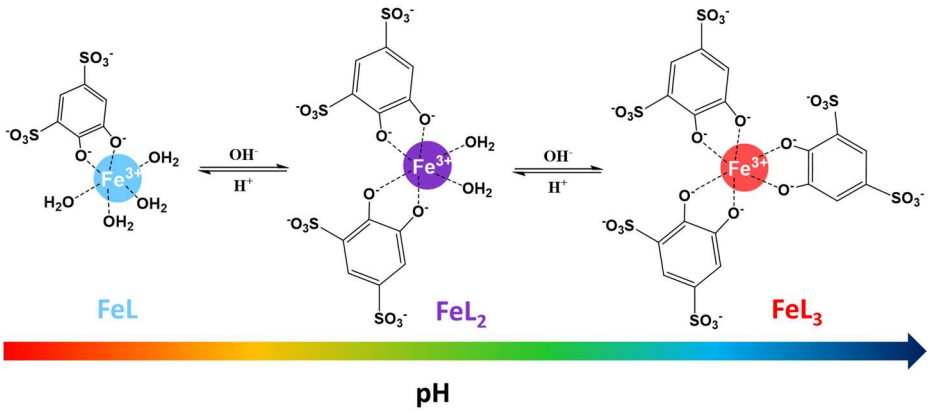

Scheme 1. Different complexes of the Fe(III)-*Tiron* system present in aqueous solution as a function of pH.

In the past, various studies have considered this system and a number of data have been reported. However, a detailed and complete characterization of each of the species present in solution is still missing. For instance, Ozutsumi *et al.* used EXAFS measurements to show that the three complexes share the same octahedral geometry characterized by Fe-O bond lengths of 200 pm.[11] UV-Vis spectrophotometry has been the main source of information on other physical-chemical properties of this system, such as thermodynamic stability, dissociation kinetics and the pH speciation.[9,10,12] These early studies have led to prove that all the complexes of the Fe-*Tiron* system are thermodynamically extremely stable. The logβ values of the q = 4, 2 and 0 species are 18.7, 33.4 and 44.8, respectively. These three complexes are paramagnetic and therefore their solutions are particularly suitable for NMR relaxometry studies. Fast field-cycling relaxometry (FFC-NMR) consists in the investigation of the dependence of the longitudinal nuclear magnetic relaxation rate ($1/T_1 = R_1$) of the solvent protons on the applied magnetic field in a dilute solution of the solute. In the case of paramagnetic complexes, the analysis of these data, the so-called NMRD dispersion profiles, allows to evaluate accurately a series of important molecular parameters related to the structural and dynamic properties of the metal ion. Among the most relevant it is worth indicating the hydration number q, the distance r_{MH} between the metallic center and the protons of the coordinated water molecule, its average lifetime τ_M in the inner coordination sphere, the molecular reorientation rate of the complex, $1/\tau_R$, the electronic relaxation times of the metal ion, $T_{1,2e}$.[13] Fe(III), with five unpaired electrons in the d orbitals, a ^6S configuration and a high magnetic moment (μ_{eff} = 5.9 B.M.), is very well suited to be

investigated through this technique. Additional information on the exchange kinetics of the coordinated water molecule(s) is provided by the measurement and analysis of the ^{17}O reduced transverse relaxation rates ($R_{2r} = 1/T_{2r}$) and chemical shift ($\Delta\omega_r$) of the bulk water as a function of temperature (280 − 350 K) at high field (11.74 T). To select the pH range in which the different complexes have a largely dominant population (>95%), an accurate species distribution diagram is required which is obtained from potentiometric and spectrophotometric titration data. These data were accurately re-measured under conditions of ferric ions and *Tiron* concentrations suitable for the relaxometric study. Finally, to complete the study we also evaluated their thermodynamic stability and kinetic inertness. We believe that the integrated use of these complementary techniques is able to provide a rather complete and accurate picture of the structure, dynamics and properties of paramagnetic species in solution not easily accessible otherwise.

6.1.2 Experimental section

Materials

For the relaxometric studies, a stock solutions of Fe^{3+} were prepared from $Fe(NO_3)_3 \cdot 9H_2O$ (reagent grade, Carlo Erba, Milano, Italy). The disodium 4,5-dihydroxy-1,3-benzenedisulfonate (Tiron®) was reagent grade (Fluka AG, Buchs, Switzerland). For the thermodynamic and kinetic investigations, the chemicals used for the experiments were of the highest analytical grade. $Fe(NO_3)_3$ was prepared by dissolving Fe_2O_3 (99.9% Fluka) in 6M HNO_3 and evaporating of the excess acid. The solid $Fe(NO_3)_3$ was dissolved in 0.1 M HNO_3 solution.

The concentration of the $Fe(NO_3)_3$ solutions was determined by complexometry with the use of standardized Na_2H_2EDTA in excess. The excess of the Na_2H_2EDTA was measured with standardized $ZnCl_2$ solution and xylenol orange as indicator. The H^+ concentration of the $Fe(NO_3)_3$ solution was determined by pH potentiometric titration in the presence of Na_2H_2EDTA excess. The concentration of *Tiron* and H_4CDTA solutions was determined by pH-potentiometric titration. All the measurements were made at constant ionic strength maintained by 0.15 M $NaNO_3$ at 25 °C.

Complexation of Iron(III)

For the synthesis of the Fe(III) chelates, 50 eq. of *Tiron* were dissolved in MilliQ water, following the addition of 1 eq. of a $Fe(NO_3)_3$ stock solution (pH = 0.5, $[Fe^{3+}]$=14.45 mM, determined by the Evans's method [14]). The pH was set to 2.51, 4.02 and 7.44 with NaOH 0.1 M in order to obtain $[Fe(Tiron)(H_2O)_4]^-$ (FeL), $[Fe(Tiron)_2(H_2O)_2]^{5-}$ (FeL2) and $[Fe(Tiron)_3]^{9-}$ (FeL3) respectively.

6.1.3 Results and discussion

Relaxometric characterization.

$1/T_1$ NMR relaxation measurements were performed as a function of pH, at 298 K and 32 MHz, to evaluate relaxivity and identify the pH range in which each species prevails (Figure 1). The ability to catalyze relaxation is called relaxivity (r_1) and measures the relaxation rate enhancement of water proton nuclei normalized to a 1 mM concentration of the paramagnetic ion. The sample was prepared following a well-established procedure reported in the literature,

using a Fe(III): *Tiron* molar ratio of 1:50.[15] In the r_1 vs pH profile of Figure 1, three different regions corresponding to the existence zones of the $[Fe(Tiron)_x]^{(4x-3)-}$ complexes are clearly distinguishable. The corresponding species distribution diagram is also shown in the same graph. The tetraaquo complex prevails in the acidic region (pH ≤ 2.2) and assumes an r_1 value of 3.5 mM^{-1} s^{-1} at pH = 2.0. The $[Fe(Tiron)_2(H_2O)_2]^{5-}$ complex is largely prevalent (> 90%) in the range of ca. 3.7 < pH < 4.9 and shows an r_1 value of 5.0 mM^{-1} s^{-1} at pH = 4.0. Finally, at pH values higher than 6.5 the aqueous solution contains only the *outer sphere* (q = 0) complex $[Fe(Tiron)_3]^{9-}$ and r_1 shows a constant value of ca. 2.9 mM^{-1} s^{-1}. From a preliminary qualitative evaluation, it is quite evident that there is no clear correlation between the relaxivity values and the hydration state of the complexes.

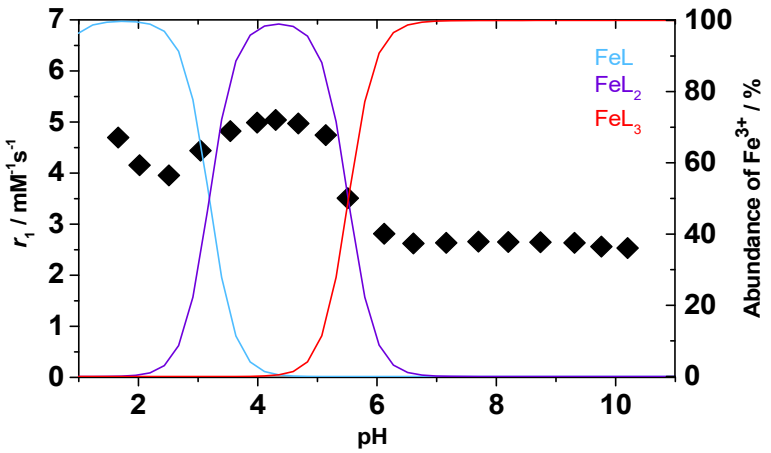

Figure 1. pH dependency of r_1 for the Fe(III)-*Tiron* system (32 MHz and 298 K, 1:50 ratio). The solid lines correspond to the percentage abundance of each of the three species.

It is well-established that the relaxivity can be considered as the sum of three contributions describing the different ways in which the modulation of the dipolar coupling between the electron magnetic moment of the metal ion and the nuclear magnetic moment of the

water protons can occur. One is associated with the water molecule(s) directly bound to the metal ion (inner sphere; IS), the other arises from water molecules interacting with polar groups of the ligand through long-lived hydrogen-bonds (second sphere; SS) and the third due to bulk water molecules diffusing in the proximity of the paramagnetic complex (outer sphere, OS):

$$r_1 = r_1^{\mathrm{IS}} + r_1^{\mathrm{SS}} + r_1^{\mathrm{OS}} \qquad (2)$$

The most important contribution is that associated with r_1^{IS}, which is directly proportional to the number of coordinated water molecules *q*. In fact, the inner-sphere relaxivity is given by the following expression:

$$r_1^{\mathrm{IS}} = \frac{[\mathrm{Fe}^{3+}]q}{55.56} \times \frac{1}{T_{1\mathrm{M}} + \tau_{\mathrm{M}}} \qquad (3)$$

In Eq. 3, T_{1M} is the relaxation rate of inner sphere protons and τ_M ($\tau_M = 1/k_{ex}$) the mean residence time of a water molecule in the inner coordination sphere of the metal ion. The relaxation rate of inner sphere protons in Fe^{3+} complexes is generally dominated by the dipole-dipole (DD) mechanism:

$$\frac{1}{T_{1\mathrm{M}}} = \frac{2}{15}\left(\frac{\mu_0}{4\pi}\right)^2 \frac{\gamma^2 g^2 \mu_B^2}{(r_{\mathrm{M-H}})^6} S(S+1) \times \left[\frac{3\tau_{d1}}{1+\omega_I^2\tau_{d1}^2} + \frac{7\tau_{d2}}{1+\omega_S^2\tau_{d2}^2}\right] \qquad (4)$$

In Eq 4, *g* is the electron *g*-factor, r_{M-H} the distance between the electron and nuclear spins, μ_B the Bohr magneton, γ the proton

gyromagnetic ratio, S the total spin (5/2 for a high-spin Fe^{3+} complex), ω_I the proton resonance frequency, and ω_S the Larmor frequency of the Fe^{3+} electron spin. The correlation time τ_{di} is given by Eq 5, where τ_R is the rotational correlation time, and T_{ie} are the longitudinal (i = 1) and transverse (i = 2) relaxation times of the electron spin.

$$\frac{1}{\tau_{di}} = \frac{1}{\tau_R} + \frac{1}{\tau_M} + \frac{1}{T_{ie}} \qquad i = 1,2 \tag{5}$$

r_1^{IS} scales with q and therefore, making the reasonable assumption of a comparable contribution of r_1^{OS} in the three complexes, we should expect that r_1 (Fe**L1**) > r_1 (Fe**L2**) > r_1 (Fe**L3**). It follows that the lack of a clear relationship between q and r_1 is connected to the occurrence of a relevant contribution of r_1^{SS}. In particular, this mechanism appears to be dominant in the case of Fe**L3** and could be attributed to H-bonding interaction between water molecules and the six sulfonic groups on the three *Tiron* ligands.

- Fe**L3**. This additional contribution can be easily appreciated by comparing the relaxation values for Fe**L3** and $[Fe(DTPA)]^{2-}$, both q = 0 complexes. At 1.5 and 3.0 T (298 K) the r_1 values are 2.8 and 3.1 mM^{-1} s^{-1} for Fe**L3** and 0.71 and 0.72 mM^{-1} s^{-1} for $[Fe(DTPA)]^{2-}$. For Fe**L3** these r_1 values are about 300% greater than the corresponding values for $[Fe(DTPA)]^{2-}$. These values are also significantly greater than those reported for several other q = 0 complexes, such as $[Fe(EHPG)]^-$, $[Fe(EHBG)]^-$, $[Fe(NOTA)]^-$ and their derivatives.[16–23] The SS contribution to the relaxivity of Fe**L3** can be assessed by measuring the $1/T_1$ ^1H NMRD profiles over a wide range of frequency values and analyzing the data using the Freed's equation for the OS mechanism and the

equations 3-5, suitable also for the SS mechanism by making some reasonable assumptions.[24] The experimental profiles, shown in Figure 2, were measured over proton Larmor frequency range 0.01-500 MHz at four different temperatures (283, 288, 298 and 310 K) and at pH = 7.4. Typical values of the Fe^{3+} complexes were assigned to some parameters that describe the OS contribution: the diffusion coefficient (D), its activation energy (E_D) and the distance of closest approach (a) of the proton nuclei of outer sphere water molecules to the paramagnetic ion (Table 1).[16] For the fit of the data also some of the parameters of the SS contribution were fixed to reasonable values. The number of SS water molecules was assumed to be five (q^{SS} = 5), r^{SS}, from the metal ion was set to 3.5 Å.

The best-fit parameters are reported in Table 1. We obtained an excellent fit of the r_1 profiles of Fe**L3** on the basis of a τ_R^{SS} of 35.3 ps and an associated activation energy, E_R^{SS}, of 15.0 kJ mol^{-1}. The parameters characterizing the relaxation of the electron spin, the mean square transient ZFS energy (Δ^2), and its correlation time (τ_v) assume values in the normal range reported for Fe(III) chelates and fully comparable to those calculated for $[Fe(CDTA)(H_2O)]^-$.[16] As previously observed, the variation of r_1 with temperature is well reproduced if the zero-field splitting energy Δ is allowed to vary with temperature, according to an Arrhenius behavior with activation energy E_Δ (Table 1).[16] From the calculated SS and OS contributions to the NMRD profile at 298 K (Figure 2) we can conclude that the r_1^{SS} component represents a contribution of about 65-70% to total relaxivity.

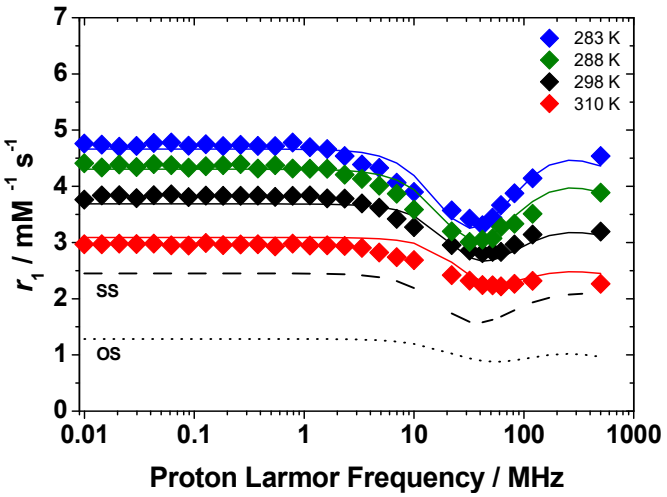

Figure 2. ^{1}H NMRD profiles of [Fe(*Tiron*)$_3$]$^{9-}$ at 283 (♦), 288 (♦), 298 (♦) and 310 (♦) K and pH = 7.4 ([Fe^{3+}] = 1.88 mM, [*Tiron*] = 94 mM). The solid lines correspond to the fit of the data. Dashed and dotted curves show the calculated second- and outer-sphere contributions to relaxivity, respectively (298 K).

- Fe**L2**. As previously mentioned, the value of r_1 of [Fe(*Tiron*)$_2$(H$_2$O)$_2$]$^{5-}$, at 32 MHz and 298 K, is 5.0 mM^{-1} s^{-1}, which is markedly higher than that of the q = 1 complex [Fe(CDTA)(H$_2$O)]$^-$ (r_1 = 2.2 mM^{-1} s^{-1}) under similar experimental conditions.[16] This simple consideration highlights the lack of a clear relationship between relaxivity and hydration state, suggesting also in this case the presence of a marked contribution of the SS mechanism. The NMRD profiles are reported in Figure 3 and need be analyzed taking into account all three contributions to r_1. Fe**L2** contains two *Tiron* ligands and therefore we can assume the presence of two water molecules (q^{SS} = 2) involved in hydrogen bonding interactions with the four sulfonate groups. Furthermore, as regards the analysis of SS and OS contributions we used the same procedure described for Fe**L3**, setting different parameters at reasonable values.

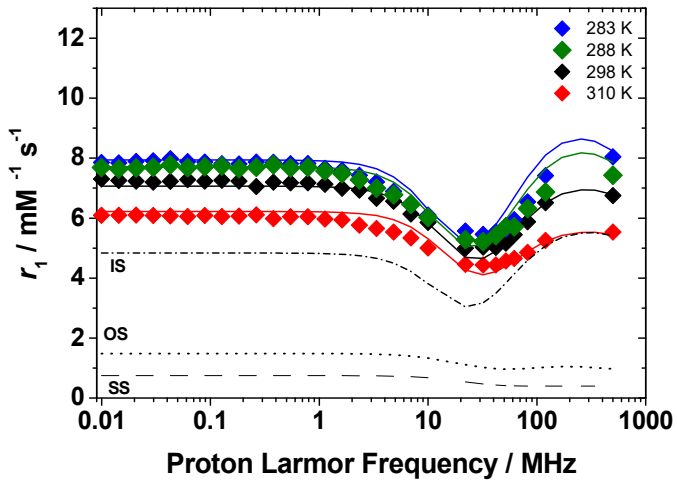

Figure 3. ^{1}H NMRD profiles (pH = 4.0) at different temperatures (283 (♦), 288 (♦), 298 (♦) and 310 K (♦)) of [Fe(*Tiron*)$_2$(H$_2$O)$_2$]$^{5-}$ ([Fe^{3+}] = 1.88 mM, [*Tiron*] = 94 mM). The solid lines correspond to the fit of the data. Dot-dashed, dashed and dotted curves show the calculated inner-, second- and outer-sphere contributions to relaxivity at 298 K.

The presence of two metal-bound water molecules requires consideration of a strong IS contribution to relaxivity (equations 3-5). Based on literature data, we fixed the metal–proton distance of the coordinated water molecules (r_{M-H} = 2.70 Å). Information on the exchange dynamics of the two bound water molecules were obtained from recording and analyzing reduced ^{17}O transverse relaxation rates ($1/T_{2r}$) and chemical shifts ($\Delta\omega_r$) data of an aqueous solution of the complex at 11.7 T (Figure 4). The transverse relaxation rates decrease as the temperature decreases, a behavior that indicates an intermediate/slow exchange regime, in which τ_M is not negligible compared to the transverse relaxation time of the two coordinated water molecules ($\tau_M \sim T_{2M}$). Such a process is dominated by the scalar

mechanism, which depends on the square of the hyperfine coupling constant $A_O/\hbar$. The chemical shifts, $\Delta\omega_r$, are directly proportional to $A_O/\hbar$, and therefore provide a complementary set of data. The ^{17}O NMR data were analyzed using the Swift–Connick equations.[25]

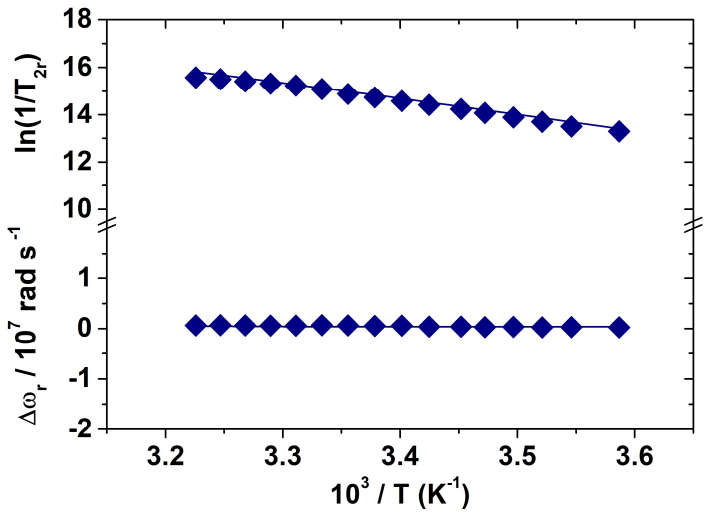

Figure 4. Reduced ^{17}O NMR transverse relaxation rates and chemical shifts of $[Fe(\textit{Tiron})_2(H_2O)_2]^{5-}$, measured at 11.74 T ($[Fe^{3+}]$ = 7.94 mM, [*Tiron*] = 39.7 mM, pH = 4.34).

We carried out a global fit of the ^1H NMRD profiles and ^{17}O NMR data, which is well known to be able to provide accurate and reliable values of the molecular parameters that influence relaxation. An excellent fit of the ^1H NMRD and ^{17}O NMR data was obtained with the parameters reported in Table 1. The analysis provided a value for τ_R (70 ps) which is entirely in line with those found for corresponding complexes of Mn(II) or Gd(III) of similar molecular mass. The values of the electron relaxation parameters, Δ^2 and τ_V, fall within the range of values typical of the previously investigated Fe(III) complexes.[16] The average

residence lifetime of the coordinated water molecules, τ_M = 272 ns, is rather long compared to those found for $[Fe(EDTA)(H_2O)]^-$ (0.9 ns) and $[Fe(CDTA)(H_2O)]^-$ (36 ns).[16] It is possible that in Fe**L2**, where the metal ion is hexacoordinated, there is a lower degree of steric hindrance near the water coordination sites and therefore a stronger interaction with the Fe^{3+} ion. Finally, the parameters relating to the SS contribution are fully comparable with those calculated for Fe**L3**, the only substantial difference being the number of second-sphere water molecules, i.e. two versus five. In summary, the relaxivity of Fe**L2** is dominated by the IS mechanism which provides a contribution of about 77% to r_1, while the SS mechanism is only about 8% of the observed relaxivity (r_1 = 6.5 mM^{-1} s^{-1}; 3T and 298 K). The latter, although rather small, is not a negligible contribution and without taking it into consideration the best-fit procedure provides unsatisfactory results.

- Fe**L1**. The presence of four coordinated water molecules in Fe**L1** would suggest an IS contribution twice greater than that estimated for Fe**L2**. This would imply a value of r_1 of about 10 mM^{-1} s^{-1} at 3 T and 298 K. Instead, the measured value is only 3.3 mM^{-1} s^{-1} and the NMRD profiles, shown in Figure 5, clearly indicate a decrease in r_1 across the entire range of frequencies. Furthermore, unlike Fe**L3** and Fe**L2**, in this case the relaxivity values decrease with decreasing temperature, a clear indication that the complex is in the slow exchange conditions ($\tau_M \geq T_{2M}$), in which the long value of τ_M represents a limiting factor for r_1. Following an approach completely similar to that used to study Fe**L2**, we measured the ^{17}O NMR values of R_2 and paramagnetic shift as a function of temperature (Figure 6) and performed a simultaneous fitting procedure of the NMRD profiles and ^{17}O data, obtaining the

parameters reported in Table 1 which allow to reproduce the experimental values very well.

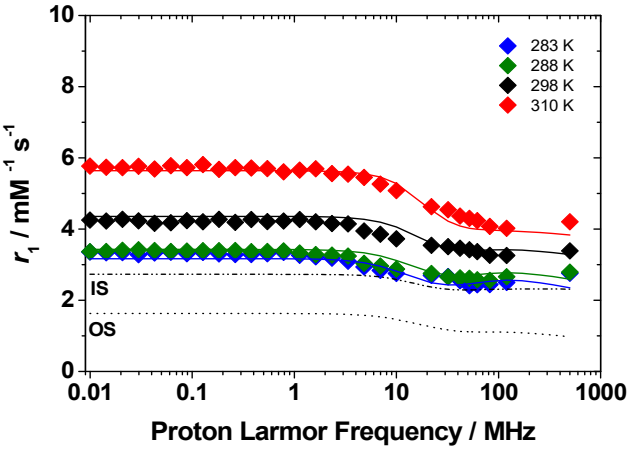

Figure 5. ^{1}H NMRD profiles (pH = 2.51) at different temperatures (283 (◆), 288 (◆), 298 (◆) and 310 K (◆)) of [Fe(*Tiron*)$(H_2O)_4]^-$ ([Fe^{3+}] = 2.09 mM, [*Tiron*] = 5.22 mM). The solid lines correspond to the fit of the data. Dot-dashes and dots indicate respectively the inner and outer-sphere contribution to relaxivity at 298 K.

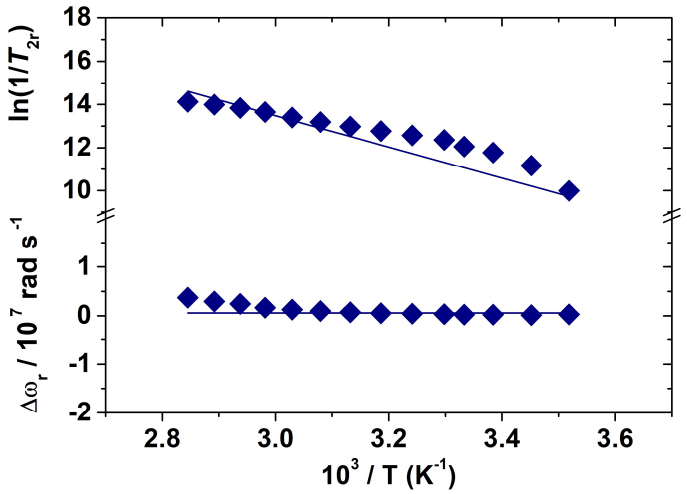

Figure 6. Reduced ^{17}O NMR transverse relaxation rates and chemical shifts of [Fe(*Tiron*)$(H_2O)_4]^-$measured at 11.74 T ([Fe^{3+}] = 8.25 mM, [*Tiron*] = 21.13 mM, pH = 2.17).

Table 1. Data obtained from the simultaneous fit of ^{1}H NMRD profiles ^{17}O NMR data*.

Parameters	$[Fe(Tiron)_3]^{9-}$ (MW = 860 g/mol)	$[Fe(Tiron)_2(H_2O)_2]^{5-}$ (MW = 628 g/mol) *	$[Fe(Tiron)(H_2O)_4]^{-}$ (MW = 344 g/mol) *	$[Fe(t\text{-}CDTA)(H_2O)]^{-}$ (MW = 416 g/mol) *,[b]
$^{298}r_1$ 60/120 MHz / mM^{-1} s^{-1}	2.8 / 3.2	5.4 / 6.5	3.4 / 3.3	2.1 / 2.4
$^{298}\Delta^2$ / 10^{20} s^{-2}	9.7 ± 0.1	12.2 ± 0.1	5.5 ± 0.1	18.1 ± 1.3
E_Δ / kJ mol^{-1}	4.6 ± 0.9	2.7 ± 1.2	3.3 ± 1.7	9.8 ± 0.5
$^{298}\tau_V$ / ps	6.9 ± 0.1	5.6 ± 0.6	9.2 ± 0.5	3.4 ± 0.2
$A_O/\hbar$ / 10^6 rad s^{-1}	/	-50.1 ± 4.8	-71.6 ± 5.7	-62.8[a]
$^{298}\tau_M{}^O$ / ns	/	272 ± 57	18000 ± 720	36.1 ± 4.4
ΔH_M / kJ mol^{-1}	/	56.2 ± 10.7	57.5 ± 2.5	51.5 ± 9.9
C_{os}	/	0.04 ± 0.02	0.05 ± 0.01	/
$^{298}\tau_R$ / ps	/	70.0 ± 5.5	34.7 ± 2.5	48.4 ± 2.3
E_R / kJ mol^{-1}	/	16.0 ± 4.9	15.0 ± 5.0	21.1 ± 2.3
$^{298}\tau_R{}^{SS}$/ ps	52.7 ± 0.2	31.2 ± 8.2	/	/
$E_R{}^{SS}$ / kJ mol^{-1}	15.3 ± 0.6	11.0 ± 1.4	/	/
q	0 [a]	2 [a]	4 [a]	1 [a]
q^{SS}	5 [a]	2 [a]	/	/
r / Å	/	2.70 [a]	2.70 [a]	2.70 [a]
r^{SS} / Å	3.50 [a]	3.25 [a]	/	/

[a] Fixed parameters. Additional parameters fixed for fitting: E_V = 1.0 kJ mol^{-1}, ^{298}D = 2.24×10^5 cm^2, a = 3.5 Å; [b] From Ref. 16

The average life time τ_M calculated is over 65 times longer than that found for Fe**L2** and of the same order of magnitude as that for the aqua ion, $[Fe(H_2O)_6]^{3+}$.[16] This is probably one of the longest reported

values for an anionic metal complex of Gd^{III}, Mn^{II}, Fe^{III}. Even the electron relaxation parameters, although falling within the range of characteristic values of Fe(III) complexes, are very similar to those reported for $[Fe(H_2O)_6]^{3+}$.[16] The hyperfine coupling constant $A_O/\hbar$, on the other hand, has a value approximately intermediate between that of $[Fe(t\text{-CDTA})(H_2O)]^-$ and that of $[Fe(H_2O)_6]^{3+}$. The molecular correlation time τ_R is quite small, in excellent agreement with the reduced molecular mass of this complex. The results of the best-fit procedure are insensitive to the consideration of the presence of a contribution from SS. The presence of four water molecules in the inner coordination sphere of the metal ion makes the IS contribution largely dominant.

In conclusion, the integrated ^1H FFC relaxometric and ^{17}O NMR data provide a set of coherent and sufficiently accurate molecular parameters that well describe the structure, the hydration state, the molecular tumbling motion and the dynamics of the solvent exchange process of the species present in the different pH ranges of the Fe(III)/*Tiron* system. This information is very useful and difficult to obtain through other experimental procedures.

Solution thermodynamics.

Acid-base properties of the *Tiron* ligand were studied by pH-potentiometry. The protonation constants ($\log K_i^H$) of the ligands, defined by Eq. (5), are listed in Table 2 (standard deviations are shown in parentheses).

$$K_i^H = \frac{[H_iL]}{[H_{i-1}L][H^+]} \qquad i = 0 \text{ and } 1 \qquad (5)$$

The protonation scheme of *Tiron* was well characterized by both spectroscopic and potentiometric methods.[9,10] These studies reveal that the first and second protonation of *Tiron* occur at two phenolate O-donor atoms.

Table 2. Protonation constants of *Tiron*, stability and protonation constants of the corresponding Fe(III)-complexes (25°C).

I	0.15 M $NaNO_3$	0.2 M KCl[10]	1.0 M KNO_3[9]
$\log K_1^H$	12.40 ± 0.01	11.96	11.78
$\log K_2^H$	7.46 ± 0.03	7.46	7.19
$\log K_{FeL}$	20.32 ± 0.01	18.61	18.8
$\log K_{FeL2}$	14.49 ± 0.02	14.77	14.7
$\log K_{FeL3}$	9.83 ± 0.02	11.06	11.60
$\log K_{FeL2H-1}$	7.86 ± 0.06	5.98	–

Comparison of the protonation constants obtained in 0.15 M $NaNO_3$, 0.2 M KCl or 1.0 M KNO_3 indicates that $\log K_i^H$ values of *Tiron* are independent of the ionic strength (Table 1). *Tiron* forms very stable complexes with Fe(III) ion.[10] Consequently, the determination of the equilibrium constants characterizing the species formed in the Fe(III)–*Tiron* system based only on pH-potentiometric studies is impossible. However, the interaction between Fe(III) ion and *Tiron* can be studied by monitoring the charge transfer absorption band in the wavelength range 400 – 800 nm. The absorption spectra Fe(III)-*Tiron* systems recorded in the -log[H^+] range 0.0 - 10.0 are shown in Figure 7. Spectra changes in Fe(III)-*Tiron* systems can be interpreted by the formation

of the [Fe(*Tiron*)]$^{-}$ (Fe**L1**, λ_{max} = 680 nm; Eq. (6)), [Fe(*Tiron*)$_2$]$^{5-}$ (Fe**L2**, λ_{max} = 562 nm; Eq. (7)) and [Fe(*Tiron*)$_3$]$^{9-}$ species (Fe**L3**, λ_{max} = 480 nm Eq. (8)) in the -log[H$^+$] ranges 0.0 – 3.0, 3.0 – 6.0 and 6.0 – 8.0, respectively.

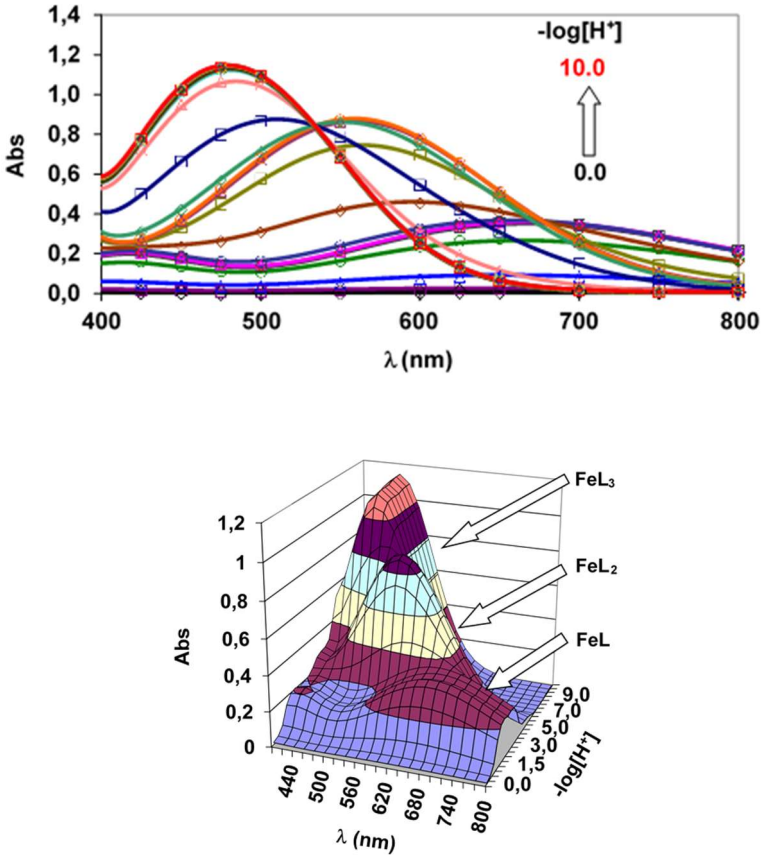

Figure 7. Absorption spectra of Fe(III)-*Tiron* system. The solid lines and the open symbols represent the experimental and the calculated absorbance values, respectively ([Fe^{3+}]=0.19 mM, [*Tiron*]=9.1 mM, 0.15 M $NaNO_3$, 25°C).

$$Fe^{3+} + \ Tiron \ \rightleftharpoons \ [Fe(Tiron)]^{-} \qquad (6)$$

$$K_{[Fe(Tiron)]^{-}} = \frac{[Fe(Tiron)^{-}]}{[Fe^{3+}][Tiron]}$$

$$[Fe(Tiron)]^{-} + \quad Tiron \quad \rightleftharpoons \quad [Fe(Tiron)_2]^{5-} \qquad (7)$$

$$K_{[Fe(Tiron)_2]^{5-}} = \frac{[Fe(Tiron)_2{}^{5-}]}{[Fe(Tiron)^{-}][Tiron]}$$

$$[Fe(Tiron)_2]^{5-} + \quad Tiron \quad \rightleftharpoons \quad [Fe(Tiron)_3]^{9-} \qquad (8)$$

$$K_{[Fe(Tiron)_3]^{9-}} = \frac{[Fe(Tiron)_3{}^{9-}]}{[Fe(Tiron)_2{}^{5-}][Tiron]}$$

The pH-potentiometric data of the Fe(III)–*Tiron* system at 1:2 metal to ligand concentration ratio indicate base consuming processes in the pH range 6.0 – 9.0. These processes can be accounted to the formation of the $[Fe(Tiron)_2H_{-1}]^{6-}$ species via the substitution of a H_2O molecule with an OH^- anion (Eq. (9)):

$$[Fe(Tiron)_2H_{-1}]^{6-} + \quad H^{+} \quad \rightleftharpoons \quad [Fe(Tiron)_2]^{5-} \qquad (9)$$

$$K_{[Fe(Tiron)_2H_{-1}]^{6-}} = \frac{[Fe(Tiron)_2{}^{5-}]}{[Fe(Tiron)_2H_{-1}{}^{6-}][H^{+}]}$$

The stability and protonation constants of the $[Fe(Tiron)]^{-}$, $[Fe(Tiron)_2]^{5-}$, $[Fe(Tiron)_3]^{9-}$ and $[Fe(Tiron)_2H_{-1}]^{6-}$ species are shown in Table 2. The species distribution of the Fe(III)-*Tiron* system are shown in Figures 8 and 9.

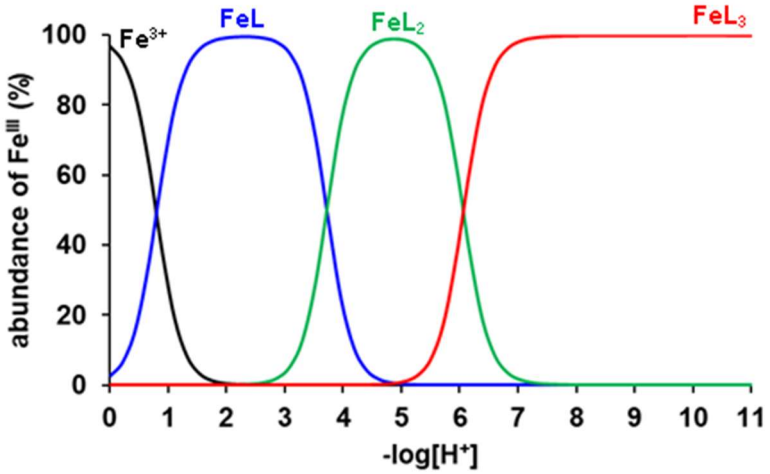

Figure 8. Species distribution of the Fe(III)–*Tiron* system ([Fe^{3+}]=0.2 mM, [*Tiron*]=9.0 mM, 0.15 M $NaNO_3$, 25°C).

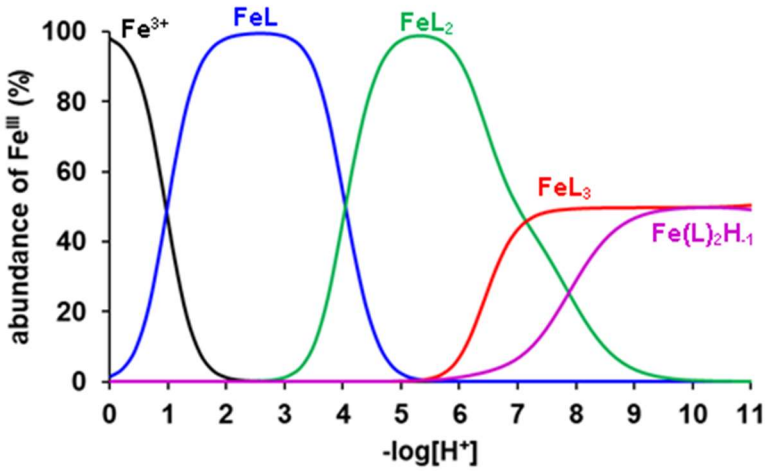

Figure 9. Species distribution of the Fe(III)–*Tiron* system ([Fe^{3+}]=0.2 mM, [*Tiron*]=5.0 mM, 0.15 M $NaNO_3$, 25°C).

Kinetic studies.

The kinetic inertness of $[Fe(Tiron)_x]^{(4x-3)-}$ was determined by following the transchelation reactions between the Fe(III)-complexes and the

CDTA ligand via spectrophotometry on the absorption band of the $[Fe(\textit{Tiron})_x]^{(4x-3)-}$ complexes (λ=562 nm) in the pH range 5.0 – 7.5. Based on the equilibrium data (Table 2), the $[Fe(\textit{Tiron})_2]^{5-}$ and $[Fe(\textit{Tiron})_3]^{9-}$ species dominates in the presence of 5 fold *Tiron* excess in the pH range 5.0 – 7.5 ($[Fe^{3+}]$ = 0.1 mM, [*Tiron*]=0.5 mM, 0.15 M $NaNO_3$, 25 °C). Transchelation reactions of the $[Fe(\textit{Tiron})_2]^{5-}$ and $[Fe(\textit{Tiron})_3]^{9-}$ species were investigated in the presence of 20 – 80 fold CDTA excess in order to guarantee pseudo-first-order kinetic conditions (Eq. (10), x=2 and 3; y=1 and 2; z=1 and 2). Some characteristic absorption spectra of the $[Fe(\textit{Tiron})_x]^{(4x-3)-}$–CDTA reacting systems are shown in Figure 10. The proposed mechanism is shown in Scheme 2. The rate and equilibrium constants characterizing the transmetallation reactions of $[Fe(\textit{Tiron})_2]^{5-}$ and $[Fe(\textit{Tiron})_3]^{9-}$ complexes are summarized and compared with those of $[Fe(EDTA)]^-$ and $[Fe(CDTA)]^-$ complexes in Table 3. Definitions and equations used for the evaluation of the kinetic data are reported in *Chapter 3*. As it is shown in Figure 11 and 12, the k_d values increase with increase of $[H^+]$ and $[CDTA]_t$ especially at pH < 6.0. The transchelation reaction of Fe(III)-complexes takes place by the relatively slow dissociation of $[Fe(\textit{Tiron})_2]^{5-}$ and $[Fe(\textit{Tiron})_3]^{9-}$ species, which is followed by a fast reaction between the free Fe(III) ion and the exchanging CDTA ligand.

$$[Fe(\textit{Tiron})_x] + H_yCDTA \quad Fe(CDTA) + H_z\textit{Tiron} \qquad (10)$$

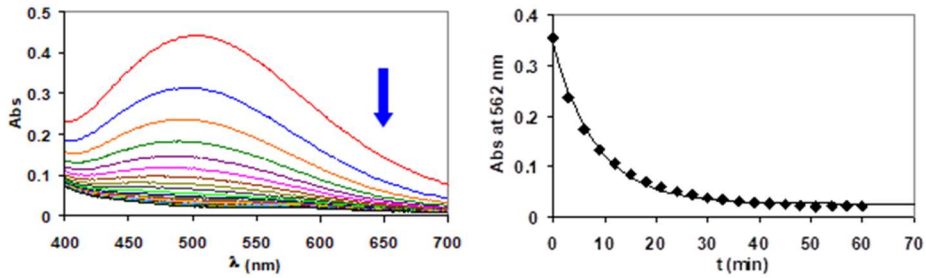

Figure 10. Absorption spectra and the absorbance values of the $[Fe(\textit{Tiron})_x]^{(4x-3)-}$–CDTA reacting system at 562 nm ($[Fe^{3+}]_t$=0.1 mM, $[\textit{Tiron}]_t$=0.5 mM, $[CDTA]_t$=8 mM, pH=6.50, 0.15 M $NaNO_3$, 25°C).

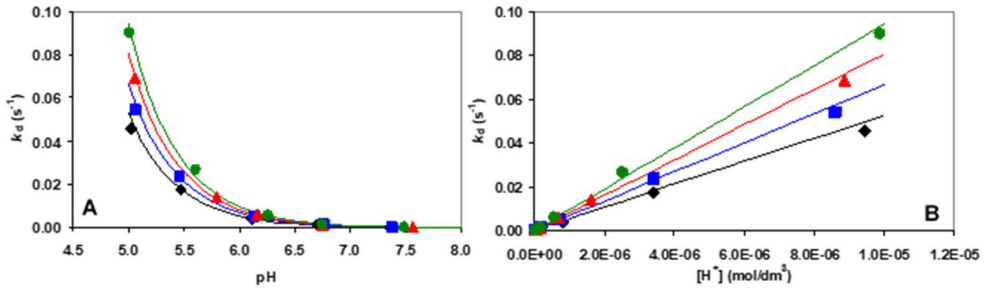

Figure 11. Pseudo-first order rate constants (k_d) characterize the transchelation reactions of $[Fe(\textit{Tiron})_x]^{(4x-3)-}$ with CDTA ligand as a function of pH (**A**) and $[H^+]$ (**B**) (x=2 and 3, ($[Fe^{3+}]_t$=0.1 mM, $[\textit{Tiron}]_t$=0.5 mM, $[CDTA]_t$=2.0 (◆), 4.0 (■), 6.0 (▲) and 8.0 mM (●), pH=6.50, 0.15 M $NaNO_3$, 25°C).

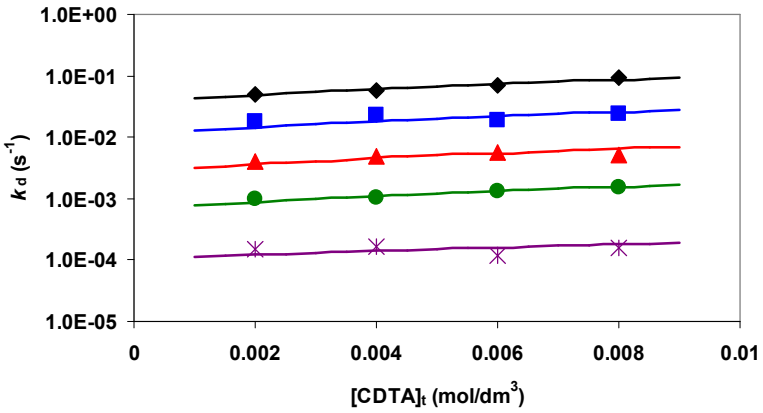

Figure 12. Pseudo-first order rate constants (k_d) characterize the transchelation reactions of $[Fe(Tiron)_x]^{(4x-3)-}$ with CDTA ligand as a function of $[CDTA]_t$. (x=2 and 3, ($[Fe^{3+}]_t$=0.1 mM, $[Tiron]_t$=0.5 mM, pH=5.04 (◆), 5.56 (■), 6.16 (▲), 6.74 (●) and 7.44 (✳) pH=6.50, 0.15 M $NaNO_3$, 25°C).

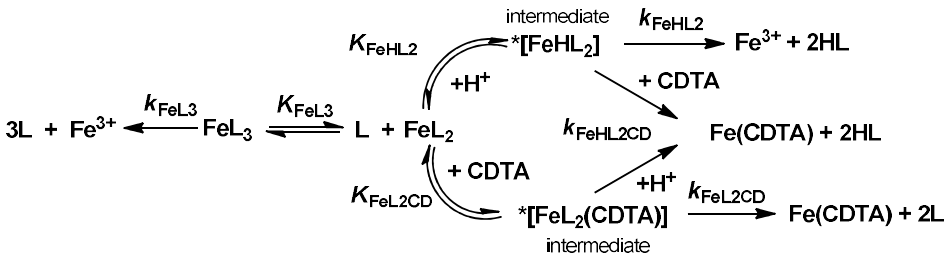

Scheme 2. Mechanism of the transchelation reaction between $[Fe(Tiron)_x]^{(4x-3)-}$ and CDTA (x = 2 and 3).

Table 3. Rate and equilibrium constants characterizing the transchelation reactions of $[Fe(\textit{Tiron})_x]^{(4x-3)-}$, $[Fe(EDTA)]^-$ and $[Fe(CDTA)]^-$ complexes (x=2 and 3, 0.15 M $NaNO_3$, 25°C).

	$[Fe(\textit{Tiron})_x]^{(4x-3)-}$	**$[Fe(EDTA)]^-$** [16]	**$[Fe(CDTA)]^-$** [16]
k_0 (s^{-1})	$(4.7 \pm 0.6) \times 10^{-5}$	5×10^{-6}	3.2×10^{-7}
k_1 ($M^{-1}s^{-1}$)	$(3.9 \pm 0.5) \times 10^{3}$	–	–
k_4 ($M^{-2}s^{-1}$)	$(7 \pm 1) \times 10^{5}$	–	–
k_{OH} ($M^{-1}s^{-1}$)	–	1.0	3.6×10^{-3}
k_{OH}^2 ($M^{-2}s^{-1}$)	–	1.4×10^{3}	1.2
$\log K_{FeL3}$	**9.20 ± 0.02**	–	–
$\log K_{FeLH-1}$	–	**7.41**	**9.58**
k_d (s^{-1}) at pH=7.4	1.1×10^{-4}	2.9×10^{-6}	2.1×10^{-9}
$t_{1/2}$ (h) at pH=7.4	1.8	66	8.9×10^{4}

FeL_2: $k_1 = k_{FeHL2} \times K_{Fe(HL2)}$; $k_4 = k_{FeHL2CD} \times K_{Fe(HL2)}$ or $k_{FeHL2CD} \times K_{FeL2CD}$; **$FeL_3$:** $k_0 = k_{FeL3}$

The transchelation reaction can occur via the spontaneous dissociation of $[Fe(\textit{Tiron})_3]^{9-}$ (k_0, Eq. (11)), proton- (k_1, Eq. (12), proton- and CDTA-assisted dissociation (k_4, Eqs. (13) and (14)) of $[Fe(\textit{Tiron})_2]^{5-}$, through the formation of a protonated $*[FeHL_2]$ ($K_{Fe(HL2)}$, Eq. (15)) and a ternary $*[FeL_2(CDTA)]$ intermediates (K_{FeL2CD}, Eq. (16)). Interestingly, the stability constant of the $[Fe(\textit{Tiron})_3]^{9-}$ complex obtained by the kinetic studies ($\log K_{FeL3}$=9.20, Table 3) agrees well with $\log K_{FeL3}$ value determined by pH-potentiometric and spectrophotometric studies ($\log K_{FeL3}$=9.83 (2), Table 2), which clearly confirms the correctness of the kinetic model used for the description of the $[Fe(\textit{Tiron})_x]^{(4x-3)-}$–CDTA reacting systems.

$$FeL_3 \xrightarrow{k_{FeL3}} Fe^{3+} + 3L \qquad (11)$$

$$FeHL_2 \xrightarrow{k_{FeHL2}} Fe^{3+} + 2H_xL \quad (12)$$

$$[FeL_2(CDTA)] + H^+ \xrightarrow{k_{FeHL2CD}} [Fe(CDTA)] + 2HL \quad (13)$$

$$[FeHL_2] + CDTA \xrightarrow{k_{FeHL2CD}} [Fe(CDTA)] + 2HL \quad (14)$$

$$FeL_2 + H^+ \rightleftharpoons FeHL_2$$
$$K_{FeHL_2} = \frac{[FeHL_2]}{[FeL_2][H^+]} \quad (15)$$

$$FeL_2 + CDTA \overset{K_{FeL2CD}}{\rightleftharpoons} FeL_2(CDTA) \quad (16)$$
$$K_{FeL_2CD} = \frac{[FeL_2(CDTA)]}{[FeL_2][CDTA]_t}$$

Since the transchelation of the $[Fe(EDTA)]^-$ and $[Fe(CDTA)]^-$ complexes with HBED take place by different pathways (the spontaneous (k_0), first- (k_{OH}) and second-order (k_{OH}^2) hydroxide-assisted dissociation),[10] the dissociation rate constants (k_d) and half-life ($t_{1/2}$=ln2/k_d) values of $[Fe(\textit{Tiron})_x]^{(4x-3)-}$, $Fe(EDTA)]^-$ and $[Fe(CDTA)]^-$ complexes have been calculated near to physiological condition (Table 3, pH=7.4 and 25°C) in order to compare the kinetic inertness of the Fe(III) complexes. The dissociation rate constant (k_d) of $[Fe(EDTA)]^-$ and $[Fe(CDTA)]^-$ complexes are about 50000 and 37 times smaller than that of $[Fe(\textit{Tiron})_x]^{(4x-3)-}$ which indicates a relatively low inertness of $[Fe(\textit{Tiron})_x]^{(4x-3)-}$ species at pH=7.4 due to the fast dissociation of the

[Fe(*Tiron*)$_2$]$^{5-}$. However, the dissociation half-life of [Fe(*Tiron*)$_3$]$^{9-}$ species dominates at pH ≥ 8.0 ($t_{1/2}$=4.1 hour, 25°C) reveals the very slow decoordination of the first *Tiron* ligand in [Fe(*Tiron*)$_3$]$^{9-}$ results in the higher kinetic inertness of [Fe(*Tiron*)$_3$]$^{9-}$ species than that of [Fe(*Tiron*)$_2$]$^{5-}$.

6.2 Polydentate ligands containing catecholic functionalities

The case of the Fe(III)-*Tiron* system clearly shows that ligands with catechol functionality can form very stable Fe(III) complexes. However, our studies show that the system exhibits low kinetic inertia ($t_{1/2}$ = 1.8 hours). This could also be partly due to the fact that *Tiron* is a bidentate ligand; in fact, we found that once the first ligand molecule dissociates, the system follows a "cascade" mechanism leading to the formation of the free metal ion. Consequently, our research was directed toward the study of new, rationally designed ligands that could form more efficient systems. With this in mind, we decided to synthesize chelating ligands with higher denticity that contain catechol groups to take advantage of the thermodynamic stability they can confer, possibly compensating for their low kinetic inertia. The ligands we propose are structures based on diamines with aliphatic chains of different lengths as a scaffold, in order to also assess the effect that scaffold length may have on complexation of Fe(III). The general structure of the ligands we investigated is reported in Scheme 1.

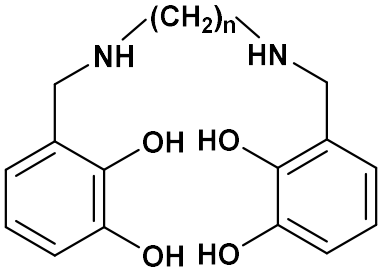

Scheme 3. General structure of the discussed ligands.

6.2.1 Experimental Section

Chemicals.

All reagents used for the synthesis of the ligands were purchased from Sigma (St. Luis, Mo., USA).

Synthesis of the ligands

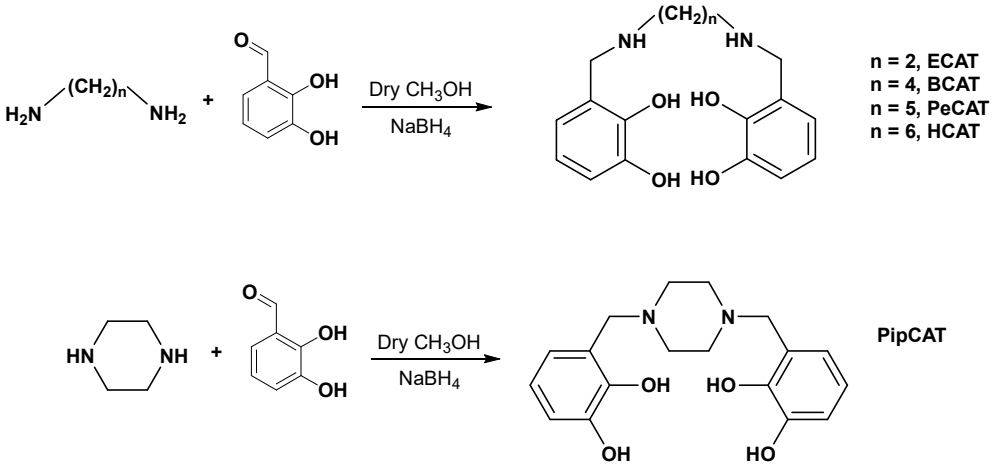

Scheme 4. General synthetic scheme of the discussed ligands.

All synthesized ligands were obtained by reductive amination of 2,3-dihydroxybenzaldehyde. Linear diamines varying in aliphatic chain

length were used. Precisely, 1,2-ethylenediamine, 1,4-diaminobutane, 1,5-diamminopentane, 1,6-diaminohexane and piperazine were used. This allowed us to prepare the following ligands: 3,3'-((ethane-1,2-diylbis(azanediyl))bis(methylene))bis(benzene-1,2-diol) (**ECAT**), 3,3'-((butane-1,4-diylbis(azanediyl))bis(methylene))bis(benzene-1,2-diol) (**BCAT**), 3,3'-((pentane-1,5-diylbis(azanediyl))bis(methylene))bis(benzene-1,2-diol) (**PeCAT**), 3,3'-((hexane-1,6-diylbis(azanediyl))bis(methylene))bis(benzene-1,2-diol) (**HCAT**) and 3,3'-(piperazine-1,4-diylbis(methylene))bis(benzene-1,2-diol) (**PipCAT**). In general, 1 eq. of the amine precursor is dissolved in dry methanol. After the complete dissolution, 2.5 eq. of 2,3-dihydroxybenahldeide are added: the solution takes on an orange/yellow colour. After 1 hour, 5 eq. of $NaBH_4$ are added to reduce the iminium ion: the system is left under stirring for 2 hours in an ice bath. Finally, a few millilitres of water are added to quench the sodium boron hydride. The sample is dried in a vacuum and taken up in ethanol. The solution is left under stirring overnight and filtered. The volume is reduced and the sample is precipitated in Et_2O and washed three times. In all cases, the samples had impurities given either by the presence of both the mono- and the bi-substituted ligand, or by the presence of unreacted catechol. For the purification procedure, the mixture were separated in a preparative column by HPLC-MS (XBridgeTM Prep Phenyl 5 μm OBDTM 19x100 mm). All ligands were characterized by NMR spectroscopy and mass spectrometry:

ECAT: MS (ESI): m/z calcd for $C_{16}H_{20}FeN_2O_4$: 304.35; found: 305.71 ($M + H^+$);

^{1}H-NMR (MeOD): δ [ppm] = 2.7 ppm (t, 4 H, -NH-C**H$_2$**-C**H$_2$**-NH-), 3.7 ppm (s, 4 H, Ph-C**H$_2$**-NH-), 6.6 ppm (m, 6 H, protons of the aromatic rings).
^{13}C-NMR (MeOD): δ [ppm] = 46 ppm (-NH-**C**H$_2$-**C**H$_2$-NH-), 48 ppm (Ph-**C**H$_2$-NH-), 117 – 120 ppm (C of the aromatic rings), 148 – 150 ppm (C bound to the –OH groups on the aromatic rings).

BCAT: MS (ESI): m/z calcd for $C_{18}H_{24}FeN_2O_4$: 332.40; found: 333.61 (M + H^+);
^{1}H-NMR (MeOD): δ [ppm] = 1.8 ppm (q, 4 H, -NH-CH$_2$-C**H$_2$**-), 3.0 ppm (t, 4 H, -NH-C**H$_2$**-CH$_2$-), 4.2 ppm (s, 4 H, Ph-C**H$_2$**-NH-), 6.7 – 6.9 ppm (m, 6 H, protons of the aromatic rings).
^{13}C-NMR (MeOD): δ [ppm] = 23 ppm (-NH-CH$_2$-**C**H$_2$-), 46 ppm (-NH-**C**H$_2$-CH$_2$-), 46 ppm (Ph-**C**H$_2$-NH-), 116 – 121 ppm (C of the aromatic rings), 144 – 145 ppm (C bound to the –OH groups on the aromatic rings).

PeCAT: MS (ESI): m/z calcd for $C_{19}H_{26}FeN_2O_4$: 346.43; found: 347.23 (M + H^+);
^{1}H-NMR (MeOD): δ [ppm] = 1.4 ppm (q, 2 H, -CH$_2$-C**H$_2$**-CH$_2$), 1.8 ppm (q, 4 H, -NH-CH$_2$-C**H$_2$**-CH$_2$), 3.0 ppm (t, 4 H, -NH-C**H$_2$**-CH$_2$-CH$_2$), 4.2 ppm (s, 4 H, Ph-C**H$_2$**-NH-), 6.7 – 6.9 ppm (m, 6 H, protons of the aromatic rings).
^{13}C-NMR (MeOD): δ [ppm] = 23 ppm (-CH$_2$-**C**H$_2$-CH$_2$), 25 ppm (-NH-CH$_2$-**C**H$_2$-CH$_2$), 46 ppm (-NH-**C**H$_2$-CH$_2$-CH$_2$), 46 ppm (Ph-**C**H$_2$-NH-), 116 – 121 ppm (C of the aromatic rings), 144 – 145 ppm (C bound to the –OH groups on the aromatic rings).

HCAT: MS (ESI): m/z calcd for $C_{20}H_{28}FeN_2O_4$: 360.25; found: 361.21 (M + H^+);

^{1}H-NMR (MeOD): δ [ppm] = 1.3 ppm (q, 4 H, -NH-CH_2-CH_2-C**H_2**), 1.6 ppm (q, 4 H, -NH-CH_2-C**H_2**-CH_2), 3.0 ppm (t, 4 H, -NH-C**H_2**-CH_2-CH_2), 4.2 ppm (s, 4 H, Ph-C**H_2**-NH-), 6.8 – 6.9 ppm (m, 6 H, protons of the aromatic rings).

^{13}C-NMR (MeOD): δ [ppm] = 25 ppm (-NH-CH_2-CH_2-**C**H_2), 25 ppm (-NH-CH_2-**C**H_2-CH_2), 46 ppm (-NH-**C**H_2-CH_2-CH_2), 46 ppm (Ph-**C**H_2-NH-), 117 – 122 ppm (C of the aromatic rings), 144 – 145 ppm (C bound to the –OH groups on the aromatic rings).

PipCAT*:* MS (ESI): m/z calcd for $C_{18}H_{22}FeN_2O_4$: 330.38; found: 331.46 (M + H^+);

^{1}H-NMR (MeOD): δ [ppm] = 3.5 – 3.7 ppm (m, 8 H, CH_2 groups of the piperazine ring), 4.3 ppm (s, 4 H, Ph-C**H_2**-N-), 6.8 – 6.9 ppm (m, 6 H, protons of the aromatic rings).

^{13}C-NMR (MeOD): δ [ppm] = 48 ppm (CH_2 groups of the piperazine ring), 115 – 123 ppm (C of the aromatic rings), 144 – 145 ppm (C bound to the –OH groups on the aromatic rings).

Complexation of Iron(III)

For Fe(III) complexation, we adapted a procedure reported in the literature.[26] In general, 1.05 eq. of the ligand are dissolved in methanol, giving a yellow solution. 1 eq. of $FeCl_3$ is then added to the system. The solution immediately takes on a greenish colour. After 10 minutes, 4 eq. of NaOH 1 M are added and the solution takes on a purple color. The sample is left under stirring for 30 minutes and then dried under vacuum. The dark powder is taken up in ultrapure water giving a clear

purple solution. After 2 hours, the solution's pH is adjusted at 6, left under stirring for 1.5 hours and then filtered on a syringe. The concentration of the solution is determined by the Evans method. For the ECAT and BCAT cases, we could not obtain a molecular complex. This is probably attributable to the fact that the aliphatic chain of the scaffold is too short to allow the formation of a complex in 1:1 stoichiometry and that instead oligomerization is thus favoured, which plausibly leads to the formation of a melanin-like compound (indeed, the formation of a black precipitate is noted).[27]

6.2.2 Results and discussion

Relaxometric characterization.

For all complexes of these catechol-based ligands, we initially assessed the dependence of the relaxivity on pH by acid-base titration and by measuring the longitudinal relaxation rate of water protons at 62 MHz and 298 K. From a preliminary analysis, we see that at acidic pH (<3) all complexes exhibit the same behaviour, which is similar to the Fe(III)-*Tiron* reference. For the Fe(III)-PeCAT and Fe(III)-HCAT systems, a further change is observed at more basic pH values, while for Fe(III)-PipCAT there is precipitation of the complex between pH 6 and 8, probably because it becomes electrically neutral.

The values of relaxivity can also give information about the hydration number of these systems. Values of r_1 of 2.4 $mM^{-1} s^{-1}$ and 2.7 $mM^{-1} s^{-1}$ between pH 4 and 6 for Fe(III)-PipCAT and Fe(III)-HCAT, respectively, suggest that the complexes could have an hydration number q = 1. In fact, these values are very similar to those of Fe(III)-CDTA (r_1 = 2.1 $mM^{-1} s^{-1}$ at 298 K and 62 MHz), for example, which has a very similar molecular mass. The slight increase in relaxivity in the case of Fe(III)-

HCAT (≈ 10-12%) compared to Fe(III)-PipCAT could be due to the fact that its molecular mass is slightly higher. Finally, for Fe(III)-PeCAT, the relaxivity value of 3.84 $mM^{-1} s^{-1}$, ranging between pH 4 and 7, can be associated with a bihydrate complex. This could be due to the shorter length of the aliphatic scaffold, which could allow the entry of a second water molecule.

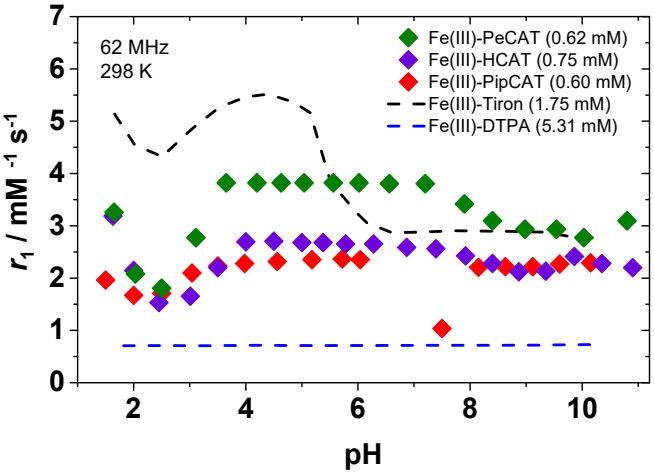

Figure 13 . pH dependency of r_1 for Fe(III)-PeCAT (◆, 0.62 mM), Fe(III)-HCAT (◆, 0.75 mM), Fe(III)-PipCAT (◆, 0.60 mM), Fe(III)-*Tiron* (—, 1.75 mM) and Fe(III)-DTPA (—, 0.62 mM) at 62 MHz and 298 K.

In order to fully understand the parameters that influence the relaxivity of these systems, we collected their NMRD profiles at three different temperatures. Furthermore, to confirm their hydration numbers and obtain accurate values for the mean residence lifetimes of bound water molecules (τ_M), we also collected ^{17}O transverse relaxation rates (R_{2p}) and chemical shifts ($\Delta\omega_r$). In this way, we are able to adequately describe the behaviour of these paramagnetic complexes in aqueous solution.

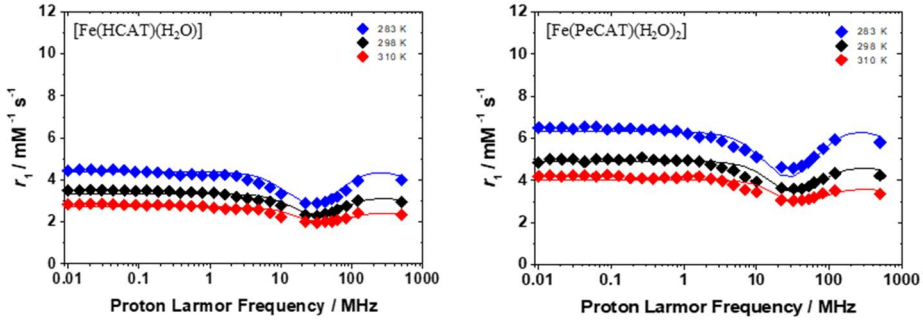

Figure 14. ^{1}H NMRD profiles at different temperatures of $[Fe(HCAT)(H_2O)]^-$ (left, pH = 7.0, $[Fe^{3+}]$ = 0.75 mM) and $[Fe(PeCAT)(H_2O)_2]^-$ (right, pH = 6.8, $[Fe^{3+}]$ = 0.62 mM).

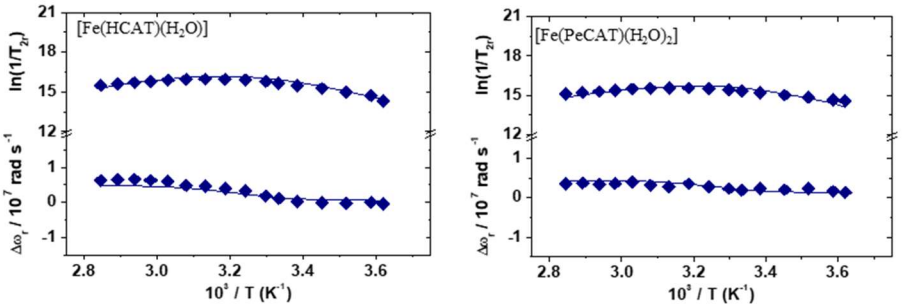

Figure 15. ^{17}O NMR reduced transverse relaxation rates and chemical shifts of $[Fe(HCAT)(H_2O)]^-$ (left, pH = 7.0, $[Fe^{3+}]$ = 1.62 mM) and $[Fe(PeCAT)(H_2O)_2]^-$ (right, pH = 6.8, $[Fe^{3+}]$ = 1.30 mM) measured at 11.75 T.

In contrast to the classical NMRD profiles of low molecular weight Fe(III)-complexes, it can be seen that in the high field region, as in the case of $[Fe(\textit{Tiron})_2(H_2O)_2]^{5-}$, the minimum relaxivity value is around 32 MHz. To our knowledge, this behaviour is typical for Fe(III)-catecholate systems and differs from other Fe(III)-complexes (e.g., the minimum for $[Fe(EDTA)]^-$ and $[Fe(CDTA)]^-$ is at 62 MHz). The reported data were simultaneously fitted by the equations describing

paramagnetic relaxation as described previously. In the case of $[Fe(HCAT)]^-$, we obtained an excellent fit of the data by assuming that the complex is monohydrate and that the value of its rotational correlation time τ_R is 54.0 ps, with which an activation energy Er of 16.7 kJ mol^{-1} is associated. Similarly, we were able to obtain an equally excellent fit of the $[Fe(PeCAT)]^-$ data assuming a hydration number q = 2, a τ_R of 45.9 ps and an associated activation energy Er of 16.0 kJ mol^{-1}. These values perfectly follow the expected linear trend with respect to the molecular mass of the complexes. As for the parameters defining the electron spin relaxation, the mean square transient ZFS energy (Δ^2), and its correlation time (τ_V), the values are in accordance with what is expected for Fe(III) complexes of this type.[16] In both cases, in order to best reproduce the temperature dependence of relaxivity, we had to integrate the dependence of the zero-field splitting energy Δ on temperature according to an Arrhenius-type trend, modulated by an activation energy E_Δ. Finally, with regard to the exchange dynamics, both complexes appear to be in an intermediate exchange regime for which the value of τ_M does not appear to be a limiting factor to relaxivity. All data obtained from the fit are shown in Table 4. Although the data obtained are promising, unfortunately the complexes seem to degrade with the passage of time. In fact, the change of the solution colour from purple to black and the formation of a precipitate can be seen after several days. We speculate that this may be attributable either to the formation of melanin-like oligomeric structures over time or to redox reactions of the catechol groups, which, upon oxidizing to quinone, may promote Fe(III) reduction.[28,29] Having completed the relaxometric characterization, the next step will be to study their thermodynamic

stability and kinetic inertia so as to understand what happens over time and, possibly, modify the design of these complexes to optimize their properties. Finally, the case of Fe(III)-PipCAT is proposed. The profiles were collected at different temperatures, and the differences are immediately noticeable. Again we noticed that the complex tends to degrade over time, changing from a purple to a black color. We hypothesized that the complex tends slowly to form poorly soluble oligomeric structures that are difficult to investigate. This might be supported by our relaxometric characterization. Especially from the data at 500 MHz. The ^{1}H NMRD profiles and ^{17}O NMR data measured at pH 5.3 are shown below. The temperature dependence of the relaxivity and the reduced transverse relaxation rates indicate the presence of a slow-to-intermediate exchange regime. However, we were unable to obtain a fit that adequately describes its behaviour. Despite some critical problems, this type of complexes remains interesting and worth of further investigation. The study will therefore continue toward the search for innovative structures based on the stabilization of the metal ion by exploiting alternative siderophores.

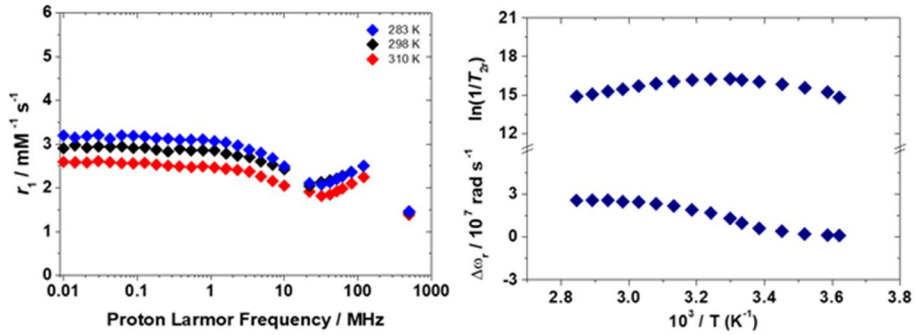

Figure 16. ^{1}H NMRD profiles at different temperatures (left, pH = 5.3, [Fe^{3+}] = 0.60 mM) and ^{17}O NMR data (right, pH = 5.3, [Fe^{3+}] = 6.41 mM) of the Fe(III)-PipCAT system.

Table 4. Data obtained from the simultaneous fit of ^{1}H NMRD profiles.

Parameters	$[Fe(PeCAT)(H_2O)_2]^-$ (MW = 434 g/mol)	$[Fe(HCAT)(H_2O)]^-$ (MW = 428 g/mol)
$^{298}r_1$ 60/120 MHz / mM^{-1} s^{-1}	3.9 / 4.3	2.6 / 3.0
$^{298}\Delta^2$ / 10^{20} s^{-2}	13.8 ± 0.1	13.0 ± 0.1
E_Δ / kJ mol^{-1}	5.6 ± 0.4	5.9 ± 1.2
$^{298}\tau_V$ / ps	5.8 ± 0.1	5.8 ± 0.4
E_V / kJ mol^{-1}	1.0 [a]	1.0 [a]
$^{298}\tau_M^O$ / ns	102.5 ± 0.8	83.1 ± 4.2
ΔH_M / kJ mol^{-1}	54.7 ± 3.5	54.4 ± 5.2
$A_O/\hbar/10^6$ rad s^{-1}	-24.5 ± 0.8	-32.4 ± 1.7
$^{298}\tau_R$ / ps	45.9 ± 1.3	54.0 ± 5.0
E_R / kJ mol^{-1}	16.0 ± 1.5	16.7 ± 5.6
C_{os}	0.3046 ± 0.001	0.1035 ± 0.034
q	2 [a]	1 [a]
r / Å	2.70 [a]	2.70 [a]
a / Å	3.5 [a]	3.5 [a]
^{298}D / 10^5 cm^2 s^{-1}	2.24 [a]	2.24 [a]
E_D / kJ mol^{-1}	20.0 [a]	20.0 [a]

[a] = fixed parameters

6.3 Conclusions

In this chapter, a detailed study of Fe(III)-catecholate systems is proposed. The case of Fe(III)-*Tiron* has represented a preliminary investigation. In particular, a thorough relaxometric characterization of all the species exhibited by this system in aqueous solution was carried out in combination with a study of their thermodynamic stabilities and kinetic inertness. As for the relaxometric part, it is very

interesting to see how phenomena of different nature can lead to deviations from the theoretical predictions. For example, assuming that the contribution from IS, if present, is the dominant one, one would have expected relaxivity trends of the type r_1 (Fe**L1**) > r_1 (Fe**L2**) > r_1 (Fe**L3**). However, the case of the SS contribution for FeL3 and the limiting effect of the slow exchange regime for FeL1 undermine this linearity. As for stability studies, the case of Fe(III)-*Tiron* clearly shows that catechols can potentially form very stable complexes, but they need to be optimized with respect to kinetic inertia

With this in mind, we synthesized a series of bifunctional ligands containing catechol groups with higher denticity to develop ligands that can maintain both high thermodynamic stability and high kinetic inertia, but without compromising their water proton relaxation enhancement effect. In addition, using the ECAT, BCAT, PeCAT, HCAT, and PipCAT series of ligands, we were able to evaluate the effects of the structure of the complex on the parameters that determine relaxivity (e.g., hydration number and electronic parameters). These preliminary studies need to be completed by spectrophotometric and potentiometric studies to obtain information on their stability and inertness. However, the case of catechol-based ligands remains a topic of great interest for future studies considering the development of rationally designed ligands for the formation of complexes combining high relaxivity and remarkable thermodynamic stabilities and kinetic inertia.

6.4 Notes and References

Author contribution: the author carried out the relaxometric measurements and their analysis under the supervision of Professor Mauro Botta. The thermodynamic and kinetic experiments were performed under the supervision of Doctor Zsolt Baranyai.

The author also provided the synthesis and characterization of the reported ligands.

(1) Lemos, V. A.; da S. Lima, A.; Santos, J. S.; Castro, J. T.; Ferreira, S. L. C. *Int. J. Environ. Anal. Chem.* **2012**, *92* (10), 1121–1134.

(2) Kim, H.-S.; Choi, H.-S. *Talanta* **2001**, *55* (1), 163–169.

(3) den Boef, G.; Ozinga, W.; van Rossum, G. J. T *Anal. Chim. Acta* **1977**, *92* (2), 387–392.

(4) Xu, Y.; Wen, Y.-H.; Cheng, J.; Cao, G.-P.; Yang, Y.-S. *Electrochimica Acta* **2010**, *55* (3), 715–720.

(5) Shahrokhian, S.; Asadian, E. *J. Electroanal. Chem.* **2009**, *636* (1–2), 40–46.

(6) K. L. Cheng, K. Ueno and T. Imamura. *Handbook of Organic Analytical Reagents*, CRC Press, Inc., Boca Raton.; **1982.**

(7) Abe, S.; Saito, T.; Suda, *Analytica Chimica Acta*, **1986**, 181, 203-209.

(8) Bhadani, S. N.; Tiwari, M.; Agrawal, A.; Kavipurapu, C. S. *Mikrochim. Acta* **1994**, *117* (1–2), 15–22.

(9) McBryde, W. A. E. *Can. J. Chem.* **1964**, *42* (8), 1917–1927.

(10) Farkas, E.; Csóka, H. *J. Inorg. Biochem.* **2002**, *89* (3–4), 219–226.

(11) Ozutsumi, K.; Uchima, Y.; Kawashima, T. *Anal. Sci.* **1990**, *6* (4), 573–577.

(12) Zhang, Z.; Jordan, R. B. *Inorg. Chem.* **1996**, *35* (6), 1571–1576.

(13) Aime, S.; Botta, M.; Esteban-Gómez, D.; Platas-Iglesias, C. *Mol. Phys.* **2019**, *117* (7–8), 898–909.

(14) Corsi, D. M.; Platas-Iglesias, C.; Bekkum, H. van; Peters, J. *Magn. Reson. Chem.* **2001**, *39* (11), 723–726.

(15) Aime, S.; Botta, M.; Ermondi, G.; Fasano, M.; Terreno, E. *Magn. Reson. Imaging* **1992**, *10* (5), 849–854.

(16) Baranyai, Z.; Carniato, F.; Nucera, A.; Horváth, D.; Tei, L.; Platas-Iglesias, C.; Botta, M. *Chem. Sci.* **2021**, *12* (33), 11138–11145.

(17) Kuźnik, N.; Jewuła, P.; Oczek, L.; Kozlowicz, S.; Grucela, Artur; Domagala, W. *Acta Chim. Slov.*, **2014**, 61, 87–93.

(18) Lauffer, R. B.; Vincent, A. C.; Padmanabhan, S.; Villringer, A.; Saini, S.; Elmaleh, D. R.; Brady, T. J. *Magn. Reson. Med.* **1987**, *4* (6), 582–590.

(19) Bales, B. C.; Grimmond, B.; Johnson, B. F.; Luttrell, M. T.; Meyer, D. E.; Polyanskaya, T.; Rishel, M. J.; Roberts, J. *Contrast Media Mol. Imaging* **2019**, *2019*, 1–10.

(20) Larsen, S. K.; Jenkins, B. G.; Memon, N. G.; Lauffer, R. B. *Inorg. Chem.* **1990**, *29* (6), 1147–1152.

(21) Hoener, B.-A.; Engelstad, B. L.; Ramos, E. C.; Macapinlac, H. A.; Price, D. C.; Johnson, T. R.; White, D. L. *J. Magn. Reson. Imaging* **1991**, *1* (3), 357–362.

(22) Kuźnik, N.; Szafraniec-Gorol, G.; Oczek, L.; Grucela, A.; Jewuła, P.; Kuźnik, A.; Zassowski, P.; Domagala, W. *J. Organomet. Chem.* **2014**, *769*, 100–105.

(23) Kras, E. A.; Abozeid, S. M.; Eduardo, W.; Spernyak, J. A.; Morrow, J. R. *J. Inorg. Biochem.* **2021**, *225*, 111594.

(24) Pierre, V. C.; Allen, M. J. *Contrast Agents for MRI: Experimental Methods*; Royal Society of Chemistry, **2017**.

(25) Swift, T. J.; Connick, R. E. *J. Chem. Phys.* **1962**, *37* (2), 307–320.

(26) Avdeef, A.; Sofen, S. R.; Bregante, T. L.; Raymond, K. N. *J. Am. Chem. Soc.* **1978**, *100* (17), 5362–5370.

(27) Enemark, E. J.; Stack, T. D. P. *Inorg. Chem.* **1996**, *35* (10), 2719–2720.

(28) Loupias, P.; Dechamps-Olivier, I.; Dupont, L.; Vanlemmens, P.; Mullié, C.; Taudon, N.; Bouchut, A.; Dassonville-Klimpt, A.; Sonnet, P. *Pharmaceuticals* **2019**, *12* (4), 160.

(29) Hostnik, G.; Tošović, J.; Štumpf, S.; Petek, A.; Bren, U. *Spectrochim. Acta. A. Mol. Biomol. Spectrosc.* **2022**, *267*, 120472.

7 Conclusions and future work

As a result of a renewed interest in the search for new Fe(III)-based paramagnetic MRI probes, an in-depth, multidisciplinary study of Fe(III)-based complexes as model systems was proposed in this dissertation. Such a multidisciplinary approach is based on the combination of relaxometric, spectrophotometric, potentiometric, voltammetric and computational data for the characterization of Fe(III) complexes in aqueous solution. In this way, we were able to help lay the groundwork for the development of these new probes.

In the first part of the project, we focused on the study of well-known model systems such as $[Fe(H_2O)_6]^{3+}$, $[Fe(EDTA)]^-$ and $[Fe(CDTA)]^-$. These preliminary results clearly suggested that high-spin Fe(III) complexes exhibit a good efficiency as potential T_1 MRI contrast agents. In particular, an important conclusion of this work is that the next optimizations should:

1) increase the pK_a of the coordinated water molecule well above physiological pH;

2) obtain kinetically inert complexes, for example by ligand rigidification;

3) shift the reduction potential of the complex out of the biological window (E^0 < 0.2 V vs. NHE), to avoid complex dissociation upon reduction and also triggering the Fenton reaction;

4) optimize the final electronic relaxation times.

In the second part of the thesis, we moved onto the study of a series of rationally designed ligands derived from the basic structure of ethylenediaminetetraacetic acid (EDTA), i.e. EDTA-BOM_1 and EDTA-BOM_2 (BOM = benzyloxymethyl). The presence of lipophilic functionalities on these ligands promotes interaction with host molecules. This interaction is potentially very useful as it restricts the molecular tumbling of the probe, thus improving its contrast efficiency. In particular, we focused on the study of the binding interaction with human serum albumin, which has already been strategically studied and applied for Gd(III)- and Mn(II)-based complexes. However, to the best of our knowledge, no such examples exist in the case of Fe(III) complexes. In addition, to evaluate the effects of the formation of supramolecular adducts with medium molecular size substrates, we studied the interaction with β-cyclodextrin (β-CD) and its oligomer (poly-β-CD). Unlike what it has been previously reported for Gd(III) or Mn(II)-based complexes, i.e. the occurrence of a relaxivity peak at proton Larmor frequencies values between ca. 20-60 MHz, in the case of our Fe(III)-chelates this peak is shifted to significantly higher frequencies (≈ 300 MHz). This shift is mainly attributable to a different contribution of the electronic relaxation time: its influence becomes detectable and important only at high magnetic fields, while for Mn(II) and Gd(III) its effects are clearly visible in the low portion of the clinical fields region due their longer values. This result represent one of the most important clue to develop optimized Fe(III)-based MRI probes. Then, although the Fe(III) complexes of the EDTA-BOM_x series cannot be considered as potential candidates for clinical *in vivo* applications, they might represent an initial platform for the future design of complexes able

to combine high efficacy, enhanced stability and inertness and non-covalent binding capability.

Finally, the last systems we analysed are the Fe(III)-catecholates. We decided to study this class of compounds since it is well-known that their siderophore nature leads to the formation of highly stable Fe(III) complexes. We started with a well-defined Fe(III)-catecholate system, the Fe(III)-*Tiron*. Its remarkable contrast-enhancing effect combined with high thermodynamic stability confirmed the potential of ligands containing catechol functionalities. As its limited applicability is known, we have taken advantage of these studies for the development of new rationally designed ligands to obtain Fe(III) complexes with possible *in vivo* applicability. Specifically, we studied bifunctional linear ligands having catechol terminations. As precursors, we considered diamines having aliphatic chains of different lengths. This allowed us to evaluate the effect of the scaffold length on complexation as well as the influence on relaxivity-defining parameters (e.g., hydration number and electronic parameters). After synthesizing and thoroughly characterizing the ligands, we obtained the corresponding Fe(III) complexes. The detailed relaxometric study of these complexes confirmed that it is possible to obtain Fe(III)-based catechol probes with interesting properties in terms of contrast enhancement. Further studies regarding their thermodynamic stability and kinetic inertia will allow us to define their future development.

Future work may concern the design of state-of-the-art ligands that can either exploit catecholic functionalities for Fe(III) stabilization that do not compromise efficacy, or even investigate other siderophore functionalities (e.g., hydroxypyridinones, hydroxamates). So, while

much remains to be done, we hope that these results may represent useful guidelines for the development of metal-diagnostic probes of improved safety, biotolerability and efficacy.

8 List of publications

1. Baranyai, Z.; Carniato, F.; Nucera, A.; Horváth, D.; Tei, L.; Platas-Iglesias, C.; Botta, M.; "Defining the Conditions for the Development of the Emerging Class of Fe^{III}-Based MRI Contrast Agents", *Chem. Sci.,* 2021, 12, 11138-11145.

2. Ravera, M.; Nucera, A.; Gabano, E.; "Freshening up Old Methods for New Students: A Colorful Laboratory Experiment to Measure the Formation Constants of Ni(II) Complexes Containing Ethane-1,2-Diamine", *J. Chem. Ed*, 2022, 99, 3, 1473–1478.

3. Uzal-Varela, R.; Lucio-Martínez, F.; Nucera, A.; Botta, M.; Esteban-Gómez, D.; Valencia, L.; Rodríguez-Rodríguez, A.; Platas-Iglesias, C. "A Systematic Investigation of the NMR Relaxation Properties of Fe(III)-EDTA Derivatives and Their Potential as MRI Contrast Agents", *Inorg. Chem. Front.* 2022, 00, 1-14 (Accepted Manuscript).

9 Acknowledgements

In questi tre anni, tutto quello che è stato il lavoro in laboratorio o la scrittura di questa tesi sicuramente è merito/colpa mia. Tuttavia, se sono cresciuto e, perché no, sopravvissuto a questo dottorato è merito delle persone con cui ho condiviso questo percorso.

Primi (e unica posizione per importanza), mamma e papà. Sono 27 anni che mi supportano e sostengono. Senza questo punto fisso della mia vita non so cosa sarei e, fortunatamente, non mi interessa neanche saperlo. Sicuramente sarei affamato però. Grazie a voi.

Ovviamente un doveroso ringraziamento va al Professor Mauro Botta e al Professor Fabio Carniato. In questi ormai quattro anni sono stati i miei mentori che mi hanno fatto crescere scientificamente in un modo che neanche avrei immaginato, "bastonandomi" quando era necessario. Grazie per avermi accolto nel vostro gruppo.

Un ringraziamento sentito va anche al Prof. Carlos Platas-Iglesias e al Prof. Zsolt Baranyai, i supervisor che mi hanno seguito nei periodi a La Coruna e a Trieste, rispettivamente. Vedere con mano cosa vuol dire collaborare con altri gruppi e imparare da voi sarà sempre un ricordo prezioso.

Infine, grazie Cibazzo. Siete 9 milioni e ho una pagina per i ringraziamenti, quindi vi ringrazierò privatamente. Ci tengo solo a dirvi che condividere con voi i momenti belli e le bestemmie è stato il punto cardine di questi anni. Soprattutto le bestemmie. Grazie.